ADHESIVE WEAR PHENOMENA IN HIGH PERFORMANCE POLYARYLETHERKETONE (PAEK) POLYMERS

A Dissertation

by

KEVIN ANDREW LAUX

Submitted to the Office of Graduate and Professional Studies of
Texas A&M University
in partial fulfillment of the requirements for the degree of

DOCTOR OF PHILOSOPHY

Chair of Committee,	Hung-Jue Sue
Committee Members,	Hong Liang
	Terry Creasy
	Mustafa Akbulut
Head of Department,	Andreas A. Polycarpou

August 2016

Major Subject: Mechanical Engineering

ABSTRACT

Adhesive wear is one of the most difficult types to study and is especially challenging for polymers. Such wear processes involve the mutual sticking of surface asperities followed by removal of debris from the bulk. This differs from abrasive wear in which debris is formed due to the penetration of hard rough asperities into the softer surface. Such descriptions have served the polymer tribology community for decades and are well suited for post-mortem analysis of wear surfaces. For instance, the presence of rippled features on the wear surface and large flake shaped debris are typical indicators of adhesive wear. However, this approach offers little insight into the underlying physics that occur at the interface. The overall objective of this research is to gain fundamental knowledge of adhesive wear phenomena in polyaryletherketone (PAEK) polymers. Ultimately, the hope is to correlate the observed surface damage and friction response with material science based explanations. Since no true adhesive wear test configuration exists, a top down approach was used in designing a set of experimental conditions. This was done with a multi-axis tribometer capable of being programmed to a wide array of displacements and trajectories. A catastrophic form of adhesive wear is termed fretting and results from the repeated slip of mutually loaded contacts. Using the multi axis tribometer PAEK polymers were studied in both multi directional sliding and fretting configurations with varied environmental conditions.

An important aspect of PEEK tribology is the surface temperature reached during sliding. Infrared thermography was used to observe the full field temperature map of PEEK during ball-on-disc sliding. Additionally, friction studies were performed with

steel and sapphire counterfaces. The results of this study illustrate the important role transfer films play in determining both the friction and temperature response of the PEEK wear interface. The formation of transfer films resembles a unidirectional drawing process. Polarized FTIR-ATR measurements were used to assess chain orientation in the friction formed PEEK on steel transfer films. The results of these studies serve to better elucidate underlying mechanisms involved in adhesive wear of PAEK polymers.

DEDICATION

To my parents

ACKNOWLEDGEMENTS

I would like to thank my committee chair, Dr. Sue, and my committee members, Dr. Liang, Dr. Creasy, and Dr. Akbulut, for their guidance and support throughout the course of this research. I would also like to acknowledge the generous support provided by the Advance Performance Polymers for Energy Application (APPEAL) Consortium members in this research endeavor. Special thanks to Hoerbiger Corporation and Dr. Tim Bremner for providing samples and research guidance.

I would like to give my most sincere gratitude to Dr. H.-J. Sue, who has provided valuable guidance and served as a role model during my stay here at Texas A&M University. I extend special thanks to Dr. Janet Wong, Annelise Jean-Fulcrand and the tribology group at Imperial College. Without their assistance much of this work would not have been possible.

Thank you to all the past and present members of the Polymer Technology Center at Texas A&M for their help and guidance. I especially thank Mohammad Motaher Hossain for his contribution to this work. Thank you to Spencer Hawkins, Kevin White and Dr. Mike Mullins for fruitful research discussions.

Thanks also to my friends, family, and colleagues for making my time here a great experience. I would like to thank Dr. Xi Zhang and her cat LingLing who have provided inspiration and support in difficult times.

Finally, I would like to sincerely thank my father, Frank Laux, my mother, Diana Laux, sister Katy Albin and her family Ray, Julia and Andrew. Without your unconditional love and support this would never have been possible.

TABLE OF CONTENTS

Page

LIST OF FIGURES

Page

LIST OF TABLES

Page

CHAPTER I

INTRODUCTION

1.1 Overview of Tribology

When materials come into contact with one another, surface forces arise that resist sliding. Early studies of these frictional forces are often credited to Leonardo Da Vinci and have been investigated by science for the past 500 years[1]. It has been found that the real area of contact ultimately determines the nature of these forces. At the micro scale, surfaces tend to be rough and so contact is between the opposing peaks and valleys often referred to as asperities. The forces that result from these asperity contacts can result in damage or wear to one or both of the materials in contact. The combined study of friction and wear constitutes the field of tribology and the broader scope of this dissertation.

Much of the current understanding of material wear behavior comes from the seminal works of Archard[2], Tabor[3, 4], and Lancaster[5] among others. Common to all of them is the notion that wear is a process and can involve multiple mechanisms. Discussions of wear mechanisms typically refer to at least one of the schemes shown in Figure 1.1. Adhesive wear is often described as the result of surfaces becoming stuck followed by shear rupture of one of the materials. Abrasive wear results from the penetration of a hard asperity into the softer surface. The repeated passage of surfaces relative to one another can produce subsurface damage that will form debris through fatigue wear. The chemical interaction of the mated surfaces may also form debris

through a corrosive mechanism. Although these illustrations offer little insight into the origins of wear, they provide some clue as to how it can be prevented. For instance, the removal of hard rough asperities through polishing will reduce the degree of abrasive wear. Adhesive wear is unique in the sense that it has the capacity to occur even between atomically smooth surfaces. Furthermore, adhesive wear has a tendency to take part in combination with other wear processes. The origins of fretting wear for instance are typically attributed to the combination of adhesive and fatigue wear processes. This multi-faceted behavior has made adhesive wear both challenging to study and prevent.

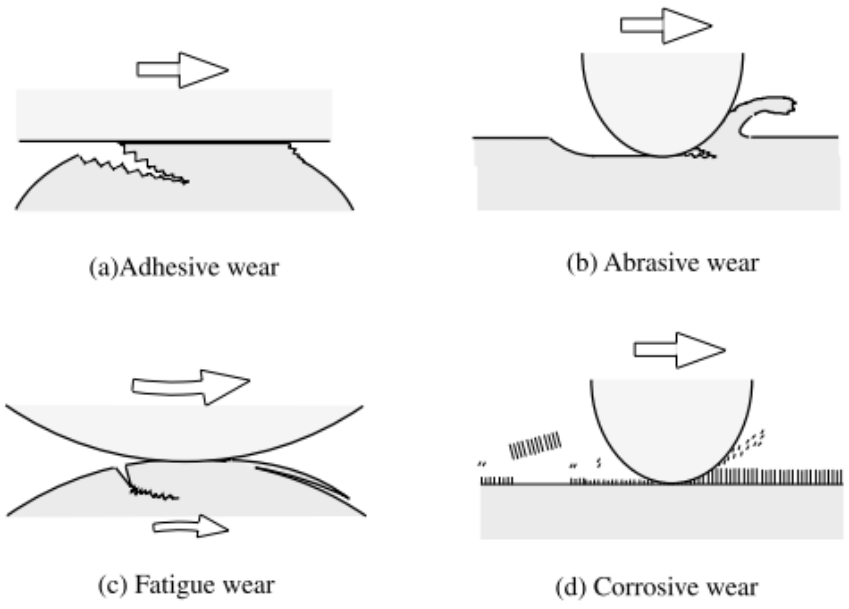

Figure 1.1. Illustration of common wear mechanisms**[6]**
(Figure reprinted from Kato, K. and K. Adachi, *Wear mechanisms.* Modern tribology handbook, 2001. **1**: p. 273-300 with permission from CRC Press)

Wear should be viewed as a system response in which the contact type and deformation state lead to surface changes that all may interact. An attempt at mapping this behavior is shown in Figure1.2 and illustrates the interconnectivity of the wear system. This complexity is especially pronounced in polymers. Polymers are viscoelastic and so bulk mechanical properties will change as a function of strain rate and temperature. This also means that the surface changes that take place during wear can then alter the deformation state and contact type. Despite the inherent challenges in studying wear of polymers, significant progress has been made over the past half-century.

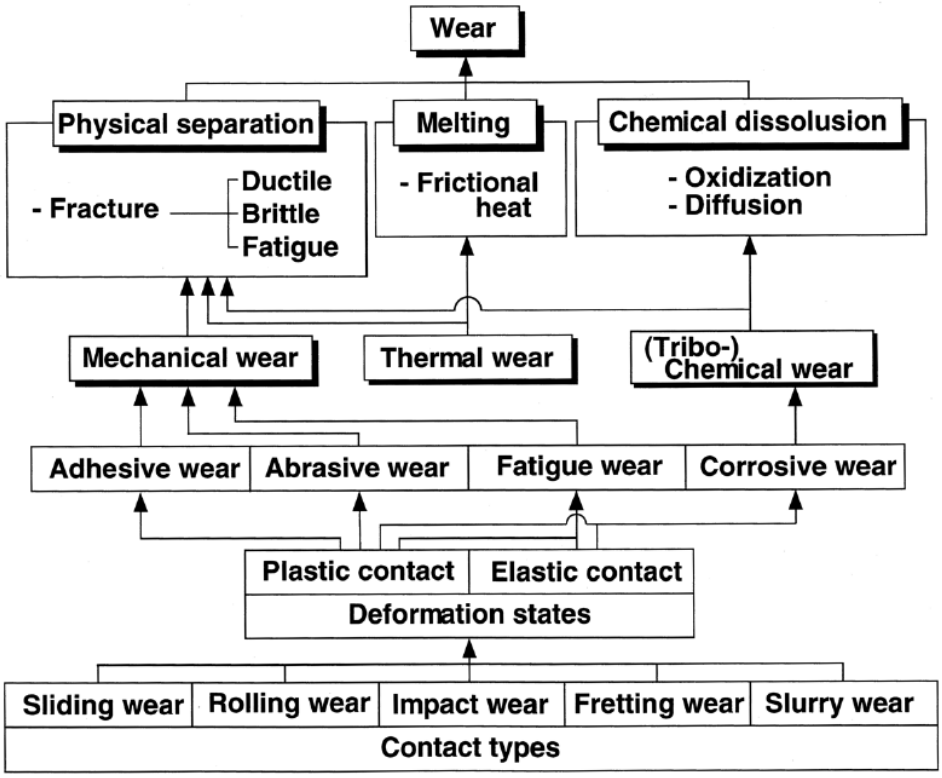

Figure 1.2. Classification of possible wear scenarios**[6]**
(Figure reprinted from Kato, K. and K. Adachi, *Wear mechanisms.* Modern tribology handbook, 2001. **1**: p. 273-300 with permission from CRC Press)

Polymers are also a broad class of materials in terms of their chemical structure and mechanical properties. This in turn has had an impact on how their wear behavior has been studied. Many of the same phenomenological wear processes occur across all material under similar contact types. Figure 1.3 shows the varied approaches taken in the study of polymer wear. Often a phenomenological approach is used in order to relate a particular set of conditions to a possible wear mechanism. However, the exact responses of elastomeric, thermosetting, glassy, and semicrystalline polymers are all profoundly different. A combined material response and generic scaling approach are thus also

necessary. The benefit of such approaches is most evident for linear aliphatic polymers PTFE and UHMWPE. In seminal work by Tabor et.al, it was found that the frictional response of these polymers could be related to their smooth molecular profiles[7]. Anisotropy in the static friction response of pre-rubbed samples resulted from preferential chain orientation that occurs on the polymer surface. Furthermore, transfer of highly oriented low friction films was detected on smooth glass substrates. These films consist of single polymer strands that are drawn as fibrils from the polymer bulk. Additionally, when bulky side groups were introduced to either polymer their characteristic tribological response disappeared. This early work linking molecular structure to friction and wear has served as a wellspring for tribology research. The transfer film formation of PTFE is often exploited to create self-lubricating bearings. Processing conditions and fillers can even be tailored to promote this behavior. Similarly, knowledge of surface chain orientation in UHMWPE has been used to explain its sensitivity to cross shearing wear environments[8]. The current practice of crosslinking UHMWPE artificial joints can be credited to this understanding. Clearly, advances in the application of polymers to tribology depend on the ability to link structure-property relations to friction and wear.

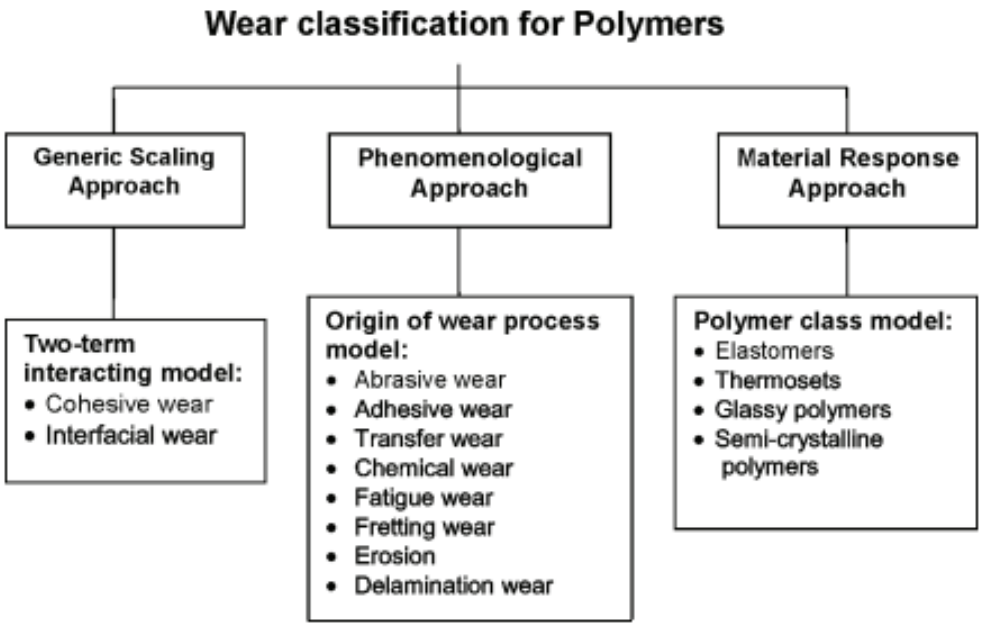

Figure 1.3. Common approaches to studying wear of polymers **[9]**
(Figure reprinted from Briscoe, B.J. and S.K. Sinha, *Wear of polymers.* Proceedings of the Institution of Mechanical Engineers, Part J: Journal of Engineering Tribology, 2002. **216**(6): p. 401-413.with permission from CRC Press)

The polyaryletherketone (PAEK) family of thermoplastics is also a well-studied group of tribologically relevant polymers. Their high glass transition temperature and resistance to most solvents make them an ideal material for application in extreme environments. Despite outstanding wear resistance, they tend to have high coefficients of friction. Often, low friction fillers such as PTFE and MoS_2 are incorporated to overcome this[10]. Still, significant work has been done to better understand the origins of unfilled PAEK wear resistance. This wear resistance is often attributed to an ability to form protective transfer films on harder metallic counterfaces. Unlike PTFE that forms transfer films due to its unique banded crystal structure, there is no specific mechanism for PAEK film formation[11]. Bahadur suggested that compacted debris becomes physically entrapped between asperities.[12] The film protects the bulk from abrasive

wear by covering hard rough asperities. However, this explanation fails to account for any tribochemical tranformations that may occur near the surface. Other researchers have focused on PAEKs susceptibility to frictional heating. It is believed that this heating process leads to the catastrophic failures seen in gears and roller bearings made from the PEEK member of this family[13]. This dissertation will thus attempt to understand how the changes that may manifest at the adhesive wear interface contribute to the overall tribological performance.

1.2 Research Scope

To further understand adhesive friction and wear mechanisms in high performance polyaryletherketone (PAEK) polymers, multi-faceted experimental and analysis approaches are needed. Such an approach involves the study of a selection of materials across a wide range of conditions capable of elucidating meaningful information. A process flow diagram for adhesive wear is given below. Briscoe utilized a similar diagram as a guide in his discussions of the phenomenon. This guide is in no way comprehensive, but it helps navigate the selection of variables for experimentation.

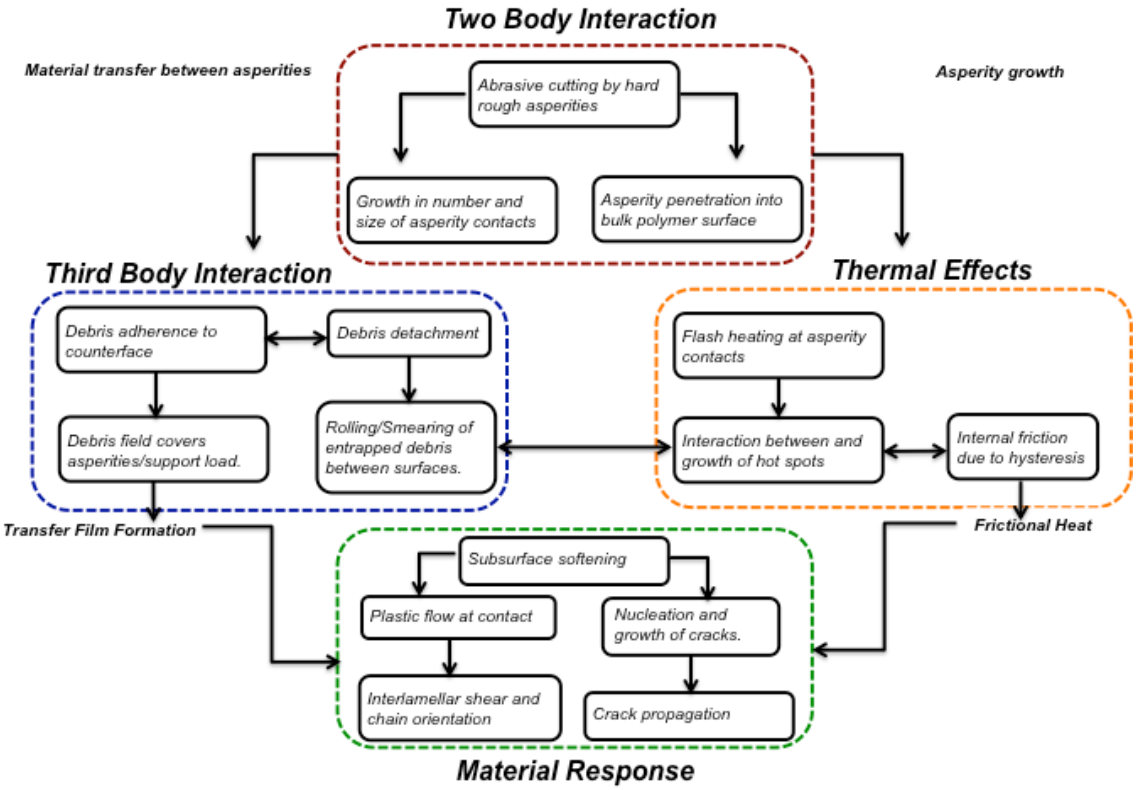

Figure 1.4. Adhesive wear process flow diagram

As the diagram in Figure 1.4 shows, the process begins with the interaction of the opposing surface asperities. The number and size of these asperity contacts depend on a number of variables. Greater normal loads will cause more asperities to come into contact. An increased plasticity index due to increased roughness or decreased material hardness will also play a role. During adhesive wear processes, the real asperity contact area may even be larger than the apparent contact area due to surface penetration. The overall material response will then be determined by these adhesively bonded asperities. With time, frictional heat will build up and can alter the material properties at the surface. Third body debris can further degrade properties, but also can support load.

Initial work will focus on contact with small displacement amplitudes and high contact pressures. This is often called fretting and it is believed that failure results from excessive surface heating. Failure may be due to the removal of large pieces of debris or fracture from crack propagation. Fillers are often incorporated into the base polymer to reduce the severity of these effects. However, the presence of water or other plasticizers can also degrade the PAEK surface. A selection of material will be tested under these conditions accompanied by appropriate post-hoc analysis. Under lighter loads and larger displacements transfer films will form which are often associated with low wear rates. However, little can be said as to how they form or contribute to wear reduction. The structure-property characteristics of such films will also be studied. Finally in situ methods will be applied to quantify the frictional heating that may take place under varied conditions.

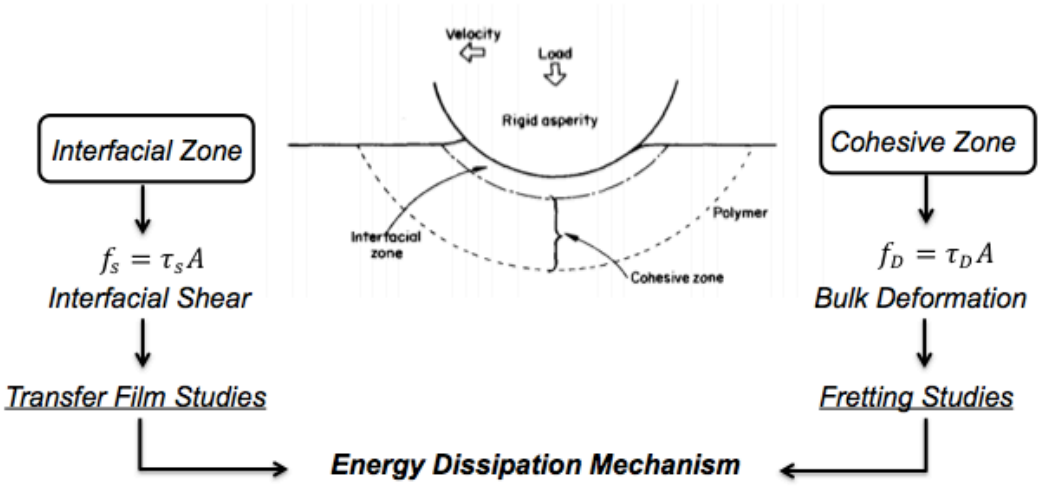

Figure 1.5. The interfacial and cohesive components of friction

As shown in the above Figure 1.5, the study of energy dissipation mechanisms requires the separation of interfacial and cohesive zones. The interfacial zone (~100nm) is largely responsible for the adhesive friction forces f_s and potential tribochemistry. The subsurface cohesive zone will then be responsible for the viscoelastic losses that contribute to frictional work. The separation of experiments into transfer film and fretting studies in effect will help isolate variables pertinent to each condition. The wear surface and debris generated from the different experimental tests will also help answer fundamental questions about the adhesive wear process:

1) Under what conditions does transfer of debris to the counterface either mitigate or promote wear?
2) Do tribochemical transformations occur at the surface that can be linked to either improved wear resistance or accelerated damage?
3) What role does frictional heating play in determining the material response?
4) Does frictional heating alone explain material behavior or do other energy dissipative mechanisms manifest during adhesive wear processes?

However, appropriate analytical methodologies need to be sensitive to the scale of damage being investigated. For instance, surface sensitive tools GI-SAXS and XPS are more appropriate for the study of interfacial phenomena than subsurface damage or bulk wear debris. A selection of appropriate analytical methodologies is shown in Figure 1.6.

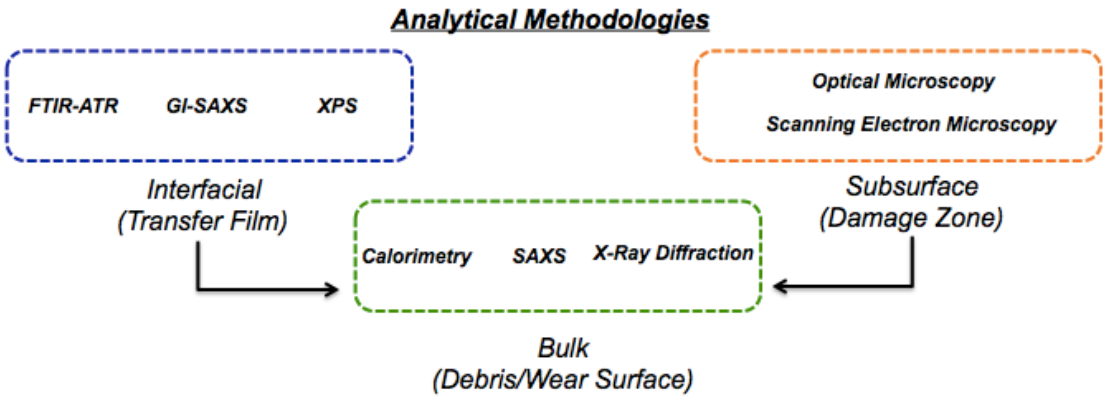

Figure 1.6. Analytical methodologies to be used in post-hoc surface analysis

The described process flow diagrams and research objectives have been incorporated into a research schema shown in Figure 1.7. As shown on the right hand side, in-situ observation will accompany the experimental studies. This work will also be supplemented with numerical modeling. It is expected that over the course of these studies new research questions will arise. These methods will help supplement the findings from wear testing and post-hoc analysis.

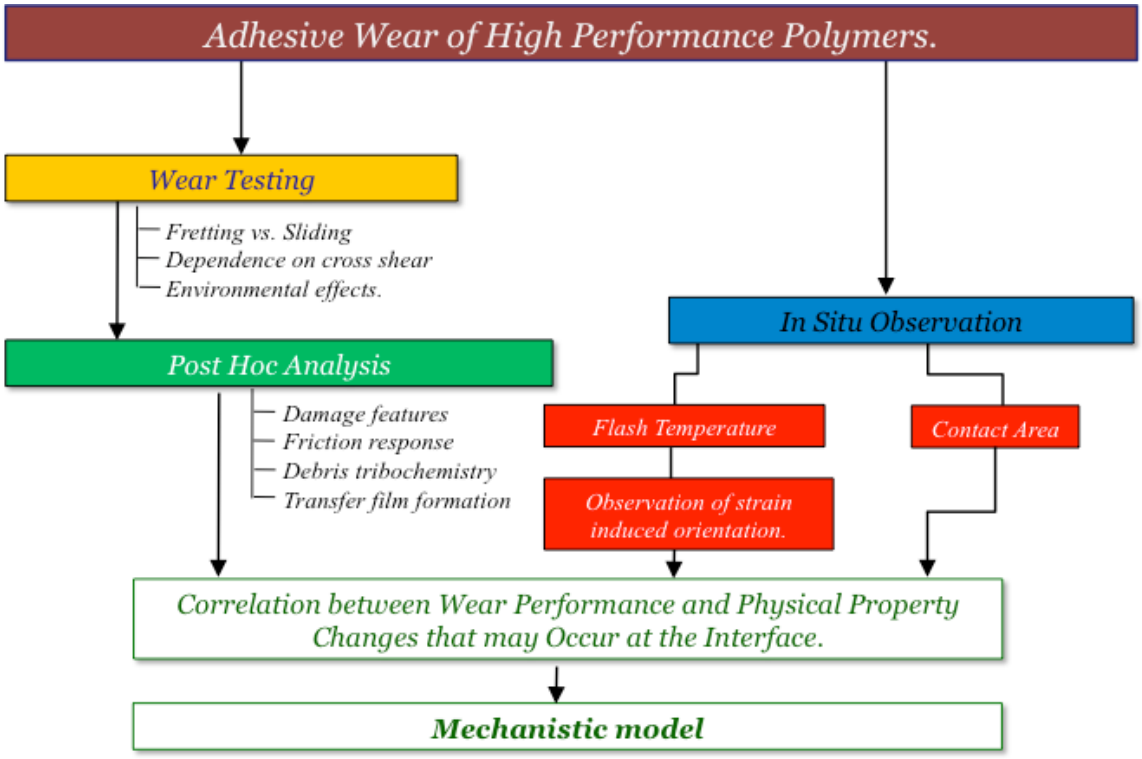

Figure 1.7. Research schema used in experimental studies

1.3 Layout of the Dissertation

The brief introduction to wear behavior presented in this chapter provides groundwork to perform a comprehensive study of adhesive wear in polyaryletherketone PAEK polymers. As discussed, no single adhesive wear test configuration exists and so a top down approach is used in designing experiments. The overall goal of this dissertation is to assign material science based explanations to the observed behavior. A literature review will be presented in Chapter II. This review will highlight work regarding wear of PAEK and relevant material behaviors.

The following Chapters III and Chapter IV will focus on experiments related to fretting. Fretting is a particular type of adhesive wear that occurs under conditions of high normal load and nominally small displacements. Using a multi-axis tribometer, test conditions have been created to help distinguish possible adhesive wear mechanisms in PAEK polymers. Analysis of wear surfaces and debris collected from the different tests will allow for discussion of possible mechanisms. Finite element modeling will also be employed to understand the stress and strain magnitude that takes place during fretting.

In Chapter V temperature measurements of the sliding surface are measured *in situ*. The measured surface temperature will then be compared to the predicted flash temperature rise. It is believed that frictional heating contributes significantly to the friction and wear behavior of PEEK. The sliding speed and pressure were selected as test variables. Separate friction measurements were also performed using both steel and a sapphire counterfaces. In Chapter VI attempts are made to understand the relationship between transfer film formation and wear performance. This chapter is a corollary to the previous chapters and builds upon previous discussions.

CHAPTER II

LITERATURE REVIEW

2.1 Wear Behavior of Polyetheretherketone

Polyaryletherketones are an ideal material for fundamental study of adhesive wear processes. The PEEK member of this family in particular has been well studied and this dissertation builds upon previous research and literature alike. A discussion of many of these findings will be presented and later incorporated into a research schema. The end goal is to provide deeper insight into suspected phenomena.

The behavior of PEEK has been investigated in a number of wear configurations[14]. Vast majorities have dealt with the wear of PEEK in pin-on-disc sliding[10]. Of particular interest has been the relationship between counterface surface roughness and wear[15-18]. Ovaert found that for unfilled PEEKs, an optimal surface roughness appears to exist as shown in figure 4[17, 19]. However, with increasing surface roughness there are only modest increases in wear. It is believed that this phenomenon can be attributed to the deposition of transfer films on the steel counterfaces. In theory, mechanically deposited films serve to protect the bulk from hard rough asperities. Laux and Schwartz later found that PEEK transfer film quality could be directly related to wear resistance[20, 21]. Most explanations contend that these films reduce wear by suppressing abrasion. Since the film modulus more closely matches the bulk, potential debris generating contact stress is reduced. However, this explanation neglects any changes in the polymer surface state that may beget wear resistance.

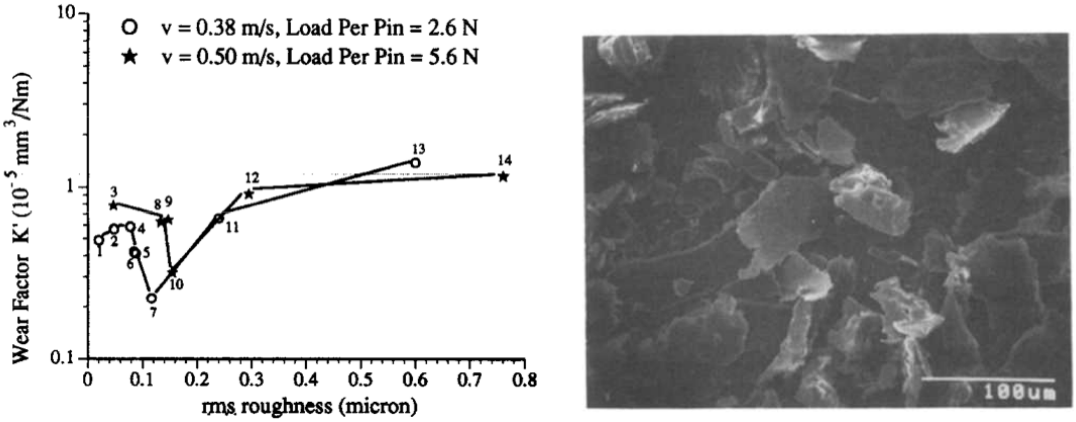

Figure 2.1. Relationship between surface roughness and wear debris formation in PEEK[17]
(Figure reprinted Ovaert, T.C. and H.S. Cheng, *Counterface topographical effects on the wear of polyetheretherketone and a polyetheretherketone-carbon fiber composite.* Wear, 1991. **150**(1): p. 275-287

The PEEK debris shape has also caused many researchers to speculate about the underlying wear mechanisms. As shown in Figure 2.1, PEEK debris tends to form as flat plate like particles. This observation is true for sliding against both smooth and rough surfaces. The above micrograph in fact depicts debris formed during sliding against a steel surface with roughness of 0.05μm RMS. Similar type debris is observed in metals and is attributed to the delamination wear process described by Suh[22]. For metals, delamination wear involves the nucleation of subsurface cracks that form through adhesive-fatigue interaction of asperities. It has been suggested that a similar explanation can be used for PEEK despite the obvious differences in how cracks form between polymers and metals. Ovaert postulated that during sliding heating takes place below the surface promoting plastic flow[17, 19]. The elevated temperature in combination with axial strain and subsurface stress leads to the formation of flat sheet like debris. Friedrich suggested that the fractal dimension of these particles could be used as a tool to assess

the severity of wear[23]. Based on debris morphology they suggested that for nominal contact pressures above 4 MPa cutting mechanisms disappear and wear is dominated by plastic flow. The contribution of sliding velocity has also been widely discussed[24-26]. With increased sliding velocity the effects of frictional heating will also increase. In some circumstances this may reduce friction and wear by promoting plastic surface flow and film formation. However, excessive velocity creates debris aggregation that will negatively impact wear resistance[26]. The apparent dependence on pressure and velocity has popularized usage of the product PV (MPa m/s) as an upper service limit for PEEK. Despite prevalent use of PV amongst manufacturers it has been proven to be a poor tool to gauge part performance.

A tremendous amount of tribochemical information is contained within wear debris. As a polymer surface is worn, frictional heating and strain can lead to changes in the polymer structure. The surface strains can then lead to chain orientation as seen in PE and PTFE[7, 8, 27, 28]. However chain rupture can also occur and result in molecular weight reduction as seen in the wear of polyamides[29]. PEEK in particular has been the subject of such post-hoc analysis[30-35].

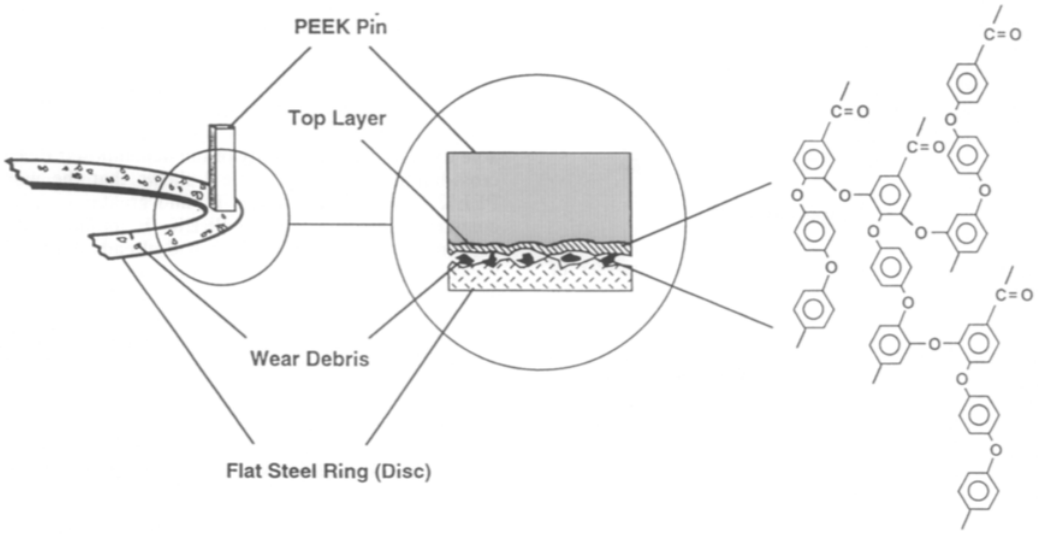

Figure 2.2. Proposed variation in PEEK chemical structure during wear process[34].
(Figure reprinted from Zhang, M.Q., Z.P. Lu, and K. Friedrich, *Thermal analysis of the wear debris of polyetheretherketone.* Tribology International, 1997. **30**(2): p. 103-111)

As shown in Figure 2.2, oxidative crosslinking is believed to result from PEEK wear against steel counterfaces. Using thermogravimetric analysis (TGA) and differential scanning calorimetry (DSC), Zhang studied the thermal properties of PEEK debris formed under varied conditions[34]. It was suggested that during wear, chain scission of the diphenyl ether segment occurs and forms oxidative crosslinks at free radical sites. They had observed changes in the pyrolysis behavior as well as a tendency for crystallization to be impeded. It was rationalized that these results were from the formation of crosslinked branches that restricted segmental mobility. Later, X-ray photoelectron spectroscopy (XPS) was used to further support this argument[32]. The appearance of a π-π^* shakeup peak in the C1S spectrum indicated the presence of single pendant phenyl rings due to chain scission. This behavior depended on contact pressure with the greatest intensity occurring at moderate (2-4MPa) contact pressures. The

change in the spectra with increased pressure was thought to be the result of chain scission occurring on different parts of the backbone that require greater thermal energy. The thermal properties of PEEK wear debris also indicate that it had been formed at temperatures near the melt. The first heat of melting for wear debris typically contains a cold crystallization exotherm[34]. This feature is often found in material that had been rapidly quenched from the melt state. The location of double melting peaks also tends to coincide with the thermal history. Usually for PEEK, an endotherm appears 10-15°C above the annealing temperature. The location of this feature has been used to determine that the PEEK wear surface may reach temperatures around 200°C [34, 35]. These studies are certainly not conclusive proof to the theories they espouse. However, they do demonstrate that the PEEK wear surface is in no way chemically inert. There is also the possibility that the polymer structure can be tailored to promote desirable tribochemistry. For instance, a more crosslinked surface would have greater load supporting capacity and creep resistance. Subtle changes in the branching or molecular weight could potentially result in more tenacious transfer films.

It has been observed that wear resistance of PEEK depends strongly on the molecular weight[10, 20, 36]. The increased molecular weight M_w will enhance a number of mechanical properties that may influence wear both directly and indirectly. With increased M_w there will also be an increased number of interspherulitic links and tie chains that can improve fracture properties. It has been suggested that abrasive wear of polymers is determined by the fracture toughness K_{IC}. Similarly, adhesive wear can

be described in terms of fatigue parameters, such as the critical length for crack growth a_c[37]. Both of these parameters have been found to depend on M_w in PEEK[38, 39].

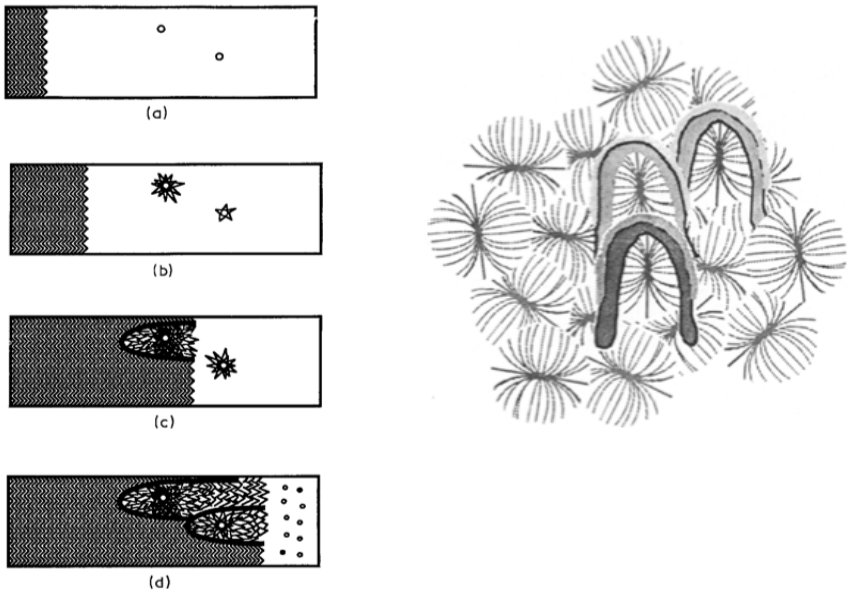

Figure 2.3. Schematic of PEEK crack propagation and fracture surface[39]
(Figure reprinted from Chu, J.-N. and J. Schultz, *The influence of microstructure on the failure behaviour of PEEK.* Journal of Materials Science, 1990. **25**(8): p. 3746-3752.)

As shown in the above Figure 2.3, microstructure plays a key role in the fracture behavior of polymers. For PEEK, the propagation of cracks can be impeded by the interaction of the crack front with the spherulite boundaries. With increased M_w there is an increased tie chain density which helps arrest crack growth[38]. It has also been observed that in lower M_w PEEK, larger spherulites occur and suffer from decreased fracture toughness[39]. This decreased fracture toughness can then be correlated with an increase in intraspherulitic fracture. Although fracture properties provide some empirical evidence for a relationship between M_w and wear resistance, it is not a direct correlation.

The apparent frictional heating at the surface means that rheological properties could also play a determining role in performance. Polymer melt viscosity and melt index increase with M_w and such properties would enhance transfer film load capacity.

The same surface plasticization that promotes protective film formation may also lead to catastrophic failures. For instance, PEEK roller bearings suffer from an adhesive wear type of pitting failure[40, 41]. Gears made of PEEK will fail similarly when there are excessive slide to roll ratios[13, 42]. It is suspected that high irreversible deformations take place at the contact and results in hysteric heating [43, 44]. Failure occurs when the opposing surfaces become compliant and adhesively weld together. Despite outstanding solvent resistance, PEEK can easily be plasticized by a number of solvents[45]. Chemicals as innocuous as water or methanol can substantially affect the hardness of the top(<1μm) surface layers. This will also severely compromise the capacity of PEEK to function as a bearing under high contact stress. Briscoe described a scuffing failure that takes place in alkane lubricated high-speed contacts and appears unique to PAEK material[46]. The loss of asperity persistence and propensity to scuff depended primarily on the applied load. These catastrophic adhesive-fatigue failures or often attributed to a scenario called fretting. However, fundamental studies of PEEK fretting are seemingly non-existent[47].

Typically, PAEK is incorporated with some low friction filler material to minimize the potential for adhesive wear[10]. These fillers are often selected without regard to how the PAEK surface chemistry contributes to friction and wear. Instead, fillers are selected based on their ability to mechanically reinforce the bulk as wells as

produce low friction transfer films. Often the filler is required to have multiple functions. PTFE is a popular choice for its internal lubrication properties and ability to form low friction transfer films. Carbon fibers will add strength but also might help dissipate heat from the surface. Chemically reactive nano-fillers such as CuS and Al_2O_3 can increase transfer film tenacity and support asperity loads[48]. It has been pointed out that although filler can improve the ultimate strength of a composite, the elongation at break is hindered. Some authors have used these mechanical properties as a guide to optimize the filler quantity in PEEK[49]. The most common selection however appears to be 10% graphite, 10% PTFE, 10% short carbon fiber. This selection of fillers can reduce sliding friction and promote transfer film formation. However, filled composites can still be vulnerable to failure under adhesive wear conditions. For instance, fretting in wet environments where the formation of protective transfer films may be hindered.

The historical studies of PTFE and PE friction anisotropy greatly accelerated their development as bearing materials. Tanaka in fact observed a similar anisotropy in PEEK and reported this amongst the unsolved problems in polymer tribology[11]. With advancing methods in simulation and spectroscopy further details on the mechanistic origins of friction and wear continue to emerge[50]. A similar type of understanding should be achievable for PAEK by studying its own unique tribological behavior from a material science perspective.

2.2 PEEK Crystal Structure

An important aspect of PAEK material is the crystallinity and morphology achieved during processing. This crystallinity is largely responsible for the outstanding

solvent resistance observed[51]. It has also been reported that crystallinity can enhance the resistance to environmental stress cracking[52] and physical aging[53]. Crystallinity can also impart some mechanical strength[54-56], hardness[14], and improvement in modulus[54-56]. A typical crystallinity for the PEEK member of the PAEK family is 30-40% but will vary with molecular weight M_w[57]. Typically, higher crystallinity X_c% is achieved in samples with lower M_w. Longer chains inhibit chain folding and so lower crystallinity is achieved for higher M_w. Within the PAEK family the crystallinity attained will also vary. Examples of the polymer repeat unit are shown for PEEK and PEK in Figure 2.4. The chemical structure consists of aromatic rings joined by either an ether or ketone linkage. The naming of the PAEK type corresponds to the presences of these ether and ketone linkages. The rigidity imparted by the ketone unit will have some impact on chain mobility. For instance the glass transition T_g increases with the ratio of ketone to ether[58]. The maximum attainable crystallinity is also affected by the flexibility of these repeat units[59]. This means that PEKK materials will likely possess lower crystallinity than PEEK.

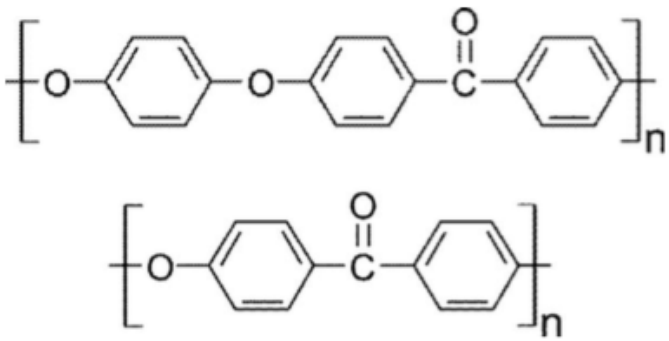

Figure 2.4. Chemical structure of the polymer repeat unit for PEEK and PEK

Upon crystallization, PAEKs adopt an orthorhombic unit cell with a planar zig-zag conformation[60, 61]. Among the types of PAEKs the crystal structure for PEEK is most studied but similar behavior occur amongst all PAEKs. A scheme for the unit cell and morphology of the crystal structure of PEEK is shown in Figure 2.5[62]. It can be seen in the schematic that the polymer backbone lines up with the c axis. During crystallization lamellae stacks are aligned with the b axis in the radial direction. The schematic also shows stacks of crystalline lamellae joined together by an amorphous region. The thickness of the lamellae will depend on thermal history and steric effects. Crystallization results from the folding of polymer chains densely packed bundles. A typical melt crystalized thickness is 5-6nm and corresponds to 10-12 aryl groups[59]. PAEK adopt a self-impinging spherulitic structure and the size of these spherulites depends upon growth kinetics. Typically PEEK spherulites have a diameter of 25-40μm and larger spherulites usually correspond to higher melting temperatures[60].

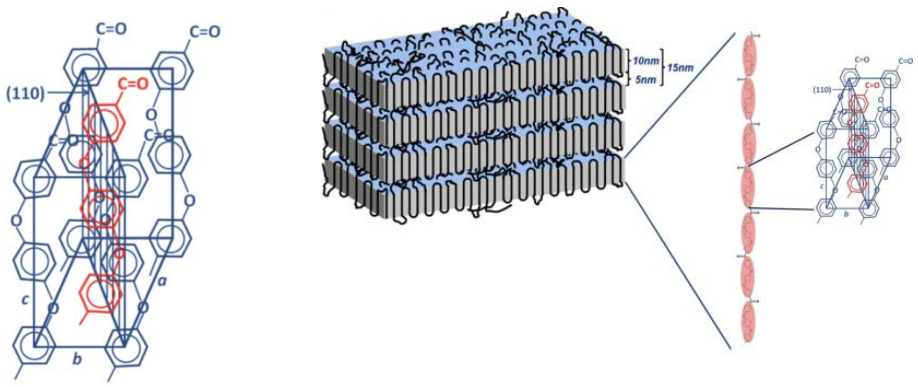

Figure 2.5. Illustration of the crystallographic unit cell and lamellar stack for PEEK.[62] **(Figure reprinted from Jin, L., et al., *Crystallization behavior and morphological characterization of poly (ether ether ketone)*. Polymer, 2014. 55(20): p. 5255-5265**

A number of uncertainties regarding the crystallization behavior of PAEK remain. In particular the double melting phenomenon observed in PEEK lacks fundamental understanding. This double melting refers to the presence of multiple endotherms in the differential scanning calorimetry (DSC) heating traces as shown in Figure 2.6. A popular explanation is the dual lamellar thickness model proposed by Cebe and Hong[63]. In theory two populations of crystals exist and these give rise to discrete melting endotherms. Bassett extrapolated on this theory and proposed less perfect crystalline regions exist between the thicker lamellae[64]. These less perfect crystals result in the lower endotherms. There are a couple of explanations for the nature of these crystalline domains. It is possible that thin lamellae are inserted between two thicker lamellae[65, 66] or the thin lamellae may bundle in stacks between stacks of thicker lamellae[67, 68]. Recent work used a combination of spectroscopy and microscopy techniques to understand this phenomenon[62]. It was suggested that the presence of ordered molecular bundles remain in the melt. These domains act as nuclei and result in the formation of small less perfect spherulites. A flash DSC technique was used to demonstrate the effects of heating rate on double melting[62]. The presence of a single endotherm with flash DSC showed that double melting results from the relatively slow heating imposed by standard DSC. Small angle X-ray spectroscopy (SAXS) was also used to calculate crystallinity based on lamellar thickness. The results produce a linear crystallinity that is nearly twice the bulk crystallinity found with DSC. To resolve the discrepancy a model was proposed in which a perfect crystal structure exists with less perfect structure extending into an amorphous region[62].

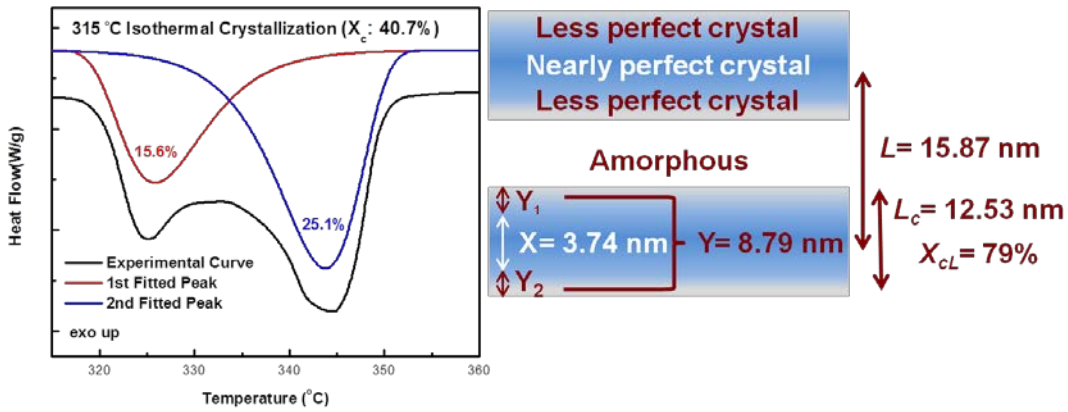

Figure 2.6. Theory regarding the double melting behavior observed in PEEK[62]. **(Figure reprinted from Jin, L., et al., *Crystallization behavior and morphological characterization of poly (ether ether ketone)*. Polymer, 2014. 55(20): p. 5255-5265**

Many uncertainties exist regarding crystallization of PAEK and a wide array of factors will contribute to the crystalline structure and morphology. It can be expected that such factors will play a role in the overall tribological response. For instance, it has been suggested that wear in PEEK increases with increasing spherulite size[10].

2.3 PEEK Structure Property Relations

Changes in a polymer's molecular structure can impact many properties. Commonly, discussion of structure property behavior concerns the mechanical solid-state behavior. With increasing M_w there is often an observed increase in elongation at break and impact strength[58]. Because M_w also affects crystallinity many properties do not change directly. For instance the tensile strength and modulus are slightly higher in lower Mw PEEK due to an increased crystallinity[55]. However, fracture toughness and impact strength will decrease with increased crystallinity[38, 39]. Table 2.1 shows how

increases in parameters for PEEK influences trends in fracture properties[38, 69]. In the melt state the rheological behavior will be affected by changes in the polymer chain structure. For instance, molecular weight M_w and the presence of branching can influence the measured zero shear viscosity[70]. The results indicate that PAEK behave as rigid rods in the melt. Samples exhibiting possible long chain branching also are more susceptible to shear thinning. The thermal stability within the PAEK class of materials will also be influenced by changes in molecular structure[70-72]. It appears that higher Mw and branching can increase the susceptibility to degradation. During degradation in oxygen crosslinks may also form following chain scission events. Most studies regarding such properties are of the PEEK member of the PAEK family but similar trends have been observed in PEK and PEKEKK. Attempts have been made to tailor structure property behavior with various processing methods. Orientation through the use of extrusion or drawing processes has been shown to significantly improve mechanical properties[73-76]. Some annealing treatments have been used to improve thermal stability[77] and the mechanical performance of PEEK composites[78]. This work will hopefully elucidate how tribological behavior depends on differences in structure of PAEKs. Processing conditions and material selections can then be made based on such knowledge.

Table 2.1. Effect of test parameters on fracture behavior of PEEK.

Testing Parameter	Impact Toughness	Fracture K_{IC}	Fatigue Crack Growth
↑ Molecular Weight	↑	↑	↑
↑ Crystallinity	↓	↓	↑
↑ Spherulite Size	-	↓	↓
↑ Aging	↓	-	-
↑ Density	↑	-	-
↑ Loading Rate	-	↓	-
↑ Temperature	-	↑	-

CHAPTER III

MULTIDIRECTIONAL FRETTING AND SLIDING WEAR*

The polyaryletherketone (PAEK) family of thermoplastics is increasingly used in engineering applications that require outstanding tribological properties. Considerable attention has thus been paid to their wear behavior in a number of environments. However, little focus has been given to PAEK response to fretting conditions. Fretting wear results from the repeated slip of mutually loaded contacts. In this study, a custom built multi-axis tribometer is used to replicate fretting of PAEK in a pin on flat configuration. This chapter concerns the experimentation and analysis of a selection of PAEK material in a multidirectional fretting and sliding wear environment.

3.1 Introduction

Fretting is said to occur when mutually loaded contacts move relative to one another with nominally small displacements. The resulting slip between asperities causes cracks to nucleate and grow with repeated motion. Damage may then manifest as fretting wear in which debris are removed from the bulk, or crack propagation through fretting fatigue[79-81]. Often, a particular wear environment is termed to be the result of fretting based solely on the appearance of the worn surfaces in contact. Such a surface is characterized by a “pock marked” or “dented” appearance. Not surprisingly, this post-

---

* This chapter is reprinted from Laux, K.A., et al., *Wear Behavior of Polyaryletherketones Under Multi-directional Sliding and Fretting Conditions.* Tribology Letters, 2015. **58**(3): p. 1-13.with permission from Springer.

hoc assessment method means that a number of parameters are believed to be the underlying cause of fretting. Many theories focus on how the retention of debris within the contact contributes to wear and act as third body abrasives. For instance, the term mutual overlap coefficient (MOC) was coined to describe scenarios in which the displacement amplitude is small enough to cause some portion of the contact to remain covered [82]. However, it has also been shown that this retained debris has the capacity to support the load between contacting bodies thereby mitigating wear. More commonly, studies of fretting involve the relationship between normal load and the critical displacement needed for slip to occur. Much of the pioneering work in fretting was done by Mindlin who derived relationships for stick-slip criteria based on Hertzian contact mechanics and elasticity[83, 84]. For a sphere on flat configuration, the shear stress distribution has a nearly infinite magnitude at the edges of the contact annulus assuming no slip occurs. Within the center of this contact a region termed the stick zone exists. Slip will thus occur when the contact has been displaced a sufficient amount to overcome the shear traction in this stick zone. Mindlin criterion for stick-slip is particularly valuable since it allows prediction of the minimum displacement for slip to occur. This knowledge allows the material response to be mapped in terms of the applied load and displacement [5, 6]. For instance, Vingsbo described fretting in metals as three different regimes that depend upon the applied normal load and the displacement of the contact [4]. With increasing displacement and decreasing load the wear behavior transitions from stick, to mixed and gross slip, until finally wear behavior matches that

of sliding. Wear is said not to occur under pure stick conditions and cracks only begin to nucleate due to slip.

Studies of fretting in metals and methods for design against fretting conditions have persisted for decades[85, 86]. However, application of fretting theories to polymers has been challenging and little fundamental knowledge exists. Interestingly, many early studies of polymer fretting focus on polymer coatings since these often serve as palliatives against fretting of metals[87-91]. The so-called velocity accommodation of polymers is believed to prevent slip conditions from occurring between the metallic components[92]. Attention was also paid to how wear debris generated by polymers may lead to tribo-oxidative wear of metallic counterfaces. For instance, Rabbe observed that debris from Polymethylmethacrylate (PMMA) bone cement used in orthopaedic applications can accelerate corrosion of titanium and steel implants[93]. However, the growing utilization of polymers in a wide variety of engineering applications necessitates study of their own unique response and failure due to fretting. Largely because of their transparent nature, PMMA and epoxy are the most commonly studied polymers under such conditions[94-99]. This transparency has allowed for in-situ observation of the contact area as well as the onset of slip. For these amorphous glassy polymers the standard fretting map technique has been successfully employed using ball on flat reciprocating tests. Chateuminois even found that Mindlin criteria could be used to predict the critical displacement for slip[95]. As might be expected, the transition from stick to slip results in transverse cracking at the contact edges. As Mindlin predicted, the edges of the contact annulus represent the highest region of shear stress

and slip will initiate cracks in this region. This behavior has also been observed in polycarbonate[100] and thermosetting bismaleimide[101].Within the gross slip regime "micro-cracks" and "rolls" are observed in the central portion of the contact and are more difficult to explain[95, 102]. In polymers, third body debris are believed to possess a load sharing capacity and may play a role in the dissipation of frictional energy. Chateuminois in fact found that these "rolls" of compacted debris have a modulus that nearly matches that of the bulk. With increased displacement the size of these "rolls" increases, but the measured fretting wear volume diminishes significantly[99]. A similar description of fretting damage has been applied to non-glassy polymers as well[47, 103]. Guo investigated a selection of polymers using a ball on flat fretting test rig and attempted to link their response to relevant material properties[103]. The observed fretting scars were reported to consist primarily of compacted and possibly melted debris. This led to the conclusion that fretting resistance is fundamentally linked to a polymer's ability to withstand frictional heating.

The polyaryletherketone (PAEK) family of thermoplastics has been increasingly used in such fretting environments, but few studies exist regarding their fretting behavior[47]. These aromatic backboned polymers are named according to the presence of ether and ketone structures in their repeat unit. Common examples include polyetheretherketone (PEEK), polyetherketoneketone (PEKK), and polyetherketone (PEK). The ratio of ketone and ether groups has an effect on chain rigidity and thus the glass transition temperature, T_g, typically increases with increasing ketone to ether ratios. Their semicrystalline nature and high T_g (150-180°C) in fact make them a desirable

bearing material in high temperature and corrosive environments. Laux and Schwartz studied the PEEK member of this family with regard to sliding wear and transfer film formation[21]. It was found that sliding path direction had a substantial influence on both wear behavior and transfer film formation. Entrapped third body debris and cross shear motion are determining factors in the sliding wear of many polymers. In theory, these factors should play a critical role in the fretting of polymers. However, it is difficult to reproduce such an environment with conventional reciprocating fretting rigs. The primary motive of this study is to produce stick-slip and ultimately fretting wear of PAEK material against steel in a pin-on-flat configuration. By controlling the nominal contact pressure and displacement trajectories, a selection of PAEK material will be studied under both multi-directional sliding and fretting environments.

3.2 Materials and Methods

3.2.1 Material

Six samples of commercially available PAEK material were used in this work and are listed in Table 3.1 along with relevant material properties. Within this selection, three PEEK materials from a single supplier were selected and are differentiated by their molecular weight, M_w. These PEEK grades are labeled A, B, and C in order of high to low M_w. Gel permeation chromatography (GPC) was used to confirm this trend for the PEEK samples and values are listed in Table 3.1 along with data for the other three PAEK samples. Samples were injection molded under controlled conditions described in previous work[21] and then machined into 6.35mm diameter pins for wear testing. Samples were also molded into bars for dynamic mechanical analysis and tensile testing.

Additionally, differential scanning calorimetry (DSC) was used to assess the degree of crystallinity for all material in this study. The percent crystallinity ($\%X_c$) was determined using the ratio of first heat melting enthalpy (ΔH_m) to the enthalpy of fusion for a perfect crystal (130 J/g)[104]. As the data shows, lower M_w PEEK typically achieves higher degrees of crystallinity compared to higher M_w PEEK under the same conditions. The increasing M_w slows down chain folding and thus lower crystallinities are commonly observed. Similarly the more sterically hindered PEKK is considerably more amorphous than PEK, PEEK, or PEKEKK. The T_g values for all samples are also reported in Table 3.1. Using dynamic mechanical analysis (DMA) T_g is located by the peak value of tan δ. Testing was performed in torsional shear mode (TA Instruments, ARES-G2). Injection molded samples were machined to dimensions of 40 x 11.5 x 3.3 mm in accordance with ASTM D790 [105]. A temperature sweep was performed with a ramp rate of 3°C/minute between 25 and 300°C. During the test, a 0.05% strain was applied with a loading frequency of 1 Hz. Tensile tests were also performed in accordance with standard ASTM D638 using type V tensile specimens. These samples were machined from injection molded stock pieces as described in ISO standard 2818. The averaged values for tensile modulus (E) elongation at break (ε) and ultimate tensile strength (σ) from four tests are given in Table 1. These tabulated results are not intended to represent a comprehensive review of all PAEK material properties, but rather to serve as a guide in understanding the results presented in this work.

Table 3.2. Compilation of material properties (molecular weight M_w, glass transition temperature T_g, crystallinity $\%X_c$) and mechanical properties (tensile modulus E, elongation at break ε, and ultimate tensile strength σ) for all PAEK used in this study.

Sample	Mw	T_g[℃]	$\%X_c$	Tensile Modulus E (GPa)	%Elongation ε	Tensile Strength σ (MPa)
PEKK	106,742	158	10	3.3	98	87
PEKEKK	66,019	176	38	4.1	22	95
PEK	100,125	167	46	4.3	12	96
PEEK-A	122,323	159	32	3.7	71	91
PEEK-B	114,362	158	42	3.8	51	82
PEEK-C	66,200	160	48	3.7	18	85

3.2.2 Sliding Wear

Typically, the study of sliding and fretting wear requires the use of separate tribometers that are specially suited for the particular type of wear in question. Sliding wear is accomplished by having the counterface continuously move relative to the normally loaded sample surface. This is often done using a pin-on-disc or block-on-ring configuration where the counterface (disc/ring) rotates and the sample (pin/block) remains fixed. Although some debris is inevitably trapped between the sample and counterface, sliding allows most debris to be expelled. This means that a fresh pin surface is constantly moving across counterface asperities. For PAEK polymers, this also means the dominant mechanism for debris removal is abrasion as hard rough asperities penetrate the softer bulk. Adhesion and fatigue mechanisms may also manifest, but are often the result of some surface plasticization. For instance, Omar demonstrated that

adhesive-fatigue wear could be promoted during sliding wear of polymers through the introduction of solvents at the wear interface[37]. In this work, the dry sliding wear of PAEK is studied using a multi-directional tribometer described by Laux and Schwartz[20, 21]. This two-axis tribometer employs two programmable linear stages (Aerotech) to move the counterface in a desired path and at a specified velocity. As the PAEK sample pins are pneumatically loaded against the planar counterface, wear is generated from their relative motion. Multi-directional refers to the motion of the sample pin with relation to the counterface asperities. The hardened (HRC 60) D2 tool steel counterfaces used in this experiment are directionally ground to a surface roughness of 0.5μm Ra. Because the surface is ground in a single direction, a circular sliding path will generate a continuously changing shear direction and thus multi-directional wear. The resulting anisotropy in the surface roughness is shown in Figure 3.1. As depicted in the profilometer traces, taller and more distant asperity peaks appear when roughness is measured perpendicular to the grinding direction. The direction of sliding relative to these asperity peaks was previously found to greatly impact how PEEK transfer films form[20, 21]. Thick transfer films are found on portions of the wear path associated with perpendicular sliding and are mostly absent when sliding parallel to the grinding direction. The presence and quality of these films was found to correlate with wear resistance[21]. The resulting cross shearing of the pin surface will also disrupt the strain hardening in the direction of motion seen for unidirectional sliding tests. For linear polymers like PTFE[106, 107] and UHMWPE[8] motion that disrupts any natural orientation will result in increased wear. The process of transfer film formation in PEEK

may lead to similar orientation phenomena. Using previous work with PEEK as a benchmark[21], sliding wear of PAEK samples will be studied with 5 MPa of nominal contact pressure. For the 6.35mm diameter pins used in this study, a normal load of 157N is used to achieve this pressure. A circular wear path with a 20mm diameter and constant sliding velocity of 200 mm/s will be used for each test. To ensure a measurable quantity of debris is generated, each test is run for 2km of sliding distance. Before each test, samples are finished to a roughness of approximately 0.2µm R_a and are ultrasonically cleaned and dried before and after each test. The volumetric wear (mm^3) is measured by weighing the samples before and after each test using a precision balance with 0.01mg resolution.

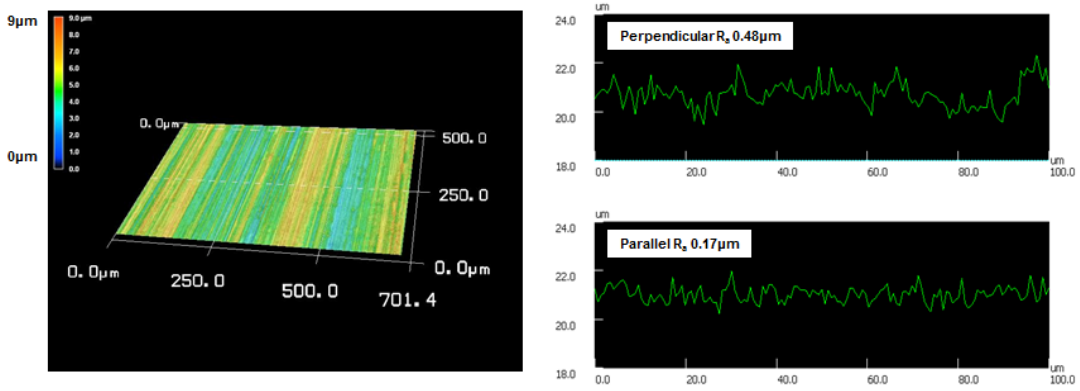

Figure 3.1. Profilometer 3D image of ground counterfaces and linear roughness measurements taken perpendicular and parallel to the direction of surface grinding.

3.2.3 Fretting Wear

Unlike sliding wear in which mutually loaded surfaces continuously move past each other, fretting is characterized by intermittent sticking and slipping of the two

surfaces. In order to produce such an environment, sufficiently high contact pressures are needed to create adhesive sticking. Additionally, one surface must move a distance great enough to break this contact before re-sticking with the adjoining surface. A ball on flat configuration is often preferred because Hertzian contact can produce such pressures with modest normal loads. As discussed earlier, this also allows for prediction of the critical displacement δ necessary for slip to occur. In nominally flat rough contact however, sticking occurs between a number of asperities of varying height and geometry. This means that a distribution of displacements is needed to describe the onset of slip within the region of contact. The displacement of these adhesive contacts will also depend on the applied normal load as well as the dynamic stiffness of the fretting rig. Friction profiles, also sometimes called friction loops, are a popular method used to map the relation between normal load and displacement for the experimental setup in question. For the 6.35mm diameter pin on flat configuration in this study, a nominal pressure of 50MPa was chosen which requires a normal load of 1570N. To determine the necessary displacement needed for slip a series of friction profiles were produced as shown in Figure 3.2. The frictional data is acquired by loading PAEK pins against the directionally ground counterfaces and reciprocating the stage at 1Hz in a single direction. The motion profile of the stage is sinusoidal without any dwell between start and stop. Since the counterface is mounted directly to a 3-axis load cell (Interface), frictional forces can be assigned to movement across or parallel to the surface roughness direction. The data in Figure 3.2A-D shows the frictional force from movement perpendicular to the counteface asperities using a data collection rate of 250Hz.

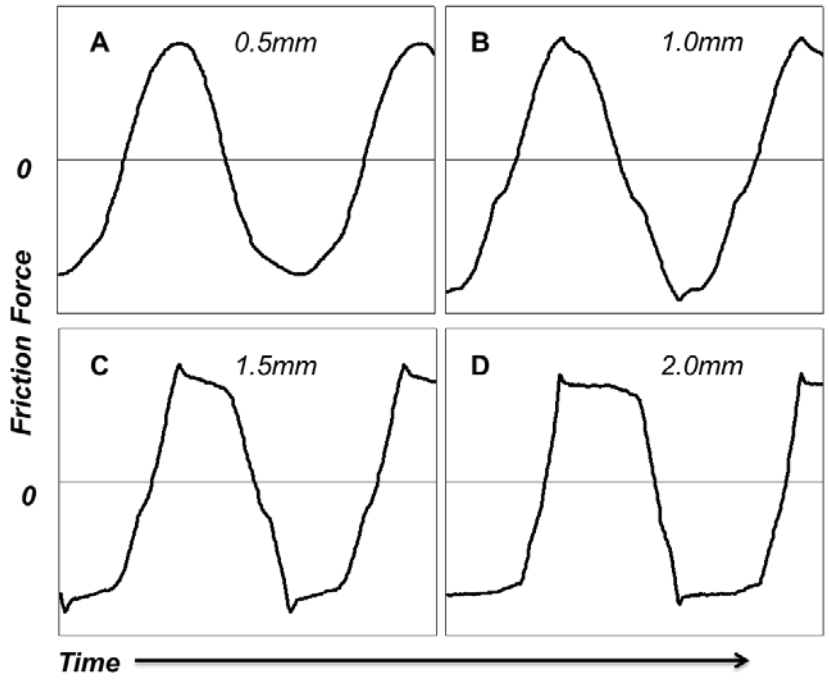

Figure 3.2. Friction profiles for PAEK pin under 50MPa of contact pressure and reciprocating perpendicular to the counterface surface roughness at 1Hz for displacements 0.5 to 2mm.

The above friction profiles indicate that at some point between 1 and 2mm of imposed displacement Δ, the local contact is able to move a sufficient distance δ to unstick asperities. In the friction profile for 0.5mm for instance, the friction force is sinusoidal and almost perfectly matches the motion profile programmed to the robotic stage. As the displacement Δ increases to 1mm, deviations in the friction profile occur at various points. The friction profile depends on the local strength of asperity contacts, but also the stiffness of the sample holder, pneumatic piston, and structure of the test rig. The deviations in the profile can be said to represent the contribution of these components to the overall stiffness of the experimental setup. As the displacement is

increased to 1.5mm and 2mm the friction profile appears flatter indicating a possible transition from mixed slip to gross slip or even sliding. It should be noted that in many fretting studies, the transition from stick to slip occurs in the micrometer range of displacement Δ. However, these studies are predominately for metal on metal fretting and use inherently stiffer loading setups such as lap-joints. Although the data in Figure 3.2 represents friction force for a single displacement direction, the same transitions were observed for both robotic stage axes, referred to as X and Y. Likewise, the surface roughness direction and PAEK type were found to give similar behaviors. As mentioned in the introduction, the viscoelastic nature of polymers presents some complications in discussing the contact mechanics involved in fretting. Polymers will undergo frictional softening over the course of an experiment and the mechanical response of the surface will change as well. A softer more compliant polymer surface will mean greater deformation by counterface asperities and an increase in the real contact area. This real contact area is sometimes called a multi-contact interface (MCI). In polymer fretting, the size of these contact patches will determine the static friction and ultimately the shear stresses generated when these contacts are broken. This growth in friction with repeated sticking and slipping of surfaces is demonstrated in Figure 3.3. A sample of PAEK is loaded at 50MPa and reciprocated across the surface roughness direction a displacement of 2mm and frequency of 10Hz. The motion profile has the same sinusoidal shape used for data in Figure 3.2. Initially the frictional force is small and marked by erratic spikes in the friction profile. After about 1000 cycles this friction force grows and an apparent steady state behavior is reached. The highlighted sections of the plot show that with

increasing cycles the friction response becomes more sinusoidal with fewer spikes. Either through an increase in contact area or a change in the elasticity of the contact surface, slip appears to become more difficult.

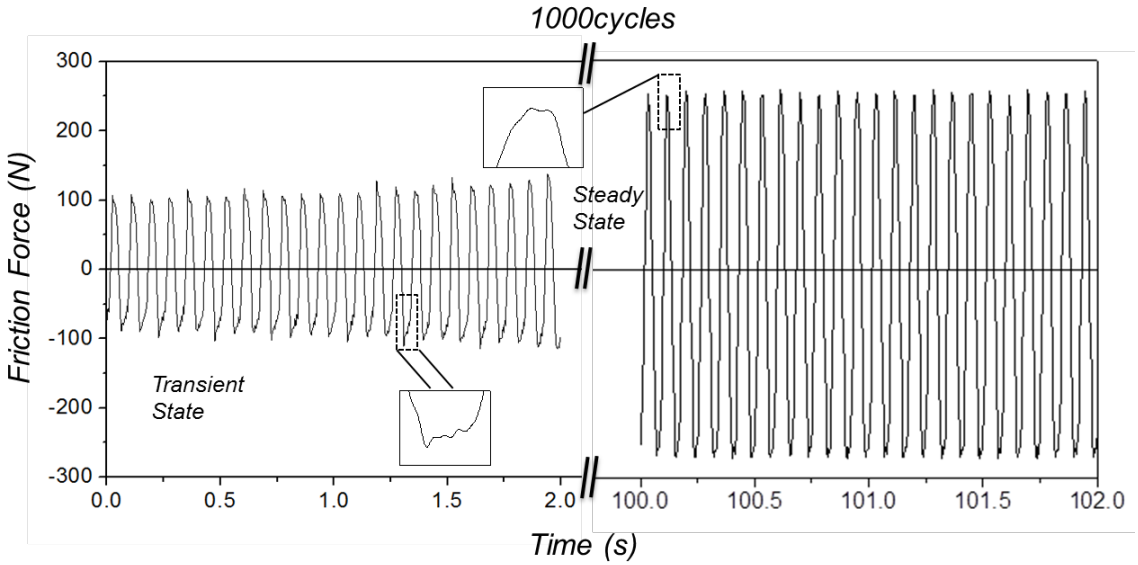

Figure 3.3. Friction force for PAEK pin under 50MPa of contact pressure reciprocating perpendicular to the counterface surface roughness at 10Hz for a displacement of 2mm.

Using knowledge gained from these preliminary studies, a computer program was written to produce a multidirectional fretting environment. Similar to the multidirectional motion for sliding wear, it is desired to have repeated cross shear of the PAEK surface across the counterface asperities. The test program moves the robotic stages through a series of 10,000 random XY data points. These data points are confined to a 2mm by 2mm space so some portion of the 6.35mm diameter pin remains continuously covered. Additionally, these random data points were chosen to have point-to-point displacement trajectories between 0.1 and 2mm with a mean value of 1mm.

Because only displacements exceeding 1mm will break the adhesive contacts, slip will occur at intermittent times and directions during the course of a test. An initial test run confirmed this desired result and it was observed that following a short transient period, slip began as indicated by a loud popping noise. To produce a comparative set of wear data for the previously listed PAEK materials, tests were run for 500,000 point to point moves. Although a frequency cannot be assigned to randomized movement, the test program completes on average 15 moves per second.

3.3 Results

3.3.1 Wear

The measured volumetric wear from the multidirectional sliding and fretting experiments are plotted in Figures 3.4 and 3.5. Under 5MPa of nominal contact pressure and 200 mm/s continuous sliding for 2km, the high M_w PEEK-A appears to have the lowest wear of all samples. As found in previous studies, a dramatic increase in wear corresponds to a decrease in M_w for PEEK. In accordance with this, lower M_w PEEK-C has a near order of magnitude greater wear than PEEK-A. The median M_w of these samples PEEK-B has wear performance between the high and low M_w samples. Amongst the other grades of PAEK, the PEK, PEKK, and PEKEKK material all have very similar performance with that of PEEK-B. In fact, Tukey t-test suggests wear behavior of these four materials are statistically indistinguishable ($p<0.05$). Although PEKK has slightly higher wear amongst this group, the result is interesting given that these materials all differ in chemical structure and mechanical properties. It should also be pointed out that transfer film formation occurred for all samples studied. The quality

of transfer film does not differ between PAEK types and is likely not the differentiating factor in wear behavior.

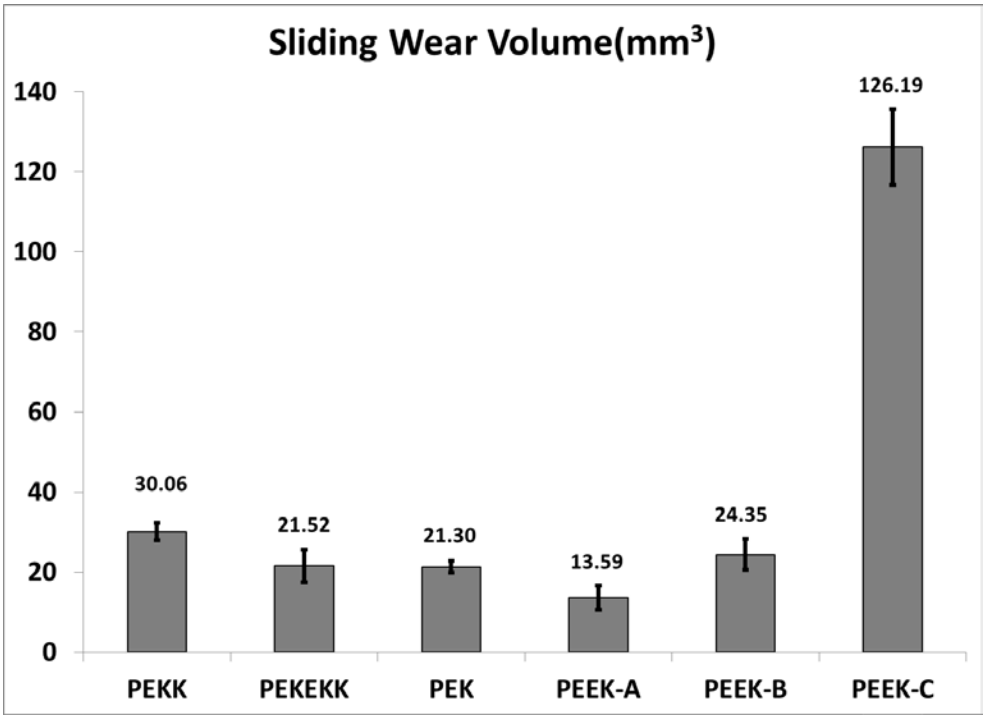

Figure 3.4. Wear results for the various PAEK materials after 2 km sliding distance under nominal contact pressure of 5.0 MPa. The bars indicate the size of standard error of the means (n=4).

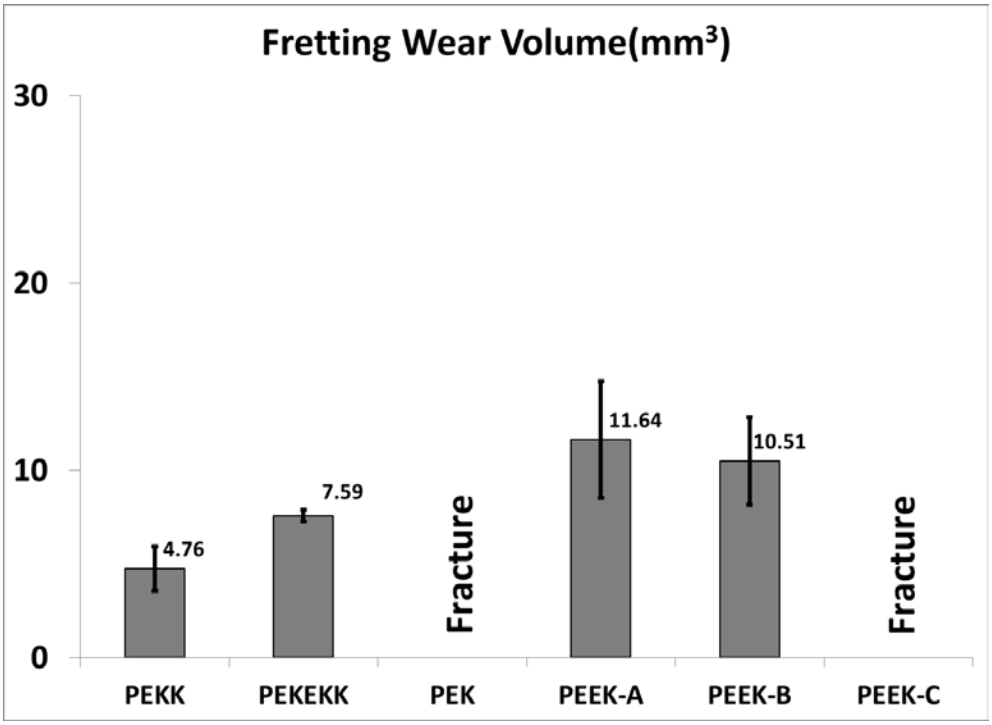

Figure 3.5. Wear results for the various PAEK materials after 500,000 point to point movements under nominal contact pressure of 50 MPa. The bars indicate the size of standard error of the means (n=4).

The results for the 50MPa multidirectional fretting shown in Figure 3.5 exhibit much different trends than that of the sliding wear. Most surprising is the behavior of PEK and low M_w PEEK-C which fractured before completing the entire 500,000 point-to-point movements. In fact, for both samples fracture was observed within the first 50,000 moves and the tests were stopped at this point. The other four samples that completed the entire 500,000 moves do not fracture, but the central region of the pin contains a large crater from where debris has been removed. Though some wear debris was expelled to the periphery, most debris is contained within this wear crater. The measured weight loss indicates some interesting trends in the volume of material removed. Comparing the high and moderate M_w PEEK for instance shows near identical

weight loss. This is surprising considering PEEK-B generated nearly twice the amount of wear as PEEK-A during sliding wear. Similarly, the PEKK and PEKEKK materials were the best performing samples in the fretting environment but exhibited only moderate sliding wear resistance. Comparison of these two data sets points to the notion that different mechanisms are responsible for the resulting behaviors. For instance, Omar suggests that in polymers abrasive wear is determined largely by fracture toughness K_{1C} and adhesive-fatigue wear depends on crack growth parameters[37].

3.3.2 Fretting Wear Surface

Figure 3.6 shows the selected images of fretting wear surfaces for the PAEK material used in the experiment. Using a violet laser confocal microscope (LCM) a number of images of the surface are first taken at 10X magnification and later stitched together using accompanying software to produce the fully assembled images below. As discussed earlier, distinct differences in sample behavior are apparent between the six PAEK materials. The most apparent features are the cracks emanating from the surface in the PEK and low M_w PEEK-C samples. These cracks propagate into the bulk of the material resulting in fracture. Though the exact start point cannot be determined, it appears that these cracks originate from the surface interior and propagate outwards. This central portion of the pin also has a melted appearance suggesting that frictional softening may play a role in the origin of these cracks. As mentioned earlier, some samples also develop a crater in the center of the pin in which wear debris collects. This behavior is found in the PEEK-A and PEEK-B material as well as PEKK and PEKEKK. However, just as the measured wear volume differs within this group the depth of the

crater seems to vary as well. The LCM is also equipped with profilometry software and allows measurement of the wear surfaces. Observation of these craters indicates that the PEEK samples are both deeper and have a larger volume than the PEKK and PEKEKK samples. Considering the measured weight loss follows the same trend, it can be presumed that most fretting wear debris is generated in the formation of these craters. There also appears to be some differences in the shape of craters found in PEKK and PEKEKK compared to the PEEK samples. In PEEK-A and PEEK-B the crater is mostly circular in shape and is deeper towards the sample center. However, both PEKK and PEKEKK samples develop shallower craters with a more oblong shape. The shape of this region also indicates that these craters had formed from cracks propagating in some preferred direction. It should be noted that flat contact between the sample and counterface was checked prior to each test so the influence of eccentric loading on wear was minimized. A possible explanation may be due to the direction of counterface surface asperities relative to sample movement. The counterfaces were ground so roughness was oriented in a single direction. Although slip occurs with motion both parallel and perpendicular to these asperities, the magnitude of surface shear forces generated likely differs. It can be presumed that the static friction forces are greater for slip perpendicular to the counterface asperities than parallel. This difference in static friction may attribute to how cracks form, propagate and eventually form craters on the PAEK surface. Visual observation of the worn sample surfaces indicates that fretting wear of PAEK depends largely on how surface cracks form and grow as the result of the mixed and gross slip condition.

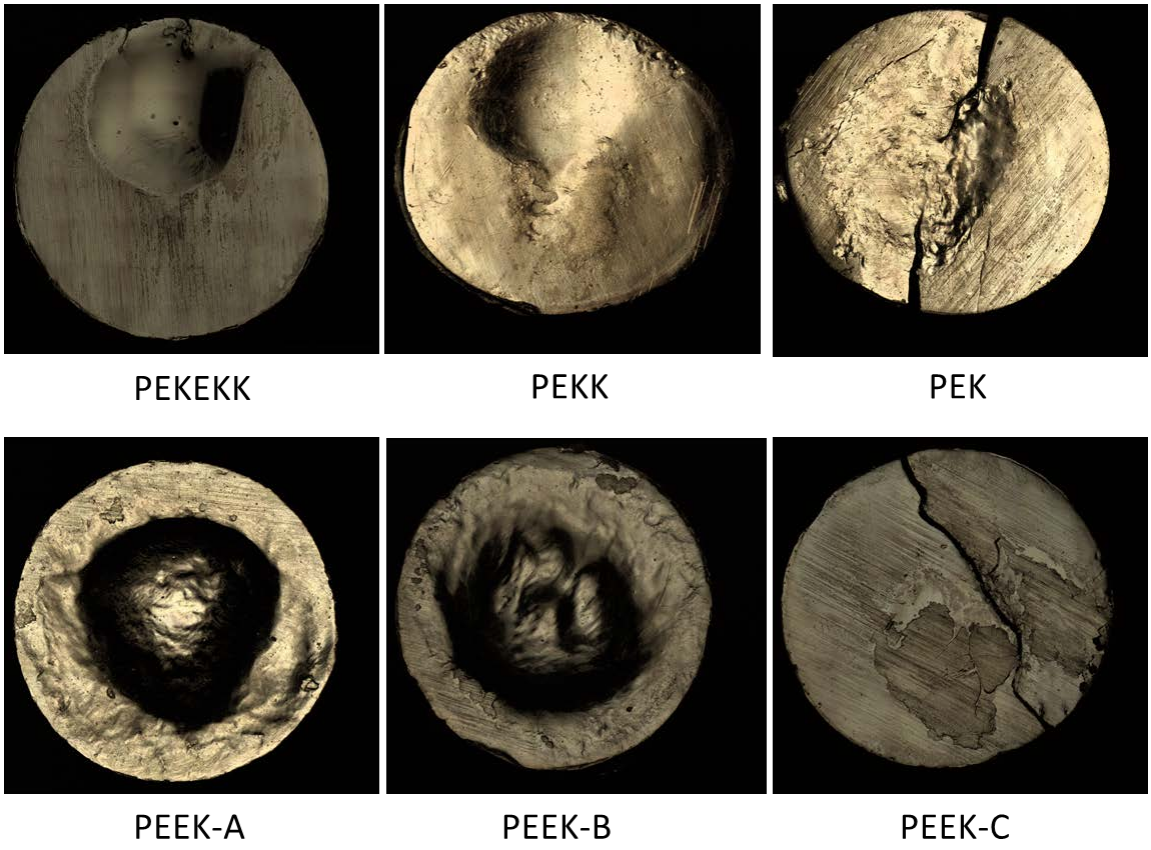

Figure 3.6. Assembled LCM images of PAEK pin surfaces after being tested under fretting conditions.

3.4 Discussion

In examining both the sliding and fretting wear data many possible explanations for material performance emerge that cannot be linked to a single material property. Wear in polymers depends largely on the contributions of abrasive, adhesive, and fatigue mechanisms. Abrasive wear results from the removal of debris from the bulk via penetration and cutting by hard rough asperities. In theory then, a material with greater toughness, tensile strength and elongation at break should be more resistant to abrasive wear. Adhesive and fatigue wear are often discussed together since surface damage

induced by adhesion often begets cracks that grow through fatigue. Adhesive wear can be imagined as occurring when junctions form between surface asperities and subsequently rupture during contact shearing. Additionally, fatigue wear is generated as the result of subsurface cracks that grow through repeated impact by counterface asperities. These simplified views of wear processes offer insight into how a material might behave in a specific wear environment. However, linking specific material properties to observed wear performance still remains a challenge. For instance, PEK and low M_w PEEK-C have similar tensile stress and strain behavior shown in Table 3.1, but their sliding wear performance differs by an order of magnitude. In fact the material demonstrating the greatest sliding wear resistance, high M_w PEEK-A, does not stand out amongst any of the tabulated mechanical properties. Studies of the wear of PEEK have suggested that M_w may play an important role in determining wear behavior[10, 20]. It was hypothesized that increased M_w increases the number of entanglements and interspherulitic links that resist the removal of debris from the bulk. Smaller spherulite size has been found to accompany improved wear resistance in many semicrystalline polymers[108]. However, most studies focus on pin on disc sliding wear and it is likely that the same material property correlations cannot be applied to fretting or adhesive-fatigue wear. For instance, PEEK-A was found to be superior during sliding wear tests but behaved similarly or worse than other PAEK material during fretting.

To better understand wear behavior in PAEKs there is a need to link structure-property relationships to underlying wear mechanisms. Differences in underlying mechanisms responsible for abrasive, adhesive, and fatigue wear are evident in the

experimental result that sliding wear resistance does not correspond to fretting wear resistance. To explain the observed fretting behavior for the PAEK material studied in this work the separate components leading to fretting wear must be further elucidated. It is believed that fretting results from the repeated sticking and slipping of mutually loaded surfaces. The loading and unloading of asperity contacts will initiate cracks that grow with repeated traversals. These cracks may lead to sample fracture or the formation of fretting debris depending on the resulting surface stress. In isotropic elastic solids, surface material strength (σ) can be linked to the sample modulus (E) and the imparted strain (ε). However, for viscoelastic polymeric material the bulk properties at the surface change as a function of time and temperature. This nonlinear stress-strain relationship renders predictive equations based on loading and displacement invalid. Furthermore, most studies of fretting in polymers have suggested frictional softening[103] and third body debris accumulation[99] is the determining factor in polymer fretting performance. These conclusions are supported by the observation that polymer fretting surfaces often consist of rolls of compacted or melted debris [95]. Although the fretting surfaces in Figure 6 show signs of melting, the overriding surface features are cracks and craters. Discussion of this observed fretting response should thus focus on how frictional softening may lead to sticking and slipping of contacts and how this ultimately produces surface cracks under the ascribed conditions.

As discussed in the introduction, the fretting experiment was designed to create intermittent multidirectional slip. Because polymers have the capacity to exhibit strain hardening through chain orientation, cross shear motion is believed to be a more severe

wear environment than linear reciprocation. Additionally, polymers are sometimes viewed as fretting resistant due to their viscoelastic response to surface traction called velocity accommodation[92]. To create intermittent multidirectional slip, the test program used in this study consisted of random point-to-point XY movements. Since only some of the resulting displacements are large enough to cause slip, the adhesive contacts are broken at random intervals. During experiments, this phenomenon is believed to have caused the reported sporadic popping noise. The velocity accommodation observed in linear reciprocation is also possibly prevented since the polymer chains cannot orient in some preferred direction. The periods of stick between slip events also may allow for the growth of asperity contacts. The static coefficient of friction depends largely on the real area of contact between surface asperities. Fundamental research in the origins of static friction has shown that asperity contacts can grow over time through creep[109]. This is sometimes called physical contact aging. In theory, the static or break loose friction will increase exponentially with time from when an adhesive contact was formed. The brief pauses between slip displacements would thus create greater static friction than would be seen in a continuous reciprocating motion. To better demonstrate this, additional linear reciprocating tests were conducted using PEK and PEEK-C. Both of these materials fractured prior to completing the 500,000 point-to-point motions in the multidirectional fretting experiment. Samples were loaded with 50 MPa of nominal contact pressure and reciprocated perpendicular to surface roughness at 10Hz as shown in Figures 1 and 2. Tests were conducted with displacements between 1 and 2mm and run for 500,000 cycles. Interestingly, neither

fracture nor audible slip occurred during any of these tests. Figure 3.7 shows the resulting surface for PEK from tests done with a displacement of 2mm. Although catastrophic failure does not occur, surface cracks are seen at the edges of a central frictionally softened region. This central region also appears striated as if it had been stretched in the reciprocation direction. Such a phenomenon is similar to the roll formation and velocity accommodation often reported in polymer fretting. These phenomenological results do not prove chain orientation or contact aging occur. However it does support the notion that intermittent multidirectional fretting presents a more severe fretting environment than linear reciprocation. Future studies on the origins of static friction in PAEK metal contact will be done and should be helpful in discussion of polymer fretting.

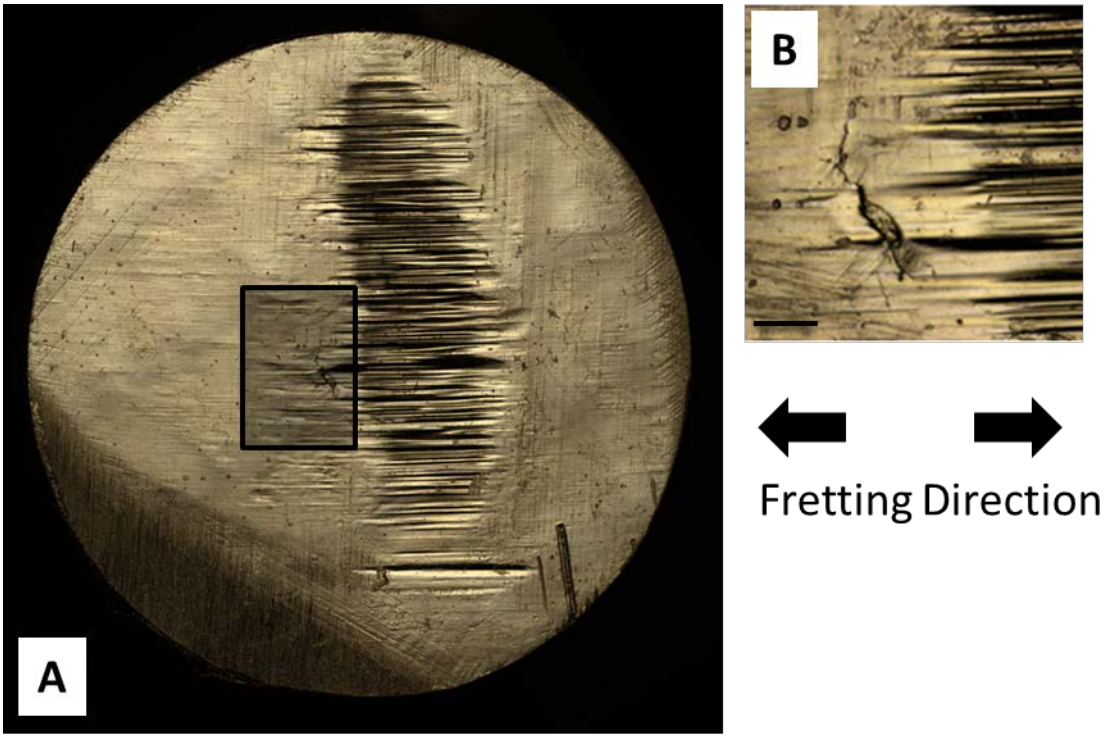

Figure 3.7. Assembled LCM image of PEK pin loaded under 50MPa contact pressure reciprocating 2mm at frequency 10Hz for 500,000 cycles. B) Magnified LCM image of the highlighted section of the pin. Scale bar 100μm.

Another phenomenon worth further investigation is the role entrapped third bodies have in fretting tests. In both the multidirectional tests in Figure 3.6 and the reciprocating tests in Figure 3.7, most debris was found adhered to the pin surface at the end of each experiment. As mentioned earlier, the displacements used were chosen to create intermittent multidirectional slip. These displacements were also confined to a 2mm by 2mm space so some portion of the 6.35mm diameter pin remains constantly covered. This overlap region will in theory be more affected by frictional heating and slip will mostly take place here. Observation that surface cracks and craters originate in the center of the pin supports this theory. It was also found that slip did not occur

immediately and required several thousand displacements until slip was audibly detected. It is likely that frictional softening promotes greater adhesion between the pin and counterface and the shearing of these adhesive contacts causes slip. However, it cannot be determined if frictional softening results from melting or merely increased surface plasticity. The surface temperatures achieved during wear remains an unanswered question in polymer tribology largely due to the difficulty of in-situ measurement. Zhang et al. studied the surfaces and debris formed during sliding wear of PEEK using differential scanning calorimetry (DSC)[34]. Their belief was that surface temperatures ranged 300-345°C based on the location of endotherms in the first heating trace of samples taken from the wear surface. Additionally, they report the appearance of a cold crystallization exotherm in the debris heating trace. This implies debris is formed and ejected from the bulk in a molten state and flash cooled. Similarly, PAEK debris collected from both the fretting and sliding wear tests in this experiment was studied using a TA Instruments Q20 DSC. Samples were heated from 30°C to 400°C at 10°C/min with nitrogen flowing at 50 ml/min. Figure 8 shows the first heating traces for sliding and fretting debris obtained from PEEK-A and PEEK-B along with a reference cut from the respective sample pin. In line with the result obtained by Zhang, both sliding and fretting samples exhibit a cold crystallization exotherm around 150°C. Furthermore, the melting endotherm for sliding and fretting debris shifts to a higher temperature nearly 15°C above that of the reference and broadens considerably. Zhang related this shift and broadening of endotherms to the reorganization and thickening of lamellae that takes place when PEEK is annealed at temperatures above 300°C[34]. It is

quite possible then that the wear surfaces reach temperatures where the material behaves in a rubbery state. For fretting, a more compliant surface would enable greater adhesion to the counterface and thus greater static friction forces. These features are seen in the first heating traces of all PAEK samples studied in this experiment with the exception of PEKK. The debris from the more amorphous PEKK material does not exhibit the cold crystallization peak seen in other samples. Additionally multiple melting endotherms appear between 300°C and 350°C. Unlike PEEK however, the crystallization kinetics of PEKK are much less understood so further analysis of this material is difficult.

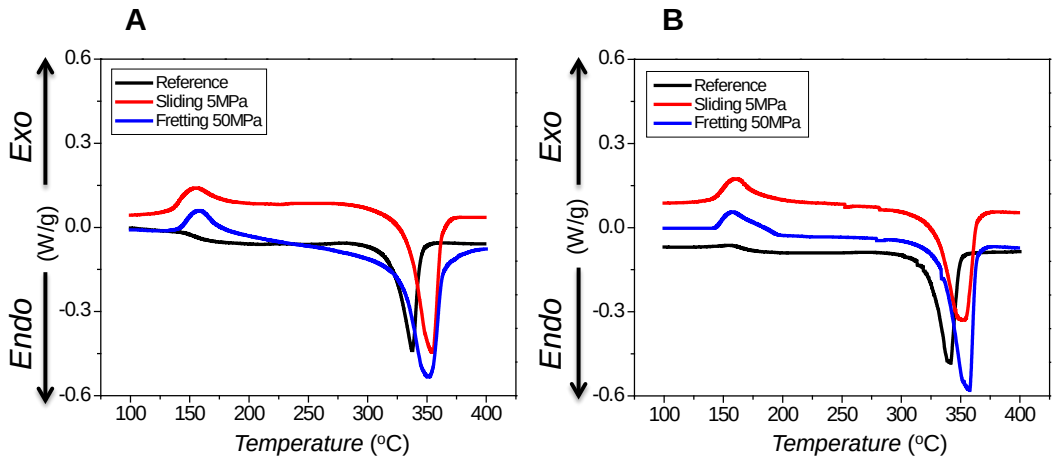

Figure 3.8. DSC first heating trace of sliding and fretting wear debris for A)PEEK-A B)PEEK-B

It should also be noted that the areas of the first heat melting endotherms increase significantly for debris from both sliding and fretting experiments. In fact for the PEEK samples in Figure 3.8, the endotherm areas imply that debris has crystallinity in excess of 50%. In light of most all PEEK crystallization studies this should not be possible.

Rather, the measured heat of melting ΔH_m likely also reflects the presence of residual stress in the crystalline phase imparted by the wear process. This behavior is commonly seen in equal channel angular extrusion (ECAE) of polymers such as polyethylene terephthalate (PET)[110]. To better understand this, samples were also analyzed with X-Ray diffraction (XRD). A Bruker D8 Discover powder XRD with a copper X-ray source was used for Bragg angles between 5 and 40 degrees. Figure 3.9 shows the measured intensity plotted with respect to Bragg angle for PEEK-A and PEEK-B. The unworn reference samples show typical prominent peaks at 19 and 23 degrees along with four additional smaller peaks[111]. However, in both the sliding and fretting debris there is a drastic change in the nature of the XRD profiles. The sliding wear debris exhibits a loss of nearly all peaks with the exception of the 19-degree peak associated with the 110 crystallographic plane. Fretting debris however appears to lose all previous peaks and a new peak appears around 30 degrees in both PEEK samples. In fretting and sliding, debris appears to be largely amorphous. The increased heat of melting in DSC studies is then likely due to residual stress and not increased crystallinity. Additionally, the sharpness and location of the new peak in the fretting debris suggests inorganic material from the metal counterface. This implies that during fretting, adhesion between the two surfaces is strong enough to actually remove fragments from the counterface. There may also be some contribution from chain scission events. For polyamide it has been found that third body debris experiences a reduction in molecular weight M_W. Marcellan studied the debris formed from reciprocating ball on flat tests using DSC and size exclusion chromatography[29]. Contrary to the changes in Figure 3.8, they observe a

reduction in both the melting temperature and heat of melting ΔH_m. This change was found to be due to a reduction in M_W and the same features are observed in the second heating trace. However, the second heating trace for the measured debris in Figure 3.8 closely matches the unworn reference. This indicates that the observed features are the result of some reversible process. It is believed that during wear of PEEK, such chain scission events are likely to result in oxidative crosslinking rather than a reduction in M_W[32, 34]. Further quantitative studies of PEEK wear debris would further help in understanding the exact tribochemistry.

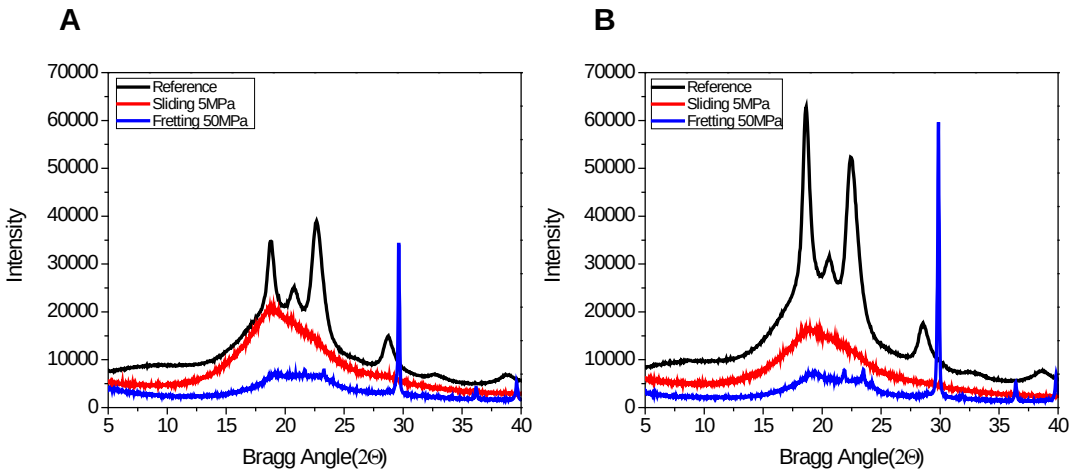

Figure 3.9. Powder X-ray Diffraction spectra of sliding and fretting wear debris for A) PEEK-A and B) PEEK-B

The final discussion point is to probe the role fracture mechanisms may play in the fretting failure of PAEK. Microstructure will play a role in the fracture and fatigue behavior of PAEK and similar mechanisms may explain the observed differences in

fretting behavior. For instance, the clear distinction between the fractured surface observed in low M_W PEEK-C and the cratered surface found in higher M_W PEEK-A and PEEK-B. Chu and Schultz found that for PEEK, the M_W has a strong influence on both microstructure and fracture[39]. Lower M_W PEEK was found to form larger spherulites and in turn suffers from decreased fracture toughness K_{1C}. This behavior was attributed to increased intraspherulitic fracture mechanisms that arise in lower M_W PEEK compared to mostly interspherulitic fracture in high M_W PEEK. Additionally, Saib studied the fatigue behavior of PEEK and observed a strong correlation between crack growth and the M_W, crystallinity, and tie chain density[38]. In particular, the lower M_W PEEK exhibited unstable crack growth compared to the Paris law type stable crack growth in the higher M_W PEEK. During fretting experiments, mixed and gross slip events are believed to lead the nucleation and growth of cracks, which should then strongly depend on microstructure. The fractured fretting surface seen in PEEK-C is indicative of unstable crack growth and propagation perpendicular to the wear surface. However, PEEK-A and PEEK-B may possess crack arresting mechanisms that are not present in PEEK-C and thus do not fail in a catastrophic manner. A similar explanation may also apply to the other PAEK material studied, but better knowledge of the relationship between failure mode and microstructure is needed.

The fracture mechanisms that occur during fretting may also be related to the apparent frictional softening that takes place on the pin surface. For instance, the fractures observed in PEK appear to originate from a melted interior region. In metals, fretting is often discussed in terms of oxidation or other tribological transformations that

lower fatigue resistance and lead to fracture. Though different transformations would take place in polymers, crack growth would be strongly influenced by the material properties at the surface. A melted interior region would in theory weaken the material and would have a diminished capacity to resist crack growth. It is also possible that material transformation may take place that improves fretting resistance. As discussed earlier, the PEKK wear debris differs from other PAEK material in its DSC heating trace. The mostly amorphous PEKK seems to undergo some friction induced crystallization not observed in other PAEKs. In-situ crystallization has been shown to improve the wear behavior of amorphous PEEK films[112] and a similar phenomenon could occur in fretting of PEKK. Because the PEKK samples are mostly amorphous, they appear transparent and can thus be easily studied under optical microscopy as shown in Figure 3.10. Samples of PEKK were tested for 50,000 point-to-point fretting movements so as to prevent material removal from the surface. In fact all PAEK samples exhibit a darkened thermal mound in the pin center during the early stages of fretting. Interrupting the test prior to the formation of debris craters allows for observation of possible subsurface transformations prior to crack growth. PEKK samples were sectioned parallel and perpendicular to this thermal mound as shown in Figure 3.10C. Using an Olympus BX60 optical microscope, samples were studied under cross polarization. Figure 3.10A shows the darkened tribologically transformed region that appears on the PEKK surface interior. When the sample is sectioned and polished perpendicular to this thermal mound, as in Figure 3.10B, the tribologically transformed material extends well below the surface. Even more interesting is the observation of a

roughly 100μm thick transition region separating the bulk sample from the thermal mound. Through frictional heating or possibly some strain-induced mechanism, PEKK undergoes an observable material transformation during fretting tests. Although this transformation cannot be linked directly to improved crack resistance, the PEKK samples outperform all other PAEK material during fretting tests. Additional energy dissipative mechanism may exist in PEKK or PEKEKK that explain their superior fretting performance and will be worth further investigation.

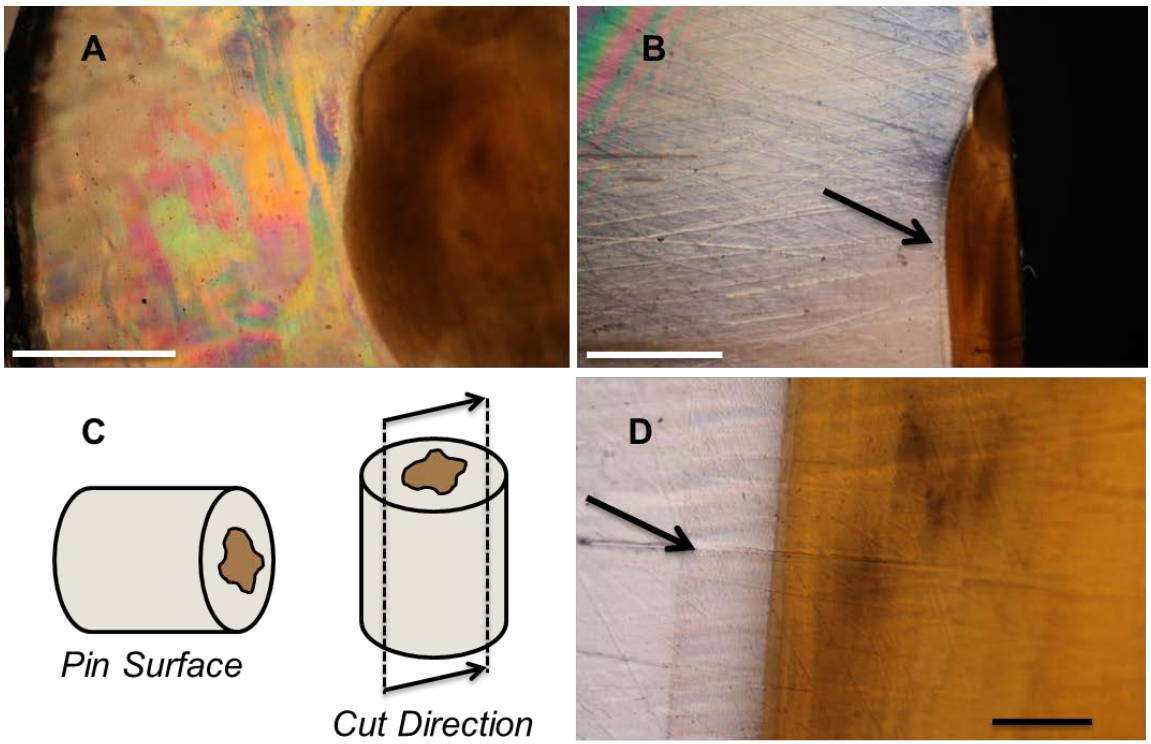

Figure 3.10. Cross-polarized optical micrographs of the PEKK fretting surface after 50,000 point-to-point moves. A) Top view with scale 1mm B) Side view of surface damage with scale 1mm C) Illustration of the pin surface features D) 50x zoom of damage features marked by the arrow with scale bar 100μm.

Although many questions raised from the results of this study cannot be completely answered, their analysis gives better insight into the nature of fretting in PAEK. Because fretting and sliding wear were studied in an identical pin-on-flat configuration it also allows for direct comparison of sample performance. Unlike sliding wear in which debris can be expelled from the contact, the entrapment of debris promotes adhesive contact between the pin surface and metal counterface. With sufficiently high displacements, slip of adhesive contacts will occur. The resulting damage from repeated sticking and slipping leads to sample failure that cannot otherwise be related to static mechanical properties or sliding wear performance. This study leads to several key conclusions that will help future studies of PAEK wear behavior in general.

3.5 Conclusions

Based on the results of this study, several conclusions can be drawn about the fretting behavior of PAEK. Sliding wear and fretting of PAEKs are governed by different mechanisms. Although a material may exhibit outstanding performance in a sliding wear environment, cratering and fracture can occur when samples are tested in a fretting environment. This fretting wear behavior also depends on how directional and intermittent stick slip is. Surface cratering and fracture occur in an intermittent multidirectional fretting environment but do not occur for a continuously linear reciprocating path. It is believed that velocity accommodation and chain orientation occur and mitigate potential surface damage. Analysis of wear debris suggests frictional softening of the wear surface also plays a key role in fretting. Greater adhesion between

the pin and counterface results from this softened surface and increases the magnitude of frictional forces. However, fretting wear of PAEKs cannot be linked to static mechanical properties. The fretting performance depends on how cracks nucleate and grow as the result of slip. Differences in fracture toughness and crack growth parameters better explain the observed surface damage. Additionally, tribological transformations such as melting or crystallization will influence the propagation of fretting induced surface cracks.

CHAPTER IV

INFLUENCE OF FILLER AND WET CONTACT ON FRETTING

Polyetheretherketone (PEEK) polymers are increasingly used in tribological applications where fretting damage occurs. Fillers are often incorporated to enhance strength and reduce friction. However, environmental conditions can severely limit their operating lifetime. Wet contact conditions in particular can lead to catastrophic failures. In this chapter, fretting of a selection of filled and unfilled PEEKs are tested in both dry and wet conditions. Analysis of the wear surfaces and debris reveal substantial differences in wear behavior. The fretting performance appears to be strongly tied to the static friction response of the material. Static friction measurement along with FEA analysis was conducted to better understand the observed phenomena.

4.1 Introduction

Polymers are increasingly used in tribological applications. Often, it is necessary for such polymeric material to function across a broad range of environments. Design challenges frequently occur since a material may offer outstanding wear resistance in one application or environmental condition but suffer in another. The polyaryetherketone (PAEK) family of thermoplastics is an attractive material for use in such varied environments. These semicrystalline polymers are resistant to most solvents and possess a high glass transition temperature (T_g) around 150°C[113]. Such properties coupled with their inherent wear resistance make PEEK a popular choice for use in extreme environments. The tribological behavior of PEEK is well reported and has been studied

in both the unfilled virgin state and with the incorporation of various fillers[10, 14, 114]. Wear resistance is often attributed to transfer films that protect against abrasion from counterface asperities[12]. For this reason, many studies have focused on the relationship between counterface roughness and sliding wear rate[15-18]. Ovaert observed that there exists an optimal surface roughness that minimizes wear[17, 19]. However, with increasing surface roughness the wear rate was mostly invariant due to the presence of transfer films[19]. Bahadur believed that these films form when debris becomes physically entrapped between asperities[12]. Though the exact role of transfer films in determining PEEK wear behavior is not fully known, much work has been done to promote their formation.

Fillers are often incorporated into PEEK to enhance desirable properties. Commonly, low friction additives such as PTFE, graphite, and MoS_2 are used to reduce friction[115]. Although PEEK has high wear resistance in its unfilled state, the coefficient of friction is higher than desired. Fillers are also chosen based on their ability in assisting the formation and functionality of the transfer films. Inorganic fillers like Al_2O_3, CuF, and CuS have been found to enhance polymer transfer film adhesion and thereby mitigate wear.[116-118] The incorporation of PTFE alone can even form films that achieve ultra low friction and wear behavior.[119] However, the addition of fillers into the PEEK matrix may come with a loss in mechanical integrity. Carbon and glass fibers are a popular choice for mechanical reinforcement. Additionally, fillers must be used in limited quantity as particle agglomeration and matrix voids can occur with high loadings. PEEK based composites are typically manufactured with filler loadings below

30%. For this reason the fill ratios of 10% PTFE, 10% graphite, 10% carbon fiber has been a popular formulation for PEEK based tribo-composites[120].

The use of polymer based bearing material in wet environments creates a number of challenges[121]. Polymers can be plasticized in the presence of solvents. It has been observed that wear increases when the solubility parameters of the polymer and liquid closely match[122]. The solvent can penetrate the polymer surface and promote stress cracking that accelerates the formation of debris. Such conditions are also said to promote adhesive-fatigue over abrasive wear. Omar suggested that plasticizers promote subsurface crack propagation resulting in the formation of large plate-like debris[37]. The deleterious effects of lubricants on polymer wear performance can also be accelerated under conditions with high contact pressures. For some polymer-lubricant pairs, plasticization of the polymer surface can occur leading to a rapid increase in friction. Briscoe termed this behavior scuffing and studied this phenomenon in PEEK at length[46, 123, 124]. Briscoe observed that the high pressures found in boundary lubrication can accelerate this scuffing failure[124]. Furthermore, frictional heating elevates the contact temperature and plasticizes more of the bulk. Recently, Berer observed that the hydrostatic pressure resulting from oil lubricants can exacerbate the propagation of subsurface cracks in unfilled PEEK on PEEK rollers[40]. Even though PEEK is resistant to most solvents, it can be plasticized in a number of environments[45, 125]. Nanoindentation and scratch studies have shown that even water can significantly soften the surface of PEEK-based materials[45]. The effects of water lubrication on the sliding wear behavior of PEEK and its composites have also been reported. For pin on

disc sliding, water lubrication generally lowers the coefficient of friction[126]. However, for most PEEK samples studied, wear rates increase significantly[126-128]. The increase in wear volume is believed to depend on the penetration of water below the PEEK surface. The high contact stress and frictional heating that occur during sliding is believed to promote this process. Yamamoto for instance observed plasticization of unfilled PEEK samples after sliding that did not occur after immersion alone[127]. The selection of filler type will also affect the performance. Glass fibers for instance are found to suffer from stress corrosion cracking in water[128, 129]. Carbon fiber based fillers were found to offer some improved performance, but generally all PEEK samples suffer in wet conditions. Unfortunately, only a small number of studies have been done so any conclusion remains speculative. Jacobs asserted that water lubricated wear rates depend primarily on counterface tribochemistry[129]. The presence of water was said to induce a hydrolysis like degradation of the PEEK. In their work they proposed that chemically inert diamond like coatings and Al_2O_3 counterfaces should be used in place of steel for aqueous environments. Water lubrication will also wash away transfer films that reduce wear in dry sliding tests. Yamatomo observed that compared to PEEK, samples of PPS were still capable of forming transfer films in wet conditions[127]. This behavior has been attributed to the bonding between sulfur compounds in PPS with iron in the steel counterface. Although PPS does not perform considerably better in wet sliding, transfer films will inherently protect against abrasion. Water is a seemingly innocuous fluid, but it can have a substantial affect on PEEK polymers in tribological applications.

Fretting is often characterized by conditions with high contact pressures and nominally small displacements. Damage occurs when adhesively bonded asperity contacts repeatedly become unstuck and slip. The static friction that results from sticking and slipping can induce surface cracks that may propagate catastrophically. Typically, fretting damage can be related to the degree of slip. The well-established Mindlin criterion for slip allows for some prediction of fretting based on contact mechanics[83, 84]. However, a lot of the theories surrounding fretting cannot be applied for polymers due to their viscoelastic nature. Typical fretting experiments are done using unidirectional reciprocation in a ball on flat configuration. However, polymers may undergo orientation hardening in the direction of strain. The polymer surface may also prevent slip from occurring through a mechanism termed velocity accommodation[92]. In the previous chapter it was demonstrated that for unfilled polyaryletherketones (PAEKs), intermittent and random slip trajectories can produce fretting damage not observed in unidirectional reciprocation[130]. Surface cratering or fracture occurred in samples depending on their fracture toughness and crack growth parameters. It is unclear though how changes in the contact conditions might affect this fretting response. For instance, the introduction of lubricating fillers will lower the frictional forces but may also result in increased slip. Some fillers may potentially reduce fracture toughness, which can increase the severity of fretting damage. Wet conditions can plasticize the PEEK surface but may also serve as a lubricant reducing the buildup of heat and expelling entrapped debris. The aim of this work is to study the influence of both filler and environmental conditions on the fretting behavior of PEEK. The resulting analysis

will then help understanding how changes in contact conditions impact the material response to fretting.

4.2 Materials and Methods

4.2.1 Materials

A total of eight different samples of PEEK based material were used in this work. Four of the samples are neat unfilled PEEK and labeled based on their molecular weight M_w. Within this selection two samples are termed low molecular weight, labeled L1 and L2, while the high molecular weight samples are H1 and H2. Gel permeation chromatography (GPC) was used to differentiate the samples and values are listed in Table 1. Additionally, relevant material properties are included in Table 4.1. All neat unfilled test specimens were injection molded under controlled conditions described in previous work[21]. Tensile tests were performed in accordance with ASTM standard D638 using type V tensile specimens. Wear samples were made from injection molded sprues that are machined into 6.35mm diameter pins. As the data shows, lower M_w PEEK typically achieves higher degrees of crystallinity compared to higher M_w PEEK under the same conditions. Mechanically, the unfilled samples are similar with the exception of the elongation at break. Although fracture testing was not performed, it is expected that such properties differ between samples. Typically, lower M_w PEEK forms larger spherulites and suffers from decreased fracture toughness K_{1C}[39]. Additionally, lower tie chain density will lead to unstable fatigue crack growth[38].

Table 4.1. Tabulated molecular weight M_w crystallinity $\%X_c$ and tensile properties for PEEK samples used

Sample	Mw (kg/mol)	$\%X_c$	Tensile Modulus E (GPa)	%Elongation at break ε	Tensile Strength σ (MPa)
PEEK L1	66.2	48	4.0	22	78
PEEK L2	75.9	42	3.7	18	85
PEEK H1	114.4	42	3.8	51	82
PEEK H2	122.3	32	3.7	71	91

It is expected that these differences will occur in the filled samples as well. The same four grades were also used to make compression-molded samples containing 10%PTFE, 10% carbon fiber and 10% graphite. The individual ingredients are introduced into a thermally jacketed high speed mixer, and mixed while maintaining temperatures well below 20 °C to avoid agglomeration of the PTFE component. The resulting powder mixture is introduced into the mold system and initially compressed to approximately 2,000 psi. Once compressed, the entire mold assembly with pre-compressed powder is placed in an industrial oven and heated to a temperature in excess of the crystalline melting point of the highest melting component to achieve a fully molten system. Once melted and at a uniform temperature throughout, the assembly is removed from the oven and re-compressed to a pressure of approximately 4,000 psi. This pressure is maintained as the temperature decreases, and the steel mold components are removed at appropriate times to avoid problems associated with coefficient of thermal expansion differences. Wear samples were molded using a 38mm diameter

cylindrical mold and then machined into 6.35mm diameter pins. A mold for tensile and compressive test specimens was also used in accordance with the ASTM standards. The relevant material properties and testing standards are listed in Table 3.2. As might be expected the introduction of filler resulted in some changes in properties compared to the neat samples. The neat specimens were all found to have a density of 1.30 g/cm^3 and moisture content at saturation of 0.4%. It appears that the filled samples differ only slightly in this regard. Mechanically, the filled samples all suffer from decreased elongation at break and tensile strength. The samples were also comparable to each other with the only notable exception being the L1 sample based on a low M_w PEEK.

Table 4.2. Tabulated material properties for filled PEEK material with accompanying standard used.

		Filled 10% PTFE, 10% CF, 10% Graphite			
Base PEEK		**L1**	**L2**	**H1**	**H2**
Density (g/cm^3)	ASTM D792	1.46	1.46	1.46	1.46
Moisture Content at Saturation (%)	ASTM D570	0.30%	0.30%	0.30%	0.30%
Hardness, Shore D	ASTM D785	79.8	80.9	80.8	82.1
Tensile Modulus (GPa)	ASTM D638	3.36	4.39	4.44	4.42
Tensile Strength at Break (MPa)	ASTM D638	36.1	63.6	68.3	64.9
Elongation at Break (%)	ASTM D638	1.90	2.2	2.4	2.7
Flexural Strength (MPa)	ASTM D790	154.2	155.13	155.8	147.8
Flexural Modulus (GPa)	ASTM D790	12.3	12	11.6	11.1
Compressive Strength (MPa)	ASTM D695	135.7	161.1	163.1	165.6

4.2.2 Fretting Test

Fretting occurs when mutually loaded contacts repeatedly stick and slip. In order to produce a fretting type of environment, sufficiently high pressures are needed. In the previous chapter a nominal pressure of 50MPa was used. In this work, the same test conditions were used as those described. To achieve such a contact pressure, the 6.35mm diameter pins were loaded against a hardened (HRC 60) D2 steel counterface with a load of 1570N. The counterfaces were all ground to have a unidirectional average roughness R_a of 0.5μm. The fretting rig used two programmable independently driven stages (Aerotech) to move the counterface against the pin. Because the steel surface was ground in a single direction, varying the sliding trajectory could control the degree of shear anisotropy. For instance, a circular path will produce a constantly changing shear direction compared to linear sliding. The resulting shear anisotropy from such motion can prevent strain hardening that occurs with unidirectional wear tests. Additionally, the fretting test requires some portion of the pin contact to remain covered throughout the experiment. The entrapment of debris and accumulation of heat in this overlapping region can accelerate fretting damage. Finally, the experiment was designed to create multidirectional and intermittent slip between the PEEK pin and a steel counterface. Polymers have been observed to undergo a velocity accommodation mechanism during linear reciprocating fretting tests [Ref.]. The viscoelastic nature of polymers means that they can comply with surface strains and prevent slip from occurring. The fretting test is designed so that adhesive contacts slip and stick intermittently so that strain compliance cannot occur. It was found that this result could be obtained by moving in a randomized

point-to-point trajectory that is confined to a 2mm by 2mm space as illustrated in Figure 4.1. The displacement trajectories have magnitudes between 0.1 and 2mm. It was found that for the test rig and loading conditions adhesive contact between the pin and the plate require displacements greater than 1mm to slip. The introduction of lubricating fillers and wet conditions might alter this slip behavior and a series of friction loop experiments were done to understand this.

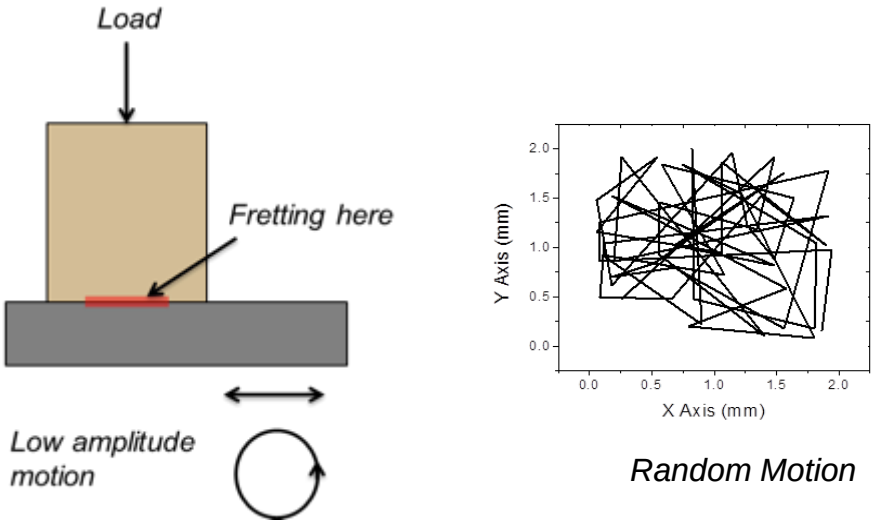

Figure 4.1. Illustration of the loading configuration and motion profile used in fretting tests.

The critical displacement δ needed for adhesive contacts to slip will depend on the normal load as well as the stiffness of the fretting rig. This behavior can be observed in the friction profiles for PEEK pins sliding against the steel surface. For this test, single direction sliding was carried out at 1Hz perpendicular to the grinding direction. The motion profile was sinusoidal and there is no dwell between start and stop. Counterfaces

were mounted to a 3-axis load cell (Interface) with a data collection rate of 250Hz. Figure 4.2A-D shows the frictional force from the filled L1 sample sliding with displacements 0.5 to 2mm. Similar to the findings for unfilled PEEK, slip only occurred for displacements exceeding 1mm. In the friction profile a displacement of 0.5mm for instance, the friction force was sinusoidal and matched the motion profile of the robotic stage. Figures 4.3 and 4.4 show the frictional force for wet contact by placing a small quantity of water on the counterface. A similar profile occurred for displacements of 0.5mm indicating that for all test conditions the surfaces remained stuck for small trajectories. As the displacement increased, a slight kink was observed in the profile. It is believed that this is due to the stiffness of the rig that must be overcome before sliding is initiated. At some displacement between 1 and 2mm the local contact was moved a sufficient distance for asperities to come unstuck. In comparing the profiles in the below figures, the most striking difference is between wet and dry sliding. For both filled and unfilled samples the friction profiles appear flatter for displacements greater than 1.5mm and indicate a state of mixed or gross slip. There is also a prominent spike in friction due to the transition from static to kinetic friction. The introduction of water to the surface appears to cause erratic spikes in the friction profile for the unfilled neat samples. This chatter phenomenon was not observed in the filled samples as shown in Figure 4.4B. It is not clear how water inhibits smooth sliding of neat PEEK samples, but there are a few explanations. The water at the surface may prevent asperities from smoothly plowing through the bulk. In effect, the water causes some asperity contacts to slip at intermittent times. A similar phenomenon is observed in rubber windscreen wipers moving across a

wet glass surface. Regardless of the underlying causes, the transition from stuck to unstuck occurs at similar displacements for all of the fretting conditions.

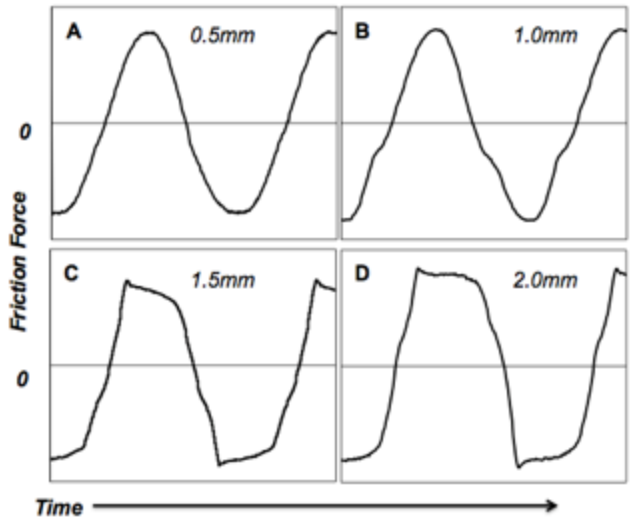

Figure 4.2. Friction profiles for a filled L1 PEEK pin under 50MPa of contact pressure and reciprocating perpendicular to the counterface surface roughness at 1Hz for displacements 0.5 to 2mm.

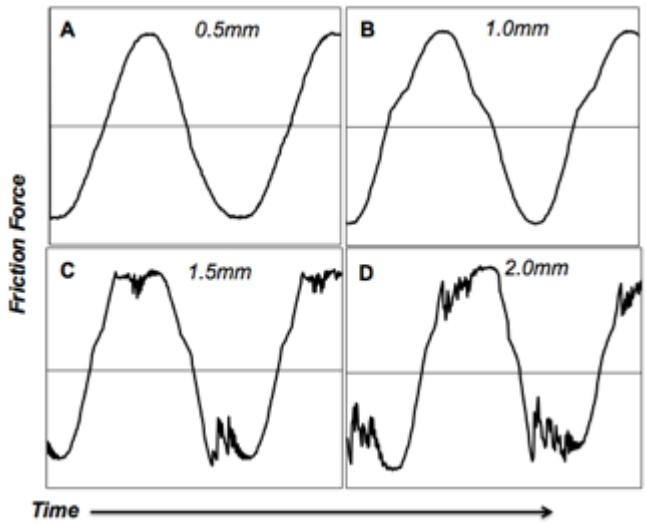

Figure 4.3. Friction profiles for a water lubricated unfilled L1 PEEK pin under 50MPa of contact pressure and reciprocating perpendicular to the counterface surface roughness at 1Hz for displacements 0.5 to 2mm.

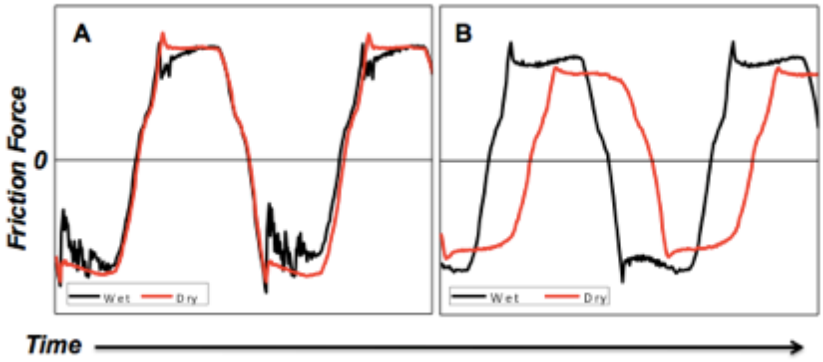

Figure 4.4. Friction profiles under dry and wet contact for A) unfilled L1 PEEK B) filled L1 PEEK under 50MPa of contact pressure and 1Hz reciprocation 2mm perpendicular to the counterface surface roughness.

Fretting experiments were performed using a test program similar to that described in the previous chapter. The program was written so that all point-to-point displacement trajectories are between 0.1 and 2mm with a mean value of 1mm. The test program moves the robotic stages through a series of 10,000 random XY data points. These data points are confined to a 2mm by 2mm space so some portion of the 6.35mm diameter pin remains continuously covered. To produce a comparative set of wear data for the previously listed PAEK materials, tests were run for 500,000 point to point moves. Although a frequency cannot be assigned to randomized movement, the test program completes on average 15 moves per second. For wet fretting studies, a basin containing the steel countefaces was filled with deionized water until the bottom half of the pin was completely submerged. Throughout the course of the test, loose debris was removed from the basin with a pipette and fresh water was added. This practice was done every hour until the completion of the experiment. Wear was measured volumetrically by weighing samples before and after each experiment.

4.3 Results

4.3.1 Wear

The measured volumetric wear results from the fretting studies are shown in Figures 4.5 and 4.6. For the low M_w L1 and L2 PEEK samples fracture occurs within the first 50,000 point-to-point movements of the experiment. For the High M_w H1 and H2 PEEK a large crater occurs within the central portion of the sample. It is believed that most of the wear debris was generated in the formation of this feature. The measured wear volume for samples H1 and H2 indicate that both samples respond similarly to the dry fretting environment. When the same four samples were tested in wet conditions new trends emerge. The L1 and L2 samples that previously fractured experience nearly twice the wear as H1 and H2. In light of sliding wear studies for PEEK material this is not surprising. However, it is surprising that fracture is inhibited simply by the introduction of water to the surface. Additionally, the wear volume for H1 and H2 samples is reduced in a wet environment. Comparing the wear volumes alone would indicate that water improves the fretting behavior of neat PEEK samples. However, further analysis of the surface can provide better explanations. For filled samples similar trends occur when comparing the low and high M_w PEEK samples as shown in Figure 4.6. The filled H1 and H2 material exhibits outstanding dry fretting resistance with only a modest amount of debris generated. Although the L1 and L2 samples generate a larger wear volume compared to H1 and H2 samples, there is no evidence of fracture or cracking. However, the introduction of water to the fretting environment appears to significantly increase the generation of debris. For the filled L2 sample wear increases

by nearly three times from dry to wet conditions. Comparison of the wear data sets suggests different mechanisms occur during the different fretting conditions tested.

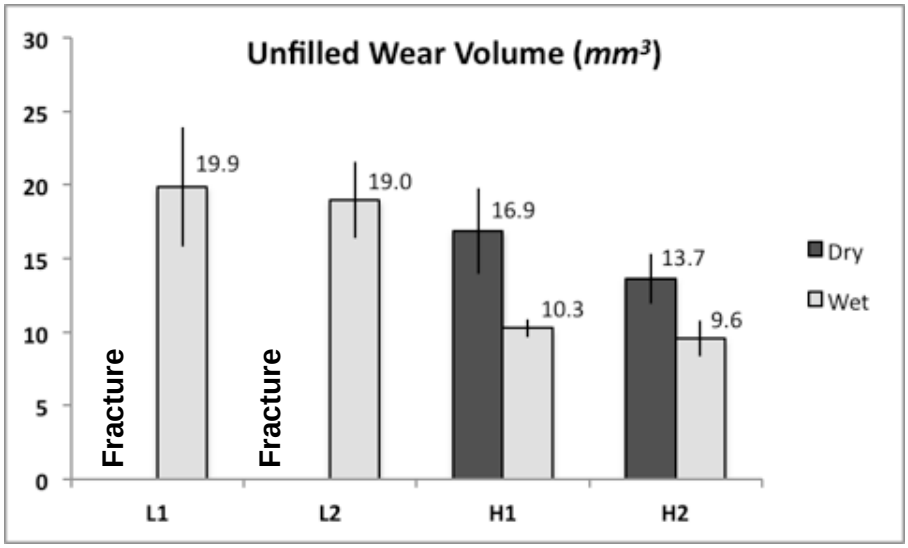

Figure 4.5. Wear results for the unfilled PEEK materials after 500,000 point to point movements under wet and dry fretting conditions. The bars indicate the size of standard error of the means (n=4).

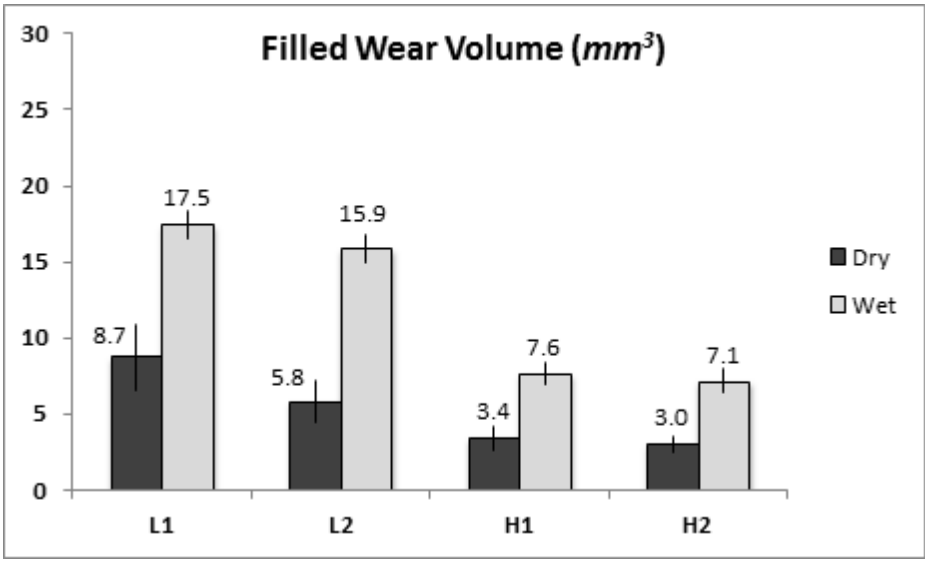

Figure 4.6. Wear results for the filled PEEK materials after 500,000 point to point movements under wet and dry fretting conditions. The bars indicate the size of standard error of the means (n=4).

4.3.2 Fretting Wear Surface

Although distinct differences occur in the measured wear volume discussed previously, the most striking difference appears when comparing the wear surfaces. Figures 4.7 and 4.8 show selected images of samples after fretting tests taken using a digital microscope (Dino-Lite). For the unfilled neat PEEK, dry fretting results in fracture or crater formation depending on the M_w of the sample. It was observed for samples L1 and L2 that cracks are able to propagate through the bulk of the specimen. In comparison, samples H1 and H2 develop craters in the central portion of the pin. It is believed that dry fretting wear results from the accumulation of heat at the pin surface. The displacement trajectories were chosen so that an inner portion of the pin remains constantly covered. Figure 4.7 illustrates this heat accumulation effect for sample H1. Within the first few thousand cycles the central portion of the pin begins to soften as shown in Figure 4.7A. This softened surface may then result in greater friction due greater asperity penetration and contact. Additionally, cracks may propagate more easily into the softened bulk and lead to fracture or cratering of the surface. The introduction of water appears to drastically influence this distribution of heat. Although sticking and slipping of the pin is audible throughout the course of a wet fretting experiment, fracture does not occur in any neat PEEK specimen. As discussed earlier, the wet fretting conditions do result in different wear volumes for the tested grades. However, debris appears to form as large flakes that are easily washed away by the water. As seen in Figure 4.8B for the low M_w L1 sample, the surface has a polished glassy hue. Even

though water promotes slip it seems to inhibit the accumulation of heat on the wear surface.

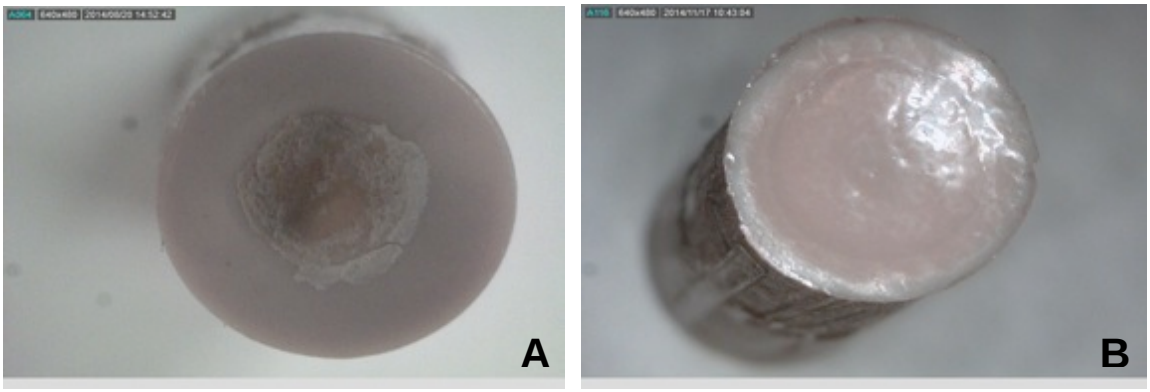

Figure 4.7. Wear surfaces of unfilled H2 PEEK after A)5,000 moves B)500,000 moves.

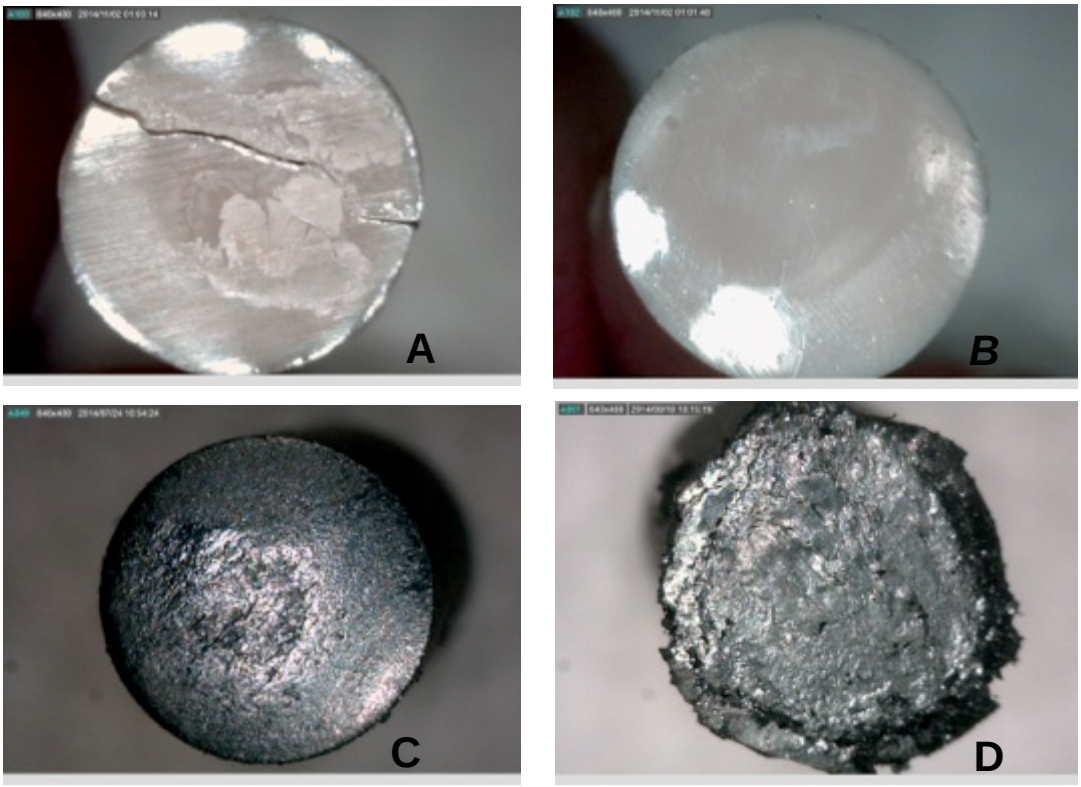

Figure 4.8. View of PEEK fretting surface for A) unfilled L1 sample dry B) unfilled L1 sample wet C) filled L1 sample dry D) filled L1 sample wet.

Figure 4.8 also depicts the wear surfaces for filled PEEK samples in both wet and dry fretting. In addition to a reduction in wear volume, fillers minimize the damage observed on the wear surface in dry conditions. It was observed that debris formed as a fine powder and collected near the periphery of the pin. There was also a layer of compacted debris under the surface. Since the filled sample contains lubricating graphite and PTFE fillers, these compacted layers will likely help reduce friction. The carbon fiber filler may also improve the dissipation of heat. However, aqueous conditions severely impact the integrity of the filled PEEK. Debris morphology appears as large smeared plates or flakes. This morphology is common to polymers experiencing adhesive-fatigue wear. In particular, the low M_w L1 and L2 samples show severe cracks around the sample periphery. Figures 4.8C and D illustrate the change in surface damage that occurs for the L1 sample in wet conditions. Figure 4.9 is a SEM micrograph (FEI-Quanta 600) taken of sample L2 after dry fretting in image A and wet fretting in image B. The region of interest in B is near cracks seen towards the periphery. The images show that wet conditions alter the surface in such a way that surface cracks form close to the surface.

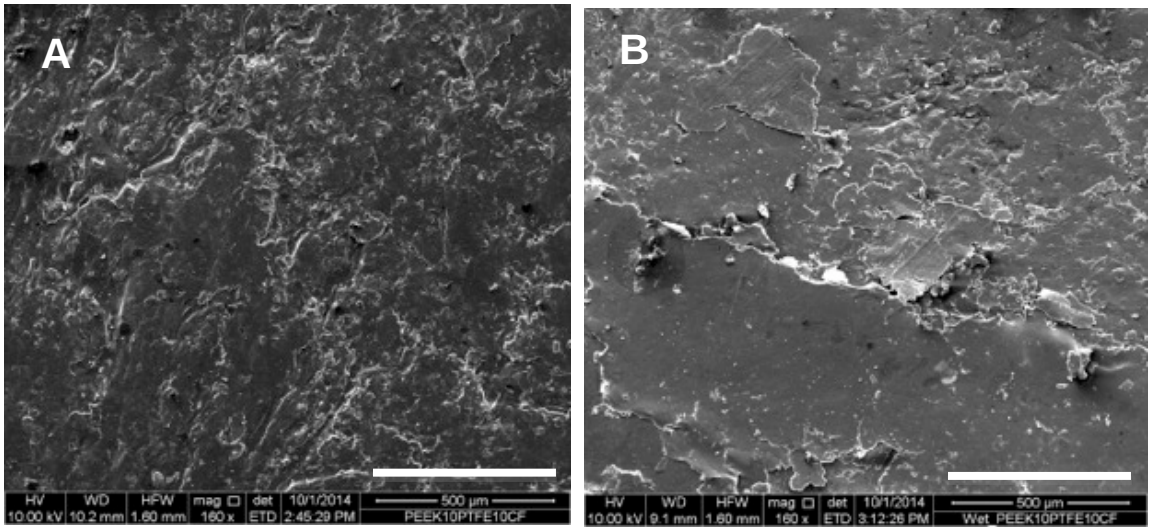

Figure 4.9. SEM micrograph of filled L1 PEEK sample following A) dry fretting B) wet fretting.

4.4 Discussion

4.4.1 Fretting Damage

Based on the results of the fretting experiments, several phenomena occur that require further discussion. Most notably, surface damage features change in character and location. For dry unfilled samples, damage is predominantly in the central portion of the pin. Previous work[130] found that the accumulation of heat in this region softens the surface and intensifies the static friction response. The increased frictional force may then initiate the formation of cracks that lead to fretting damage. However, the cratering and fracture that occur in dry conditions do not occur during wet fretting tests. It is assumed that water helps quench the surface and prevent the buildup of heat. It is also likely that some change in the contact loading occurs between test conditions. Water trapped between the pin and counterface will exert hydrostatic pressure on the pin surface. It has been observed that for oil lubricated PEEK rollers, hydrostatic pressure

can force fluid into microscopic surface cracks. The filled samples appear particularly sensitive to this effect. As seen in Figures 4.8D and 4.9B, cracks are visible across the entire surface. These cracks are most prominent in a ring near the periphery. Even though the unfilled specimens do not exhibit this cracking, the damage in a wet environment is predominantly near the edge as seen in Figure 4.8B. This suggests that the maximum stress occurs near the edges during wet fretting. Observation of the samples from the side shows a splaying feature as seen in Figure 4.10. During the fretting test, the counterface moves in a randomized path with trajectories confined to a 2mm by 2mm square. The test conditions were such that strain is imparted radially outward from the surface. For the dry samples, cratering takes place and the stress distribution is pushed radially outward over the course of the experiment. This can explain the splaying seen high M_w H2 samples in Figure 4.10D. However, in wet conditions all filled samples exhibit this feature. Comparing Figure 4.10A and 4.10C, it appears that the lower M_w L1 sample fractures more easily compared to the higher M_w H2 samples. Even though there is some difference in the elongation at break between samples, differences in mechanical properties alone cannot explain sample performance. It is likely that the lower M_w L1 sample surface can be softened more easily in the wet fretting environment. It can be observed in Figure 10b that this splaying does not take place for the L1 sample in a dry environment. The addition of lubricating fillers PTFE and graphite effectively lowers friction and thereby reduces the radial surface stress. The addition of water both prevents the formation of lubricating transfer films as well as

softens the wear surface. However, to understand this measurement of the static friction response is needed.

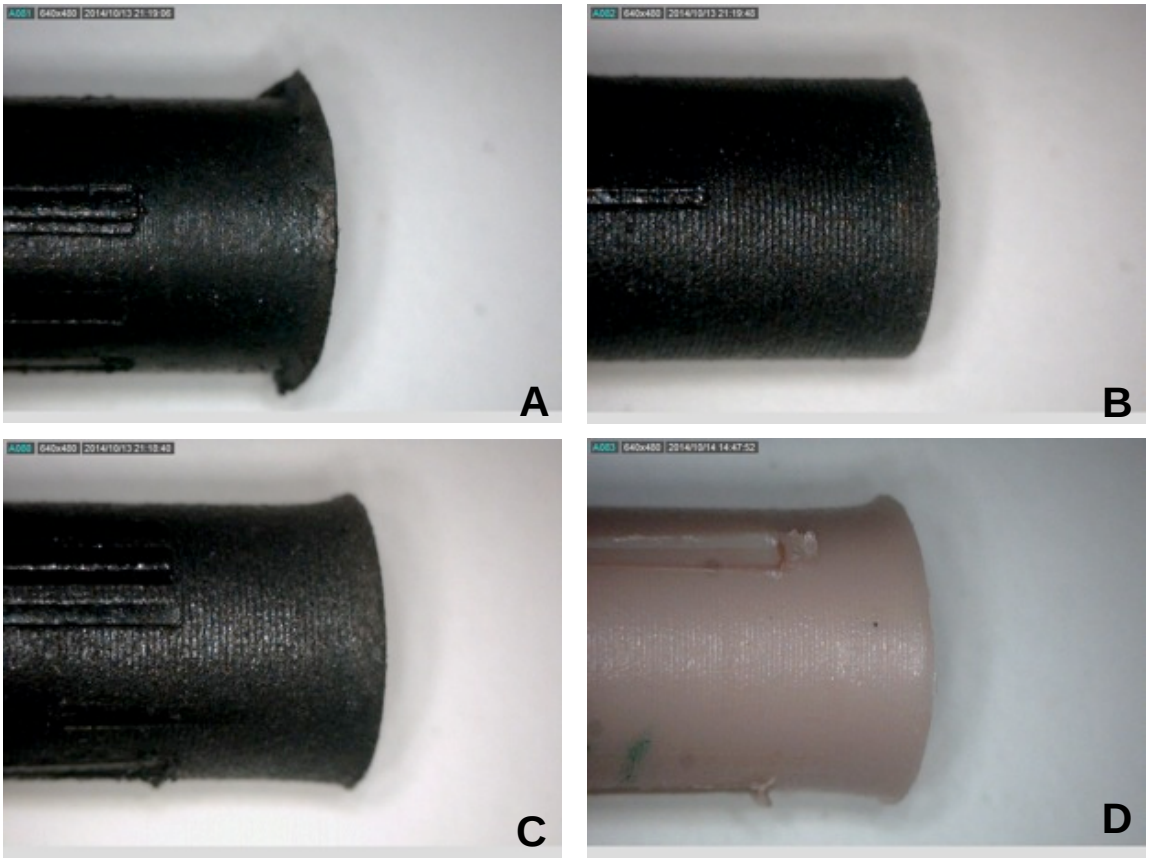

Figure 4.10. Side view of PEEK fretting surface for A) filled L1 sample wet B) filled L1 sample dry C) filled H2 Sample wet D) unfilled H2 sample dry.

4.4.2 Contact Stress Distribution

To better understand the stress field distribution during fretting damage, FEM simulation was performed using the supercomputing facilities at Texas A&M University. A model of a PEEK pin loaded against a rigid sliding body was created using the ABAQUS/ Explicit® software package (V. 6.12)[131].The dimensions of the FEM

computational domain are shown in Figure 4.11. Eight-node 3D linear brick elements were adopted in the FEM modeling. Nodes on the top surface of the PEEK pin were restrained in all three directions to simulate the clamping condition. The FEM simulation was divided into two steps. During first step, the rigid sliding body moves up to the PEEK pin to produce a 1600N load on the pin. In the second step, the rigid sliding body reciprocates 2 mm distance back and forth at a speed of 2 m/s. To define the contact between the rigid body and PEEK pin during the fretting process, general contact algorithm in ABAQUS® was used. To describe the frictional behavior of the interacting surfaces, isotropic Coulomb friction model was used. The rate effect was not considered in this simulation work along with the assumption that no heat is generated during the process. Since the numerical analysis was performed primarily to understand the stress field distribution during fretting damage, the above assumption can be considered reasonable. A piece-wise linear true stress-strain curve was used to describe the constitutive behavior of the PEEK pin in the dynamic stress analysis. To simplify the modeling complexity, mechanisms involving node or element separation and viscoelasticity of polymers were not included. A more realistic material constitutive model and a comparable speed will have to be considered along with heat generation during the fretting process in the future for quantitative modeling. The surface coefficient of friction ($\boldsymbol{\mu}$), Young's modulus ($\boldsymbol{E}$), Poisson's ratio ($\boldsymbol{\nu}$) and yield stress ($\boldsymbol{\sigma_y}$) were assumed to be 0.3, 3.5 GPa, 0.4, and, 140 MPa, respectively. The yielding and post-yield behavior was assumed to follow the stress-strain curve generated in the uniaxial compression tests.

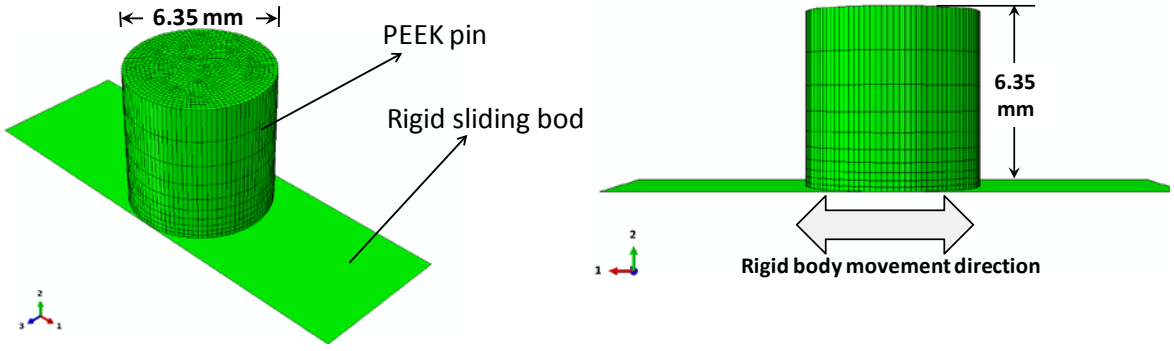

(a)

(b)

Figure 4.11. FEM simulation model - a) 3-D view; b) front view.

Figure 4.12 shows the stress field distribution in the PEEK pin when the rigid sliding body reciprocates against it. The arrow indicates sliding direction of the rigid body with arrow in both directions indicating that the rigid body is at the center. According to the numerical analysis, the stress magnitude is higher at the bottom surface of the PEEK pin indicating that the stress generated is primarily due to friction between the pin and rigid sliding body. Additionally, the highest stress magnitude can be seen at the bottom trailing edge of the pin. As the rigid body reciprocates, the position of the highest stress magnitude in the pin changes accordingly. The same spot of the bottom edge feels the highest stress magnitude alternatively. This alternating stress condition can be the reason for splaying phenomenon observed in the samples. For unfilled sample, the heat is accumulated during the fretting process which softens the mid-portion of the sample and causes craters in the middle of the pin. Wet condition helps dissipate this heat and as long as the stress magnitude does not exceed the yield stress of

the material, no splaying of the sample can be observed. For filled samples, the filler reduces the tensile strength of the material significantly as shown in Table 4.2. The wet condition may further weaken the bottom of the sample over time causing the splaying phenomenon to occur in wet filled sample. It should be noted that the surface of both PEEK pin and rigid sliding body is considered smooth in the numerical modeling. However, both contacting surface may not be sufficiently smooth during the experiment. As a result, local deformation and damage mechanisms at the asperities may also play a major role in the contact stress distribution.

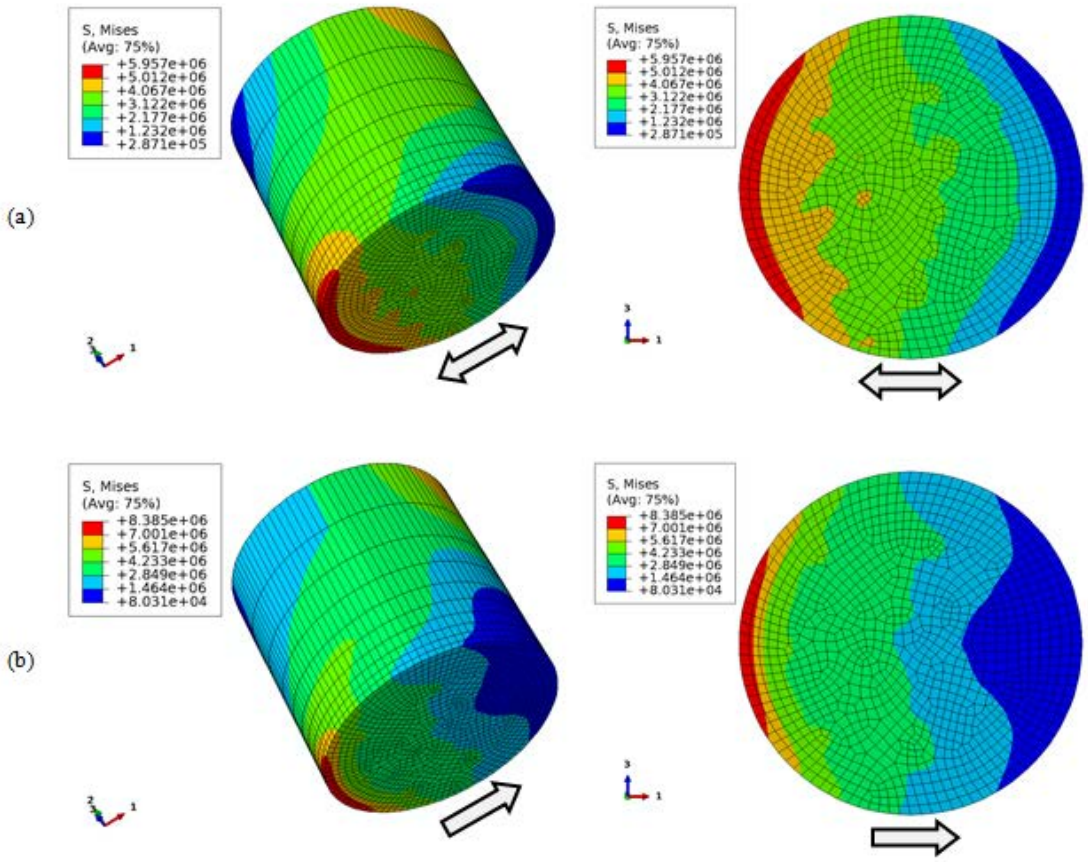

Figure 4.12. von Mises stress contour of the PEEK pin when the rigid sliding body - a) at the center; b) moves to the right; c) at the center; d) moves to the left.
(Left images show the 3-D view and right images show the bottom view; the rigid sliding body is removed for better visualization; the arrow indicates sliding direction of rigid body, direction in both ways mean the rigid body is at the center)

Figure 4.13 continued

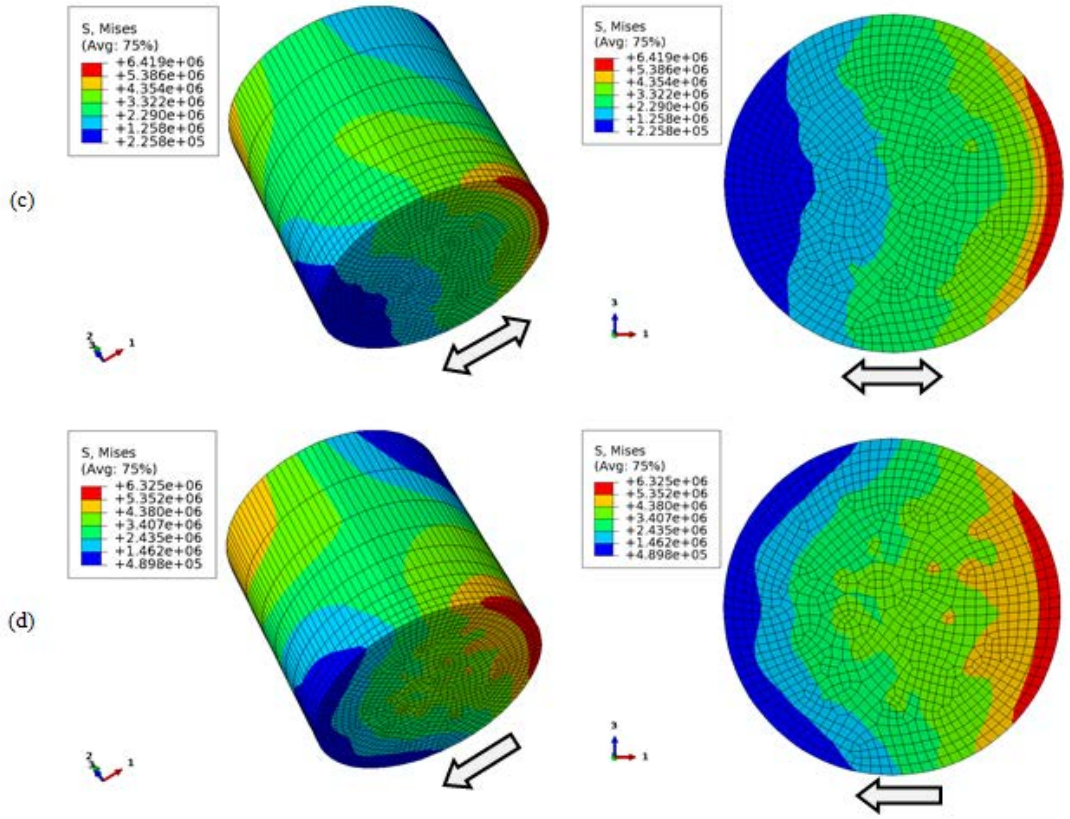

4.4.3 Static Friction Response

During the fretting tests, surface forces arise that resist sliding. In the experiment, a 50MPa contact pressure was selected in order to create adhesive sticking between the pin and counterface asperities. Additionally, the test rig was programmed such that surfaces would unstick and slip intermittently. This transition from stuck to unstuck releases energy. The repeated sticking and slipping of contacts can then lead to catastrophic failures observed in fretting. In order to quantify how static friction changes between test conditions, a stop-go methodology is used. Typically, studies focus on the

kinetic friction that results from pin on disc sliding. However, prior to sliding there exists static or break-loose friction force that is always greater in magnitude. This behavior however is still poorly understood.

Baumberger described the static friction behavior of rough surfaces by imagining an interface consisting of many single asperity contacts[109]. The friction response will then depend on the real contact area as well as the strength of each individual asperity contact. Static friction will also depend on the way in which material in and around the contact are sheared or ruptured during sliding. During a stop-go test, the contacting surfaces are rubbed together for a sufficient period of time to form adhesive contacts. The motion is then stopped for some prescribed hold time and then the surfaces are once again slid past one another. Although the experiment is simple by design, a wealth of information can be obtained from the measured frictional forces. The shape and size of the static friction peaks can then help understand the severity of a potential fretting environment. Figures 4.13 and 4.14 demonstrate a test using unfilled PEEK specimen L1. The test parameters were selected to best replicate the static friction that might occur during a fretting test. The pin is loaded against the counterface with a 1570N load and the stage then reciprocates at 10Hz with a displacement of 2mm for 1000 cycles. Motion is paused to allow the asperity contacts to grow. The surfaces are then slid apart and the tangential forces are recorded. Figures 4.13 and 4.14 also show a stop-go experiment with different sliding speeds after a pause. In Figure 4.13, sliding after pause is 100 mm/s over a distance of 10mm. Figure 4.14 is an identical test condition except the speed is slowed to 10 mm/s. It can be observed that for both tests, friction grows with an

increasing number of cycles. It is believed this is due to the formation of a multi contact interface. The reciprocating surfaces result in frictional softening and asperity penetration into the bulk. During the dwell period, this adhesive contact causes a holding force opposite the direction of sliding. For both slow and high speed tests, a spike in friction is observed before sliding. In Figure 4.13 the process of breaking asperity contacts and initiating smooth sliding takes place in about 0.1 seconds. This process is much slower in Figure 4.14 where the transition from static to kinetic friction occurs gradually. In a fretting environment, the breaking and reforming of adhesive contacts is believed to occur rapidly and so a 100 mm/s sliding speed best simulates this process.

In Figure 4.15A, a zoomed-in view of the transition from Figure 4.13 is shown. With a data collection rate of 250Hz, the static friction and kinetic friction response can be clearly distinguished. Typically, stop-go experiments seek to understand how the magnitude of static friction changes with hold time[132]. This behavior is often referred to as physical contact aging and results from the growth of asperity contacts by creep. Attempts were made to measure this behavior with hold times in seconds varying across several decades. Although measurable static friction spikes occur in every instance, little evidence of contact aging was found for PEEK sliding against steel counterfaces. It is possible that the data collection rate is too slow to distinguish the subtle changes in static friction. Furthermore, contact aging measurements are usually done for polymer on polymer pairs with very small loads. For instance, a surface force apparatus can distinguish the changes in contact aging that results from surface crosslinks and free chain ends[133]. However, the friction profiles from stop-go measurements of PEEK on

steel allow for behaviors to be observed and related to the fretting environment. Analysis of the changing stick-slip behavior can be equally valuable[134].

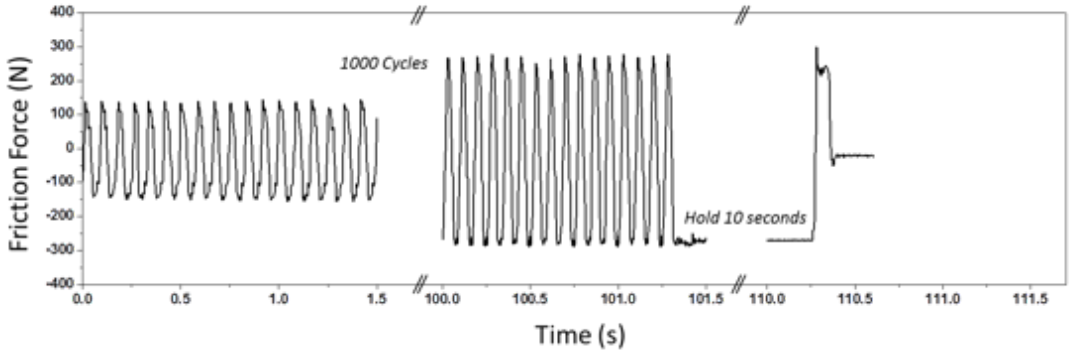

Figure 4.14. Friction force during 1,000 cycle stop-go experiment with 100mm/s slide velocity after 10 second hold.

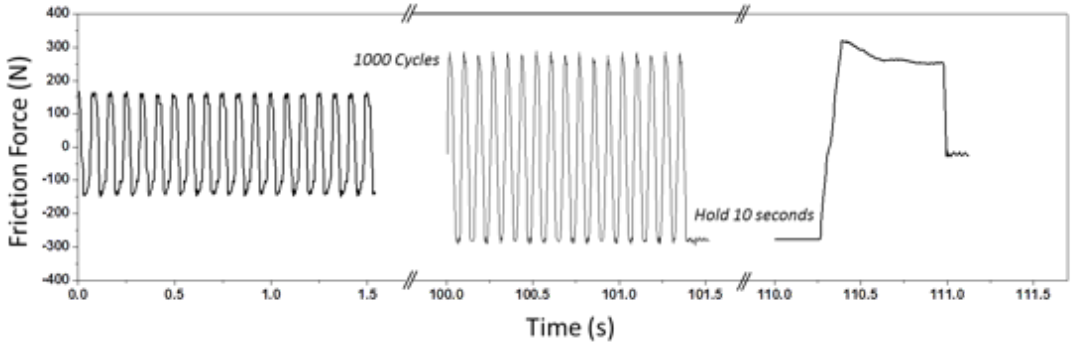

Figure 4.15. Friction force during 1,000 cycle stop-go experiment with 10mm/s slide velocity after 10 second hold.

Figure 4.15 shows how surface roughness affects the friction response for an unfilled L1 sample. According to Bowden and Tabor, friction can be broken down into components of plowing and adhesion[135]. Adhesive friction depends largely on the real contact area and possible bonding between material pairs. However, plowing will be

greatly affected by the plastic deformation of asperities. The effects of these friction components are evident when comparing the perpendicular and parallel sliding friction profiles. For sliding perpendicular to the surface grinding direction, a sharp stiction spike occurs followed by an increasing kinetic friction trace. When sliding is parallel to the surface roughness, static friction diminishes and the kinetic friction decreases with increased sliding distance. This trend in friction suggests that sliding direction alters how easily the hard steel asperities deform the PEEK surface. Perpendicular sliding results in asperities cutting into the bulk and quickly reforming adhesive contacts. This grinding angle effect has been observed in similar studies of steel pins sliding over ground steel surfaces[136]. Additionally, for the filled L1 sample in Figure 4.16 both adhesive and plowing components are altered sliding perpendicular to surface roughness. In light of the different fretting performances between samples, this result makes sense. The filled samples contain lubricating graphite and PTFE that will reduce adhesion to the counterface. The kinetic friction trace also exhibits smooth sliding compared to the plowing phenomena seen in the unfilled specimen. Observation of the counterface in Figure 19A shows debris transfer to the surface not seen with the unfilled specimens. This transferred debris likely aids in the reduction of friction during sliding. This also indicates that counterface asperities more easily cut through the softer surface of the filled specimen. The filled samples improved fretting performance can likely be attributed to this reduction in traction force.

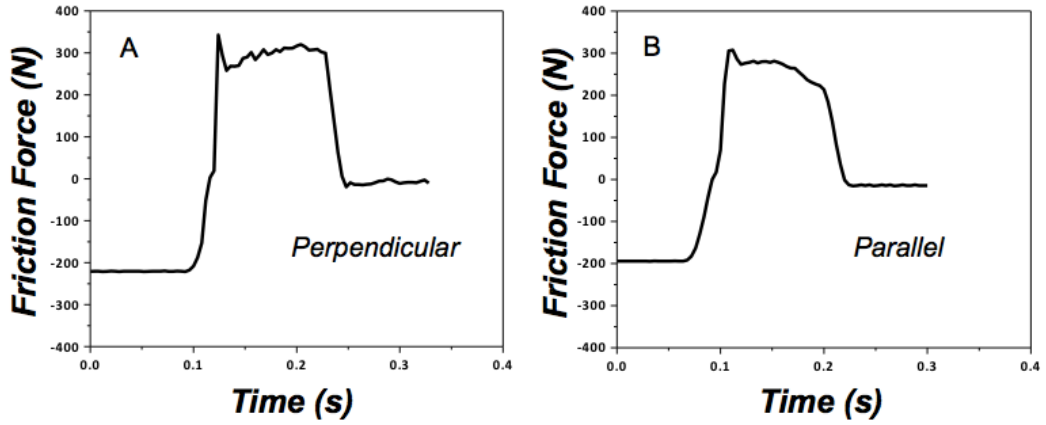

Figure 4.16. Stop-go friction profiles for unfilled L1 PEEK A)perpendicular sliding B)parallel sliding

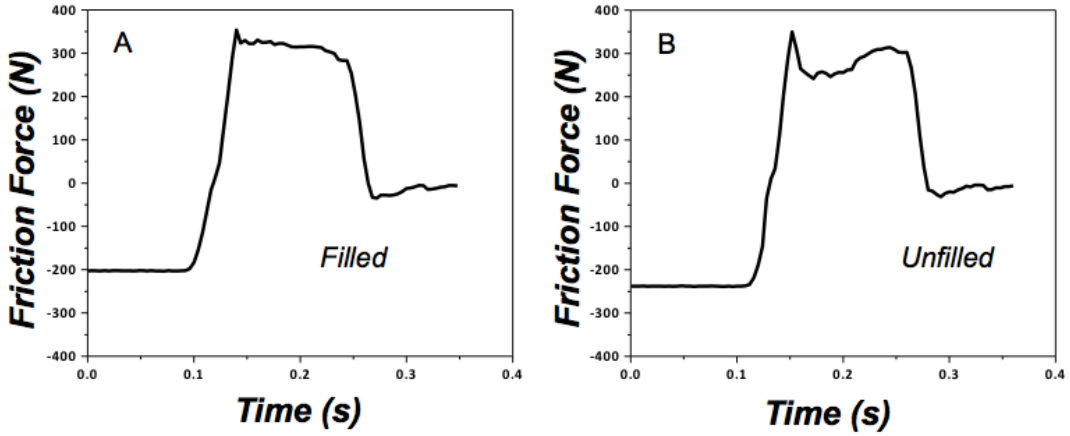

Figure 4.17. Stop-go friction profiles for A)filled L1 PEEK B)unfilled L1 PEEK

It was observed that the for water lubricated fretting, both filled and unfilled PEEK behaved differently compared to dry conditions. Water may quench the surface of the unfilled sample and prevent the build up of heat. The transfer film that reduces friction in filled samples will also be washed away as a result of water. However, it is expected that water lubrication will also alter the static and kinetic friction response. Stop-go experiments were performed for neat and filled samples with water lubrication

as shown in Figure 4.17 and 4.18. Samples were also soaked in deionized water for 3 weeks and tested immediately after removing samples from the water. This has been shown to be sufficient time to saturate as well as plasticize the surface of PEEK[45]. From the friction profiles, it can be seen that water lubrication has a much different effect on the unfilled and filled samples. For the neat unfilled L1 sample in Figure 17A, water lubrication results in irregular sticking and slipping. Additionally, the magnitude of the static holding force and kinetic friction are reduced. Although slip occurs more easily under water-lubricated conditions, less energy is released in the breaking of adhesive contacts. This may in part explain why fracture did not occur for the L1 and L2 samples in wet conditions. In contrast to this, the filled sample in Figure 18A exhibits an increasing kinetic friction under wet conditions. The magnitude of the friction forces are also significantly reduced compared to testing in dry conditions. Although the lower friction force implies water offers some lubrication, the trend in kinetic friction suggests more severe plowing. When samples are soaked in water different trends emerge. For the unfilled L1 PEEK sample in Figure 17B, soaking in water appears to have little effect on either static or kinetic friction. However, the filled sample experiences both a stiction spike as well as a decreasing kinetic friction trace. Observation of the counterface after a stop-go test gives some explanation for this. In Figure 19B the counterface shows a transfer of large debris flakes following a stop-go friction test. The lubricating effect of this debris can explain the trend in kinetic friction. However, this behavior can also explain the observed fretting damage for the filled samples under water lubrication.

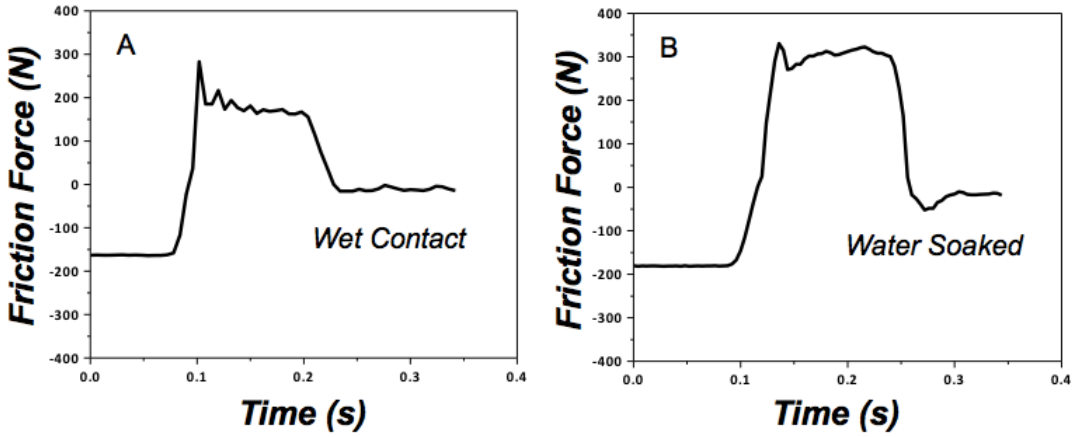

Figure 4.18. Stop-go friction profiles for unfilled L1 PEEK A)wet contact B)water soaked

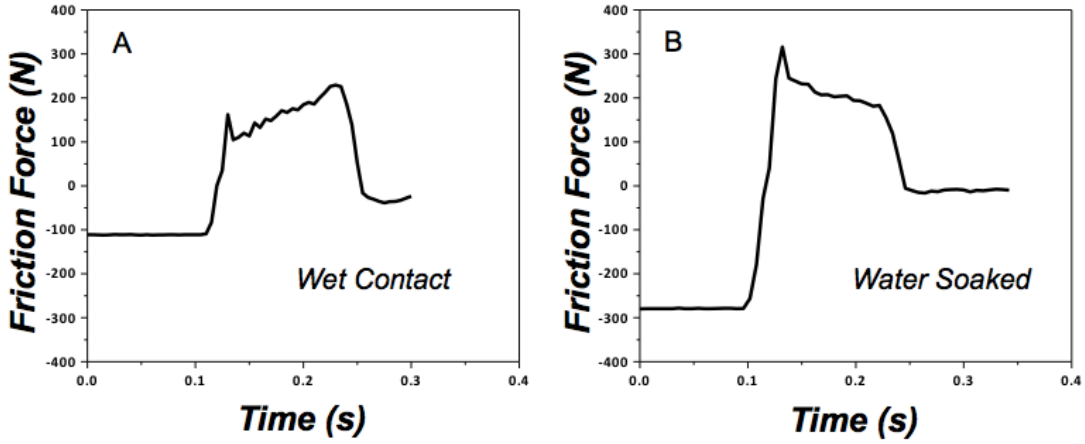

Figure 4.19. Stop-go friction profiles for filled L1 PEEK A)wet contact B)water soaked

It can be seen that the introduction of filler to the PEEK base material reduces the magnitude of the static friction force. However, when the same filled sample is soaked in water, the smooth sliding behavior disappears. For water soaked samples stiction occurs followed by decreasing kinetic friction. Water lubrication however results in an increased plowing effect. This decreased interfacial shear strength and increased asperity

penetration can exacerbate the formation of cracks. Under the hydrostatic pressure conditions used in wet fretting, water can be forced into these cracks. It is believed that this behavior is inherently linked to the observed fretting response. Fretting of filled PEEK in water results in increased wear as well as the appearance of cracks on the surface. Furthermore, splaying is observed towards the pin periphery. This splaying phenomenon likely results from the increased stiction during wet fretting.

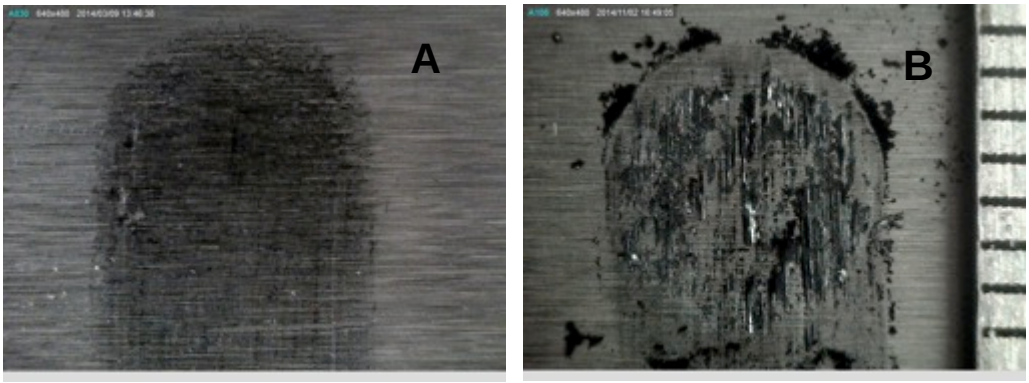

Figure 4.20. Counterface surface following stop-go experiment with A)Dry filled L1 B)water soaked filled L1

The performance of PEEK based polymers in a fretting environment depends on the shear stresses generated when adhesive contacts are broken during slip. This work illustrates how changes in surface properties can affect this behavior. For unfilled PEEK, significant frictional heating can occur during repeated stick slip cycles. The softened material can be easily sheared from the bulk. An aqueous environment can inhibit the build up of heat on the surface and prevent catastrophic fractures. Lubricating fillers such as PTFE and graphite can lower frictional forces and reduce tractive shear stresses.

However, it remains difficult to predict fretting behavior for a particular environment a priori. As a part of this work it has been demonstrated how static friction measurements can be used to give some foresight into fretting behavior. A stop-go experiment can be used to capture the friction response that results from sticking and slipping of adhesive contacts.

4.5 Conclusions

Based on the results of this study, several conclusions can be drawn about the fretting behavior of PEEK and its composites. A selection of four PEEK materials of varying molecular weight were used in both unfilled neat form and with the inclusion of 10% PTFE, 10% graphite, 10% carbon fiber. Using a multi-axis tribometer, a test program was created that produces multidirectional and intermittent slip. Tests were performed in dry and wet conditions and results varied drastically between test environments.

1) The dry fretting behavior of unfilled PEEK is observed to result in fracture or cratering depending on sample molecular weight. Lower molecular weight samples were found to fracture during the first few thousand cycles of fretting tests. Observation of the surface indicates that frictional heating occurs during dry fretting in the central portion of the pin. The softened surface promotes greater adhesion between the pin and counterface and increases the magnitude of the frictional forces.

2) In water lubrication, the unfilled PEEK no longer exhibits fracture or cratering during fretting. The change in damage results from the fact that water will remove debris from under the wear surface and also dissipate heat. However, water promotes slip between

the pin and counterface. The more erratic friction that results also causes an increase in wear volume generated.

3) Despite the loss in tensile strength and elongation at break, samples with lubricating fillers exhibit outstanding fretting resistance. This fretting resistance can be attributed to the friction response seen in stop-go experiments. Lubricating fillers promote smooth sliding and inhibit the formation of adhesive asperity contacts.

4) Water has a deleterious effect on the fretting performance of filled samples. Both the wear volume and severity of damage increase in wet fretting conditions. The molecular weight of the base PEEK material has the biggest effect on wet fretting performance. For all samples, surface cracks and splaying occur towards the periphery of the pin. Friction measurements show that wet conditions increase the static friction response as well as the degree of asperity plowing. This friction response coupled with the hydrostatic contact pressure can promote the formation of cracks on the pin surface.

5) Stop-go friction experiments are a valuable tool in understanding and predicting the fretting response of polymers in varied environments. Fretting depends both on the magnitude of friction forces during slip as well as how easily asperity contacts reform. The stiction spike and kinetic friction trace observed in stop-go experiments can effectively replicate a stick-slip event during fretting.

CHAPTER V

INFLUENCE OF SURFACE PROPERTIES ON FRICTION AND HEAT

An important aspect of PEEK tribology is the surface temperature reached during sliding. However, most knowledge of frictional heating in PEEK is based on post-hoc analysis of debris and wear surfaces. In this chapter, infrared thermography is used to observe the full field temperature map of PEEK during ball-on-disc sliding. Additionally, friction studies were performed with steel and sapphire counterfaces. The results of this study illustrate the important role transfer films play in determining both the friction and temperature response of the PEEK wear interface.

5.1 Introduction

Wear in polymers remains challenging to study due to the inherent complexity of the process. The viscoelastic nature of polymers means that bulk mechanical properties will change as a function of strain rate and temperature. Adhesive chemical bonds at the wear surface between the polymer and counterface may occur. Polymers can undergo changes in structure though chain scission or crosslinking events. These dynamic properties all must be considered when describing the wear surface[9]. It is common for descriptions of polymer wear phenomena to involve the interfacial surface temperature[137]. A substantial decrease in polymer mechanical properties can occur at elevated temperatures such as the glass transition T_g or melting T_m. Conditions in which excessive surface temperatures are reached are often avoided but prediction of such thermal softening is challenging. The combination of pressure and velocity is believed to

greatly contribute to the surface temperature[24, 138, 139]. However pressure and velocity alone tell very little of how surface temperatures arise. To gain better insight into the heat generated during sliding direct observation of the surface is needed. This work will focus on understanding how frictional heat manifests during sliding of polyetheretherketone (PEEK) polymers. This high performance semicrystalline polymer is valued for its solvent resistance as well as high glass transition (T_g ~150°C) and melting (T_m~350°C) temperatures[58]. Such properties have enabled PEEK to be used in tribological applications where temperatures and corrosive environments would preclude the use of many materials. PEEK has seen use in oil and gas exploration[125], biomedical applications[140], and space environments[141] to name a few. Limits on operating conditions are often ascribed to excessive heating that results from friction[24]. To avoid such conditions, it is not uncommon for an upper value of pressure and velocity to be assigned to PEEK based components[10, 23, 25, 142, 143]. This work seeks to provide deeper insight into the origins of frictional heating that occur in PEEK polymers.

5.1.1 Frictional Heating

When two surfaces rub against each other, frictional heat is generated and the temperature at the rubbing interface rises. Depending on test conditions and material properties of the rubbing pair, the interfacial temperature, T_s, can be substantially higher than the stated test temperature. This is particular true when rubbing surfaces are rough. For rough surfaces, the real contact area is often much smaller than the size of the nominal contact area[144-146]. The asperity contact pressures may also be much greater

than that predicted by Hertzian contact mechanics. The high local pressure and friction can also give rise to exceedingly high temperatures[147].

The actual magnitude of T_s is important for accurate descriptions of polymer wear phenomena. Potentially, this heat can be great enough to soften or even melt the polymer surface. Severe wear associated with melting temperatures are likely initiated by the buildup of small thermal transients[137]. Many studies have observed rippled and stretched wear features that suggest the surface was strained in a rubbery state[21, 36, 148]. Analysis of wear debris often shows changes in molecular structure that indicate surface temperatures near melting are reached[35, 130]. Ludema and Rhee utilized mass spectroscopy to detect chemical decomposition products that may occur during severe polymer wear[149]. The detection of chemical vapors corresponding to melting implied that such temperatures have been reached at the rubbing interface. Archard determined a maximum temperature for polymer pairs based on a model for load-controlled friction[150]. They observed that predicted temperatures near the glass transition corresponded with severe wear in Perspex sliding pairs. Polymers are also typically good insulators and so heat cannot easily be conducted away from the surface. Ettles suggested that for polymers, a limiting condition should occur based on the thermal softening point[137]. This thermal control model has been supported by empirical observations of polymer friction[108, 137, 139]. However, observations of interfacial temperature are largely speculative and based on post hoc analysis. Detection of this interfacial temperature requires *in situ* measurement of the contact.

The flash temperature concept has been used to model the temperature distribution that results from a moving heat source[147, 150-153]. In sliding contacts, friction generates heat that will dissipate at the interface. The interfacial temperature distribution that develops can be estimated based on material properties and sliding speeds. Models have been proposed for a variety of Peclet numbers and shapes of heat source[154]. Early work attempted to confirm these models through the use of buried thermocouples, dyes, temperature sensitive films [154]. However, advances in infrared (IR) thermography have enabled *in situ* studies of frictional heating to be performed with great accuracy. *In situ* studies are valuable as they enable direct comparisons with flash temperature models[155-158]. The real contact area, frictional forces, and contact temperature can all be directly measured. This means analytical solutions can be proposed and verified for a number of sliding conditions[155, 156].

In situ frictional heating studies of polymers so far have focused largely on rubber and other soft elastomers[155, 158-160]. These materials have low elastic modulus and thus large real contact areas and friction can occur at low pressures and sliding speeds. These test conditions are however orders of magnitude below operational pressures and velocities commonly experienced by many engineering polymers. In this work, polyetheretherketone (PEEK) polymer, a high performance engineering polymer, will be studied across a range of pressures and speeds in which frictional heating is believed to become significant. The upper limits on the combination of pressure and velocity vary between applications. For instance, a thrust washer configuration may operate with a nominal pressure of ~1MPa and speeds of 4m/s[161]. In academic studies

pin on disc and block on ring sliding tests are common. A typical max pressure is ~4-6MPa with maximum speeds between ~1-2m/s[10, 23, 36]. In this experiment a PEEK ball on sliding disc configuration will be used. During sliding, the surface temperature will be monitored with *in situ* IR thermography.

5.1.2 PEEK Tribochemistry

The polyaryletherketone (PAEK) family of thermoplastics, with polyetheretherketone (PEEK) being the best-known representative, is an often-studied group of semicrystalline polymers[58]. A number of authors have focused on PEEK wear behavior[10, 14, 19, 162]. Comparisons in terms of friction and wear resistance are often made with polytertrafluoroethylene (PTFE). PEEK is in fact often filled with PTFE to reduce friction. However on its own PTFE suffers from high wear rates[119]. In a study by Burris, they report for unfilled PTFE a coefficient of friction μ~0.1 and wear rate $K \approx 6 \times 10^{-4} \frac{mm^3}{Nm}$[119, 163]. In the same study, unfilled PEEK had outstanding wear resistance $K \approx 1.9 \times 10^{-6} \frac{mm^3}{Nm}$ but tended to have high coefficients of friction μ~0.4[119, 163]. PEEK wear resistance is often attributed to an ability to form protective transfer films on harder metallic counterfaces[19, 21]. Unlike PTFE that forms transfer films due to its unique banded crystal structure, there is no specific mechanism for PAEK film formation[7]. When PAEK is rubbed against metal, Bahadur suggested that compacted polymer debris becomes physically entrapped between asperities of the countersurface[12]. A polymeric film is eventually formed, and protects the bulk polymer from abrasive wear by covering hard rough asperities.

Many studies have attempted understand the role thermal and tribochemical effects have on the wear of PEEK. Using thermogravimetric analysis (TGA) and differential scanning calorimetry (DSC), Zhang studied the thermal properties of PEEK debris formed under varied conditions[34]. It was believed that during wear, chain scission of the diphenyl ether segment occurs and forms oxidative crosslinks at free radical sites. They had observed changes in the pyrolysis behavior as well as a tendency for crystallization to be impeded. It was rationalized that these results were from the formation of crosslinked branches that restricted segmental mobility. Later, X-ray photoelectron spectroscopy (XPS) was used to further support this argument[32]. The appearance of a π-π^* shakeup peak in the C1S spectrum indicated the presence of single pendant phenyl rings due to chain scission. This behavior depended on contact pressure with the greatest intensity occurring at moderate (2-4MPa) contact pressures. The change in the spectra with increased pressure was thought to be the result of chain scission occurring on different parts of the backbone that require greater thermal energy. The thermal properties of PEEK wear debris also indicate that it had been formed at temperatures near the melt. The first heat of melting for wear debris typically contains a cold crystallization exotherm[34]. This feature is often found in material that had been rapidly quenched from the melt state. The location of double melting peaks also tends to coincide with the thermal history. Usually for PEEK, an endotherm appears 10-15°C above the annealing temperature. The location of this feature has been used to determine that the PEEK wear surface may reach temperatures around 200°C [34, 35].

These studies are certainly not conclusive proof to the theories they espouse. They do demonstrate though that the PEEK wear surface is in no way chemically inert. According to Bahadur, the chemical activity between the filler and counterface can enhance the tenacity of polymeric transfer films[116, 117, 164]. Jacobs used this logic to investigate the effect of counterface material and aqueous environments on sliding wear of PEEK[129, 165]. Based on measured wear rates they suggested that chemically inert diamond like coating (DLC) or alumina Al_2O_3 counterfaces should be used in place of steel [129, 165]. Figueiredo recently used Raman spectroscopy to detect adhesive transfer between neat PEEK and various counterfaces[166]. Low surface roughness and surface energy was believed to minimize the adhesion tendency as well as tribo oxidative wear[166]. These observations all indicate that wear behavior of PEEK depends strongly on tribochemistry and temperature effects. However, these theories can be further supported by in-situ studies.

5.2 Materials and Methods

PEEK balls were rubbed against steel and sapphire discs in a ball-on-flat configuration. Friction and interfacial temperatures were recorded at various sliding speeds and contact pressures. Both steel and sapphire discs were used for friction measurements while only sapphire discs were used for temperature measurements.

5.2.1 Materials

PEEK ball samples were made from a commercially available Victrex 450G injection molded bar stock. The 19 mm diameter balls were machined from a single 25 mm diameter rod on a 3-axis CNC lathe to ensure reproducibility between samples. Steel

and sapphire discs for friction measurements were purchased from PCS. The materials properties of the balls and discs are listed in Table 5.1. Contacts are formed when a PEEK ball is pressed against a disc. The ball is always stationary while the disc rotates at a programmed speed. The labeling PEEK-sapphire and PEEK-steel denote contacts formed between a PEEK ball, and sapphire disc or steel disc respectively.

Table 5.1. Material properties of disc substrates.

Material (source)	Dimensions	Hardness	Roughness, R*a* (nm)
19 mm PEEK balls (Victrex)	19 mm diameter	85 Shore-D	1500
MTM Steel AISI 52100 disc (PCS)	46 mm diameter	760 HV	< 10
MTM Sapphire disc (PCS)	46 mm diameter	2000 HV	< 20
Sapphire disc	100 mm diameter	2000 HV	7

5.2.2 Friction Measurement

Coefficients of friction were measured using a mini traction machine (MTM) from PCS instrument under pure sliding conditions[167]. An illustration of the MTM test rig is shown in Figure 5.1. Tests were done by pressing a 19 mm diameter PEEK ball on a rotating disc. A new disc specimen was used for each test. Discs were cleaned with toluene in an ultrasonic bath and washed with acetone before use. The PEEK balls were also washed with acetone to remove surface contaminants. The balls were then rinsed in deionized water and thoroughly dried before each test. All tests were conducted

at 25°C. In this study, the effect of speed and load on friction coefficient was investigated. Friction was measured across a range of loads between 1N and 40N at a fixed sliding speed of 100 mm/s. The change in friction as a function of sliding speed was also measured at a fixed load of 10N over sliding speed range of 1 to 4000 mm/s. The test equipment measures friction as the average of five data points taken at the desired load and speed. Each test point represents approximately a 5 second period of sliding measured by a force transducer. The duration of sliding is roughly 12minutes for fixed load increasing speed tests and 3 minutes for fixed speed increasing load tests.

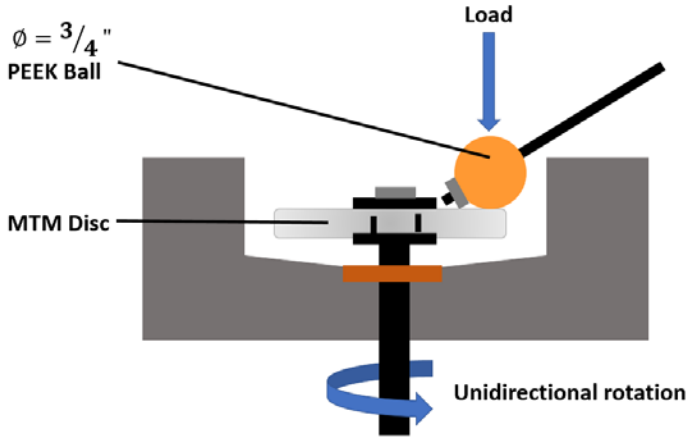

Figure 5.1. Illustration of MTM test and sample configuration

5.2.3 Temperature Measurement

The interfacial temperature of a rubbing contact, T_s, was examined with IR thermography. Details of the setup and calibration procedures are described in[157]. Briefly, the rubbing contact was created with an EHL rig (manufactured by PCS

instrument), where a stationary PEEK ball is pressed against a rotating sapphire disc from the bottom. A sapphire disc was used as the counterface because it fully transmits infrared radiation in the wavelength range of 3 – 5 μm. As the contact heats up, infrared (IR) radiation is emitted. An infrared camera X6540SC (FLIR), placed above the contact, can then detect the IR radiation emitted from the contact (see Figure 5.2). The camera had a 320 x 256 focal plane array with a 5x lens and 6.3 μm resolution. The observables are IR intensity images.

In order to detect T_s with IR thermography, a calibration is required. From such calibration the relationship between T_s and the amount of detected photon counts by the IR camera is obtained. This was done with a stationary contact formed by pressing the PEEK ball against the sapphire disc. Calibration for temperatures above ambient was performed with the ball partially immersed in a silicon oil bath. The EHL rig allows the oil to be heated to a predetermined temperature. A thermocouple was placed inside the PEEK ball just below the contact to estimate T_s. Once the estimated T_s from the thermocouple matched that of the oil bath, the IR signals detected by the camera are recorded. This was performed for a temperature up to 110°C. The above described process was conducted twice with two different sapphire disc, one of which was coated with Aluminum. This is because IR signals obtained with the uncoated sapphire disc, $C_{Uncoated}$, contain contributions from both the contact interface and the heated sapphire disc. Due to aluminum low IR emissivity, the IR signals from the coated disc, C_{Al}, comes only from the heated disc. The IR signal from the contact is then $C_{Uncoated} - C_{Al}$. The interfacial temperature can be obtained using the relationship: $T_{contact} = f(C_{Uncoated} -$

C_{Al}). These calibration curves can be found in appendix 6.1 and are used to create temperature maps with IR intensity images.

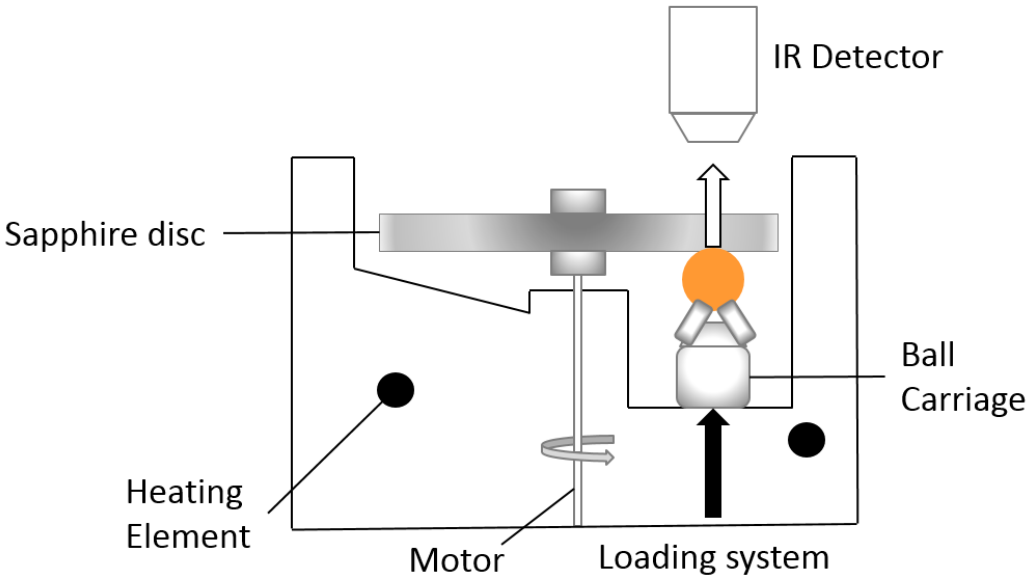

Figure 5.2. Illustration of In-Situ IR measurement

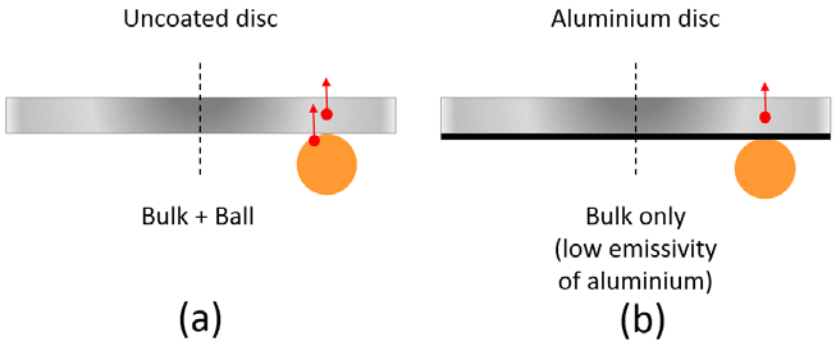

Figure 5.3. Discs used for IR calibration curves.

5.3 Results

5.3.1 Friction With Constant Sliding Speed

Friction measurements were performed with load and sliding speed as variables. Tests were repeated at least 2 times to verify observed friction trends. As shown in Figure 5.4, for a fixed speed of 100 mm/s the coefficient of friction μ, which is the ratio between frictional force, F, and applied normal force W, drops with increasing load. Fitting a power series to the PEEK-sapphire contact (circles, Figure 5.4) and PEEK-steel contact (squares, Figure 5.4) data gives $\mu = 0.33W^{-0.15}$, and $\mu = 0.5W^{-0.1}$ respectively. This behavior has been observed in polymers previously [168-171]. This is inconsistent with Amonton's laws for friction which states μ remains a constant. Note the validity of Amonton's laws would require that the real contact area, A increases proportionally with the applied normal load, W, i.e. $A \propto W$. If $A \propto W^n$, hence $F \propto W^n$, μ reduces with increasing W and $\mu \propto W^{n-1}$ [35]. The nature of the contact would govern the value of n, with $\frac{2}{3} < n < 1$ for deformations ranging from fully elastic smooth surfaces to plastic deformation of asperities of rough surfaces. With high sliding speed, frictional heating can soften the polymer surface, which will influence the proportionality between load and friction. For thermally controlled friction, $\mu \propto W^{-1}$ for full contact and partial contact $\mu \propto W^{-0.25}$ have been suggested[137]. Ettles based this relationship on observations of a rapid drop in friction with increasing load reported for several polymers[172-175]. These trends were not correlated to a measured surface temperature but phenomenological evidences of surface melting. The observation that the critical load for softening shifted to lower loads with increased speed implied

softening resulted from frictional heating[137]. It can be assumed that for the test conditions used in Figure 5.4, thermal effects are not significant.

Comparison of μ for PEEK-steel and PEEK-sapphire contacts shows that μ for PEEK-steel contacts is nearly twice that of PEEK-sapphire contacts. Observation of the steel counterface after friction tests (see Figure 5.14A) shows the presence of small debris not found on the sapphire surface. The debris also appears well adhered to the surface. A number of explanations can account for both the transfer of debris and differences in friction. It is possible that debris formed as the result of plastic yielding of the PEEK surface. The yield strength for PEEK is approximately 98MPa in tension and 125MPa in compression[176, 177]. Under sufficiently large loads the yield strength of the PEEK surface may have been exceeded in the contact. Assuming Hertzian contact (see appendix section 6.2) a nominal pressures of 75MPa occurs for PEEK-steel at the maximum 40N load. This pressure is below the yield strength but the real asperity contacts are likely much smaller than a Hertzian contact. The small size of transferred debris (see Figure 5.14A) supports this. The resulting high localized pressures at asperity contacts will also give rise to a larger shear stress. Debris can be removed from the bulk if the adhesive force between the PEEK and the counterface exceeds the bulk shear strength of the PEEK. The resulting shear stress in the asperity contacts may have been great enough to shear debris away from the bulk. However, this does not explain the difference in behavior between PEEK-steel and PEEK-sapphire friction. Friction is governed by both the elastic-plastic deformation of sliding bodies and their adhesion to one another[178, 179]. Plastic deformation of surface asperities will change the contact

area and thereby affect the value for friction. Hard counterface asperities may also penetrate and cut into the softer polymer surface and contribute to friction. Since steel and sapphire counterfaces are of similarly low roughness (R_a = 10 – 20 nm) such plowing components of friction are likely not significant. Differences in friction between PEEK-steel and PEEK-sapphire result from changes in contact area and adhesion between the contacting bodies. Furthermore, deposition of PEEK debris to the steel increases the adhesion between the surfaces. This increased adhesive friction is observed under all loads and suggests debris transfer may have occurred readily. This potential contribution of debris transfer to adhesive friction will be further discussed.

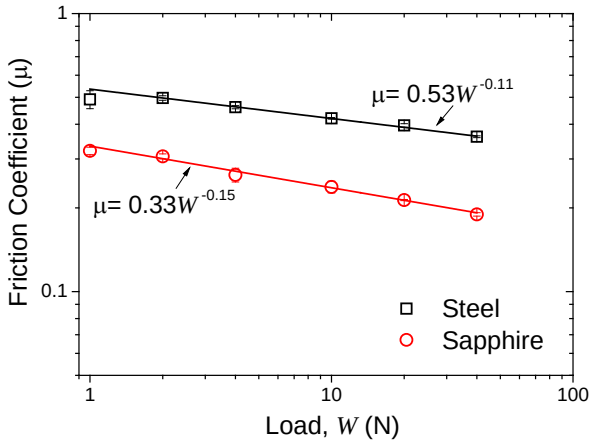

Figure 5.4. Evolution of friction coefficient μ with increasing load W when PEEK balls were rubbed against steel and sapphire discs. The sliding speeding was 100 mm/s. The duration of each test was 150 s.

5.3.2 Friction With Constant Load

How coefficient of friction of PEEK-steel contact and PEEK-sapphire contact varies with sliding speed U at a constant load of 10 N is presented in Figure 5. Results for PEEK-sapphire contact (open circles in Figure 5.5) shows that μ increases gradually at U ranges 1 – 50 mm/s, then more rapidly until a maximum is reached and then drops off around U = 1 m/s. Similar observations have been seen previously [137, 174]. The increase in friction can be attributed to growth in asperity contacts with increased sliding. During this initial period sliding speed is low and frictional heat does not become significant. The contact area changes as the result of mechanical deformation of surface asperities. As the contact area grows from partial to full contact a greater proportion the PEEK surface contributes to the overall frictional force. With increased speed a transition point where friction drops may occur. This transition is often attributed to thermal induced softening or melting after which friction of polymer enters the "thermal control regime"[137]. In the thermal control regime, the contact temperature may approach the glass transition temperature T_g of the polymer. The PEEK surface softens and thus slides more easily and friction rapidly drops with $\mu \propto \frac{1}{\sqrt{U}}$[137]. With a PEEK-steel contact (open squares in Figure 5.5), μ grows rapidly initially until $U \approx$ 10 mm/s, after which it reaches a plateau. μ sees a slight drop before increasing again around $U \approx$ 1 m/s but it is difficult to conclude if a transition has occurred based on Figure 5.5 alone.

Observations of the steel counterfaces after the test show thick transfer films (see Figure 5.14C) not seen on sapphire counterfaces. The deposition of debris on the steel counterface and the eventual formation of a transfer film can explain the different friction behaviors between PEEK sliding against steel and sapphire. This transfer film formation will likely influence the adhesive friction and contact temperatures. The role transfer films play in such processes will be further discussed. The results obtained with constant speed friction tests at U = 100 mm/s and W = 10 N (Figure 4) are also included in Figure 5 (solid symbols). Since none of these values fall within the range of speed where μ falls with increasing U, it supports that thermal effects were not important for results with constant speed conditions (Figure 5.4) within the tested range.

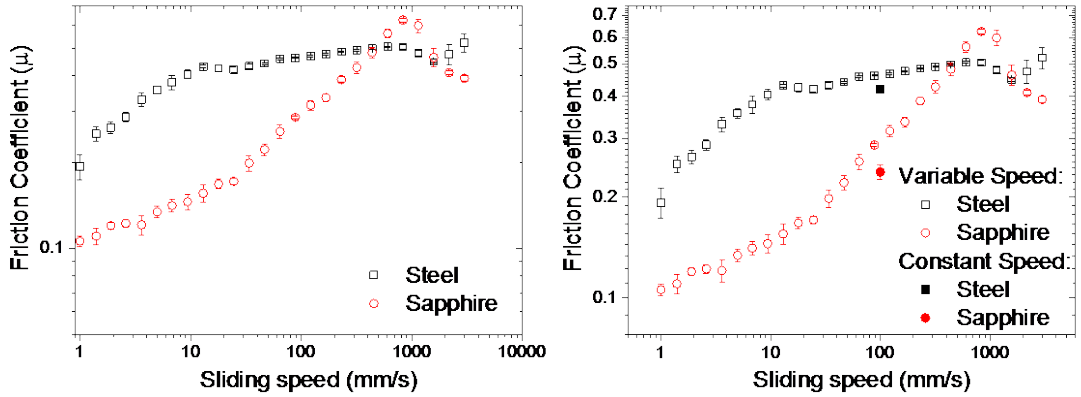

Figure 5.5. Evolution of friction coefficient μ with increasing speed **U** when PEEK balls were rubbed against steel and sapphire discs. The load was 10 N. The duration of each test was 700 s.

5.3.3 Temperature Rise During Friction Test

To understand how friction μ and surface temperature T_s evolves during rubbing, a thermocouple was used to detect the counterface temperature just behind the trailing edge of the contact T_{sn}. T_{sn} is used to estimate T_s and T_{sn} is likely to be lower than T_s. A steel counterface was used with a 10 N constant load and velocities $U = 10$ mm/s, 100 mm/s, 2 m/s, and 4 m/s. Each tests lasted 5 mins. The change in μ and T_{sn} with time are shown in Figure 5.6 and 5.7 respectively. For all velocities tested, μ grows within the first few seconds of sliding, after which a steady state is reached. Lower velocities 10 mm/s and 100 mm/s exhibit a plateau in friction coefficient for the duration of sliding. However, faster sliding speeds 2 m/s and 4 m/s the friction values fluctuate much more with time. The stable μ observed with low sliding speeds is accompanied by low stable $T_{sn} \approx 20$°C as shown in Figure 5.7 However, for U = 2 m/s and 4 m/s tests T_{sn} grows continuously. Temperatures also appear to trend towards a plateau at longer sliding times. For U = 4 m/s T_{sn} has reached above 130°C after 300 s. In this case, it is likely that T_s is higher and may approach the PEEK's glass transition temperature T_g ~ 150°C. The high temperature may explain the more erratic nature of μ obtained at high U.

The plateau $\mu \sim 0.5 - 0.6$ in all conditions match relatively well with results obtained from the constant load friction test (open square in Figure 5.5, and section 5.3.2). In addition, the transition from stable μ at low U to more fluctuating μ at high U in Figure 5.6 coincides with observation in Figure 5.5, with stable μ with U < 1 m/s and μ with larger scatter thereafter. In all cases, some adhered debris was found on the steel counterface and is similar to the debris observed in constant load tests (see Figure

5.14A) discussed in section 3.2. The deposition of debris to the counterface is likely to play a significant role in how friction and surface temperatures evolve. Thus the observed discrepancy in μ may be due to the amount of time allowed for adhered debris to form.

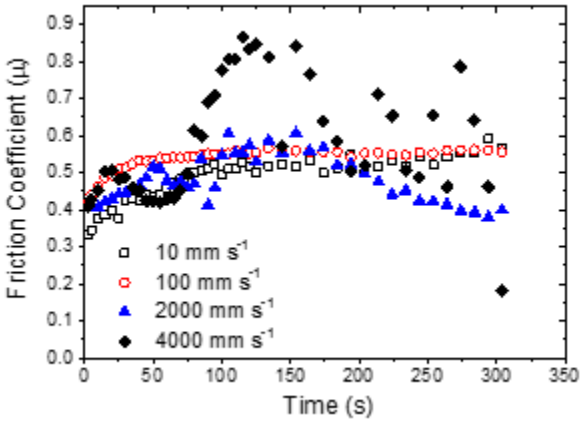

Figure 5.6. Evolution of friction over time for PEEK sliding against steel.

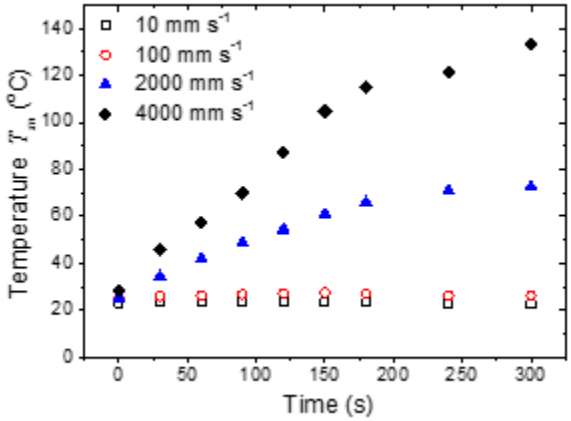

Figure 5.7. Evolution of surface temperature over time for PEEK sliding against steel.

5.3.4 Surface Temperature With IR Thermography

The contact temperature produced by PEEK-steel contact was estimated at a position of the counterface as close to the trailing edge as possible in section 5.3.3. In order to directly measure the contact temperature during rubbing, IR thermography is applied to PEEK-sapphire contacts as outlined in section 5.2.3. The effects of applied load W and sliding speed U on contact temperature T_s, in the form of temperature maps, are shown Figures 5.8 and 5.9 respectively. The range of loads and speeds were selected to allow for comparison with results obtained with friction tests (as shown in sections 3.1 – 3.3).

Temperature maps obtained at U = 100 mm/s sliding speed with W between 1 N and 40 N are shown in Figure 5.8. Across the entire range of loads studied, a maximum contact temperature rise of 3.5°C (i.e. T_s = 28.5°C) occurs (see Figures 5.8 and 10A). While T_s remains relatively unchanged, the contact area, which can be estimated by the width of the temperature distribution in Figure 5.8, grows with increasing normal load. In addition, the contact area is not continuous, but rather is made of patches at low loads (W = 1 – 5 N). With increasing load, partial contact develops into full contact. These observations supports that for load controlled friction, in the case of PEEK against sapphire (see constant speed friction test results presented in Figure 5.4 (section 3.1)), thermal effect is not important. Provided the PEEK ball is not in contact with any third body debris, the same observation may be extended to PEEK sliding on steel.

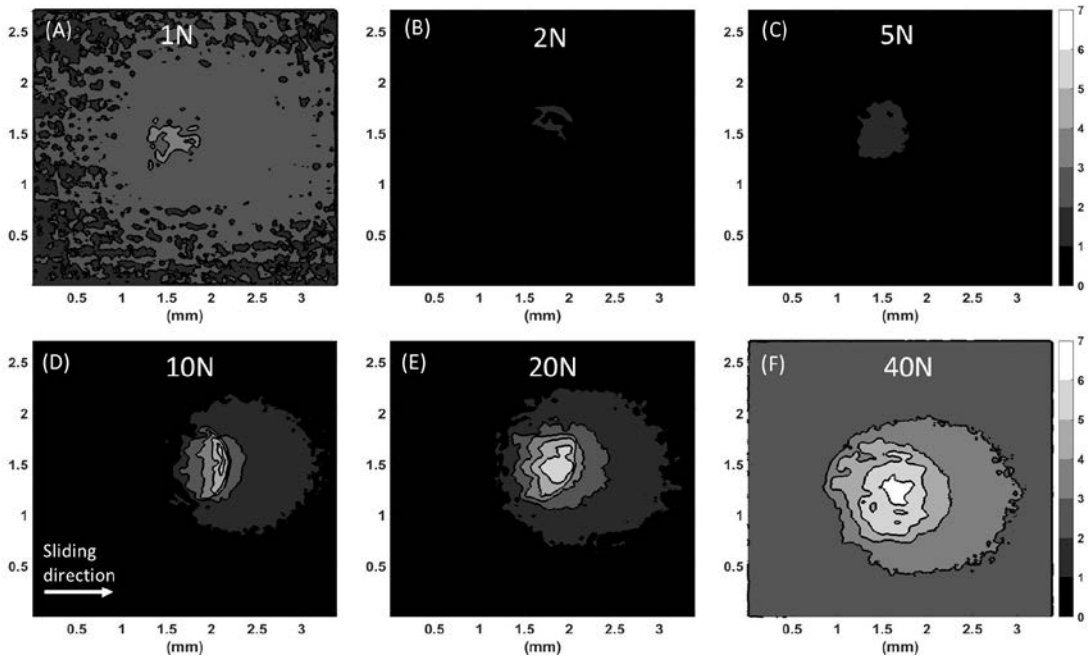

Figure 5.8. Maps of surface temperature rise $\mathbf{T_{IR}}$ for constant load **W** = 10N and increasing speed **U** for stationary PEEK ball against sliding sapphire counterface. Each image correspond to the temperature at time = 5 minutes. The color scale shows the local temperature rise in the contact.

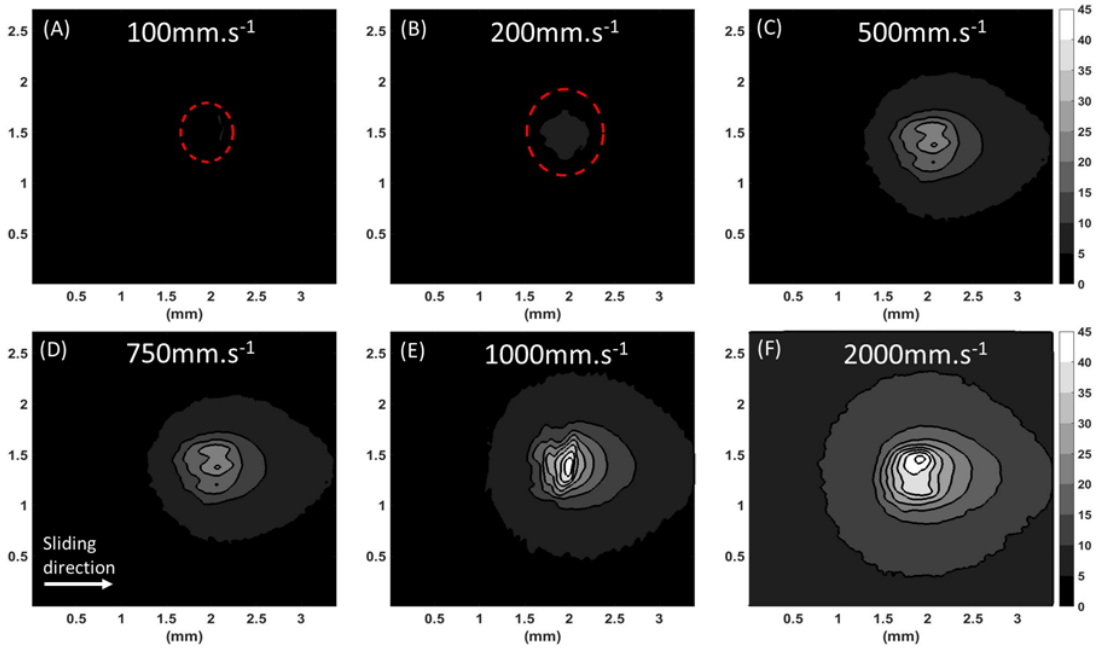

Figure 5.9. Maps of surface temperature rise $\mathbf{T_{IR}}$ at constant speed U = 100mm/s and increasing load W for stationary PEEK ball against sliding sapphire counterface. Each image correspond to the temperature at time = 5 minutes. The color scale shows the local temperature rise in the contact.

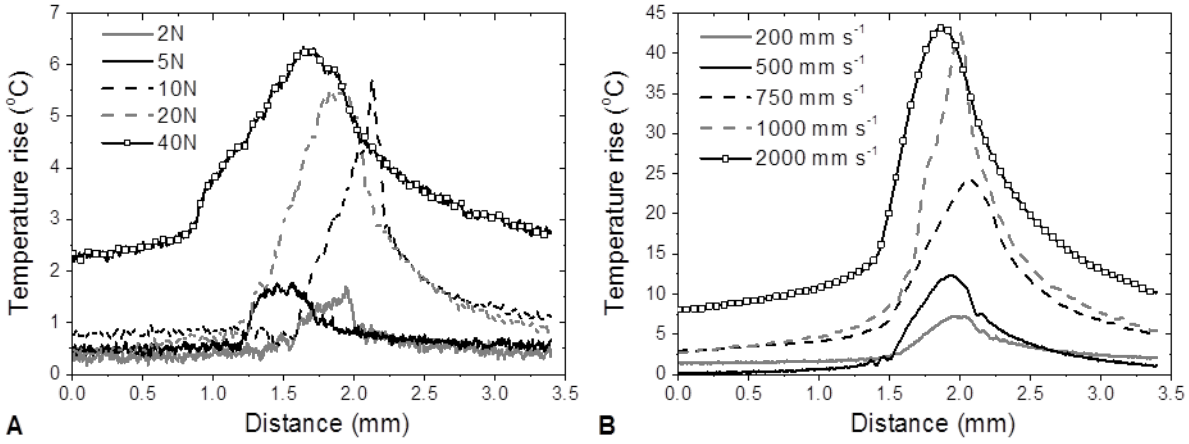

Figure 5.10. Profile of the average temperature rise $\mathbf{T_{IR}}$ across the center of the contact: (A) constant U = 100 mm/s (Figure 4) and (B) constant W = 10 N (Figure 8).

The temperature maps for PEEK-sapphire contact with a constant 10N load at various velocities are shown in Figure 5.9. The corresponding temperature profiles are

presented Figure 10B. For U = 100 – 200 mm/s, only slight temperature rise is observed. With increased sliding speeds significant changes are observed in both the contact shape and the contact temperature. For U above 1 m/s a temperature rise of 40°C is observed, giving a maximum surface temperature of about 65°C. These observations can be used to explain how coefficient of friction μ changes with U for PEEK-sapphire contact (open circles, Figure 5 in section 3.2). Assuming that the real area of contact A_r corresponds to the hottest sections of the temperature maps, both Figures 5.9 and 10B show that A_r grows with speed until U = 500 mm/s. This is accompanied by a modest temperature rise at U = 500 mm/s (7°C average) in Figure 10B. This supports that the initial increase of μ with U for PEEK-sapphire contact in Figure 5.5 can be explained by an increase in true contact area.

For U above 500 mm/s, a distinct hot zone has been established, with further increase in U giving higher T_s. Nevertheless maximum T_s observed is 65°C and is below any thermal transition for PEEK such as T_g ~150°C. This is insufficient to cause the PEEK to soften and allow the thermal-control model to be applied to explain how μ decreases with U at high U for PEEK-sapphire contact shown in Figure 5.5. The observed drop in μ indicates decreased interfacial shear strength, but can occur due to a number of reasons. The most likely explanation stems from differences in heat dissipation between the experiments. For sliding speeds above 1 m/s significant heat drag is observed in Figure 5.10B. This phenomenon is commonly found for conditions with large Peclet numbers[156]. Since the sapphire disc has a higher thermal conductivity than the PEEK ball, most of the frictional heat generated at the interface is

conducted into the moving sapphire body. Based on the partition equation in the appendix Section 5.6.3 it can be assumed that a majority of heat is conducted into the sapphire disc. The portion of the frictional heat is conducted into the disc $\alpha_{disc} > 0.97$ for all sliding speeds tested. Heat will also be dissipated from the disc to the surroundings through convection. The resulting temperature distribution in the disc can be described by the Peclet number $Pe = \frac{Ua}{\chi}$, where a and χ are diameter of the contact and thermal diffusivity of the disc respectively. Laraqi has analytically shown that for $Pe > 20$ considerable heat drag develops[156]. In Laraqi's analysis there appears to be a threshold velocity where $Pe > 30$ and the partition coefficient no longer changes. At such a sliding speed they suggested that a thermal balance arises between frictional heat generated in the contact and heat removed due to convection[156]. Unless all of the heat generated at the contact is dissipated into the surroundings the surface temperature will rise with increased sliding. Rowe demonstrated this affect with a rubber half sphere sliding against an IR transparent CaF_2 disc under both forced and natural convection[155]. The reduced heat transfer efficiency of natural convection resulted in a continuous rise in surface temperature with increased sliding[155].

For the experimental conditions used in this study the Peclet number reaches 20 at 1.08 m/s and 30 at 1.62 m/s. The observation of heat drag in Figure 8 is similar to the response predicted by Laraqi[156] and observed by Rowe[155]. High sliding speeds may prevent some of this heat from being conducted to the surroundings. The amount of retained heat at a specific location will depend on how much time it has in dissipating the heat between two subsequent contacts with the PEEK ball. Since the sapphire discs

for friction tests (sections 5.3.1 – 5.3.3) and IR thermography (section 5.3.4) are 46 mm and 100 mm respectively. The smaller disc used for friction tests would give less time for heat to be removed. In addition, temperature maps were collected using a sliding time of 5 minutes but friction experiments in Figure 5.5 took roughly 12 minutes to complete. Hence higher surface temperatures may reach PEEK T_g during friction measurements due to this retained heat. The drop in friction observed at 1 m/s may be the result of temperatures above the glass transition. The relationship between surface temperature and sliding conditions will be further discussed.

5.4 Discussion

5.4.1 Flash Temperature

Frictional heat generated at a contact causes contact temperature to rise. The hottest flash temperatures should then correspond to regions of the highest friction and contact pressure. Average flash temperature rise for PEEK-sapphire contact can be estimated using Jaeger's solution assuming a uniform circular source[152]. A number of models can be used such as that by Tian and Kennedy [153] or Archard[150]. Rowe *et. al* derived a partitioned flash temperature solution for a moving heat source based on these models and an equation based on Jaeger's model is used for the predicted temperature rise[155] (see Appendix section 5.6.3 for details). Since the heat flux density $\dot{q}$ due to friction μ is $\dot{q} = \mu pU$ where p is the average normal pressure and sliding speed U (see appendix section 5.6.3), assumptions on p and μ need to be made. Note that for PEEK-sapphire contact, the real contact area changes with increased sliding speed. The temperature maps allow for observation of how temperature is

distributed within the contact but not pressure or friction. This means that measured surface temperatures may deviate from the predicted flash temperature depending on assumptions made in the calculation. In this case, the pressure and contact area are assumed to be Hertzian and μ is a constant. Flash temperature predictions are done for the constant load condition W = 10 N using both nominal and maximum pressure as well as the mean $\mu = 0.3$ and maximum $\mu = 0.6$ (see Figure 5 for μ value). Predicted flash temperature rise T_f (lines) and maximum local surface temperature rise T_{IR} (open squares) from IR thermography are shown in Figure 5.11. Note T_{IR} (squares, Figure 11) and T_f (nominal) based on average pressure and mean μ = 0.3 (solid line, Figure 11) match relatively well. However, T_{IR} are lower than T_f predicted using the maximum values for pressure and friction coefficient.

Both the observed (from IR thermography) and predicted temperatures are well below any possible PEEK thermal transition such as T_g ~150°C. In fact the predicted nominal flash temperature would require a sliding speed of 48 m/s to reach such a transition. The maximum temperature rise is about 40°C as shown by the temperature maps obtained by IR thermography (Figure 5.9). The temperature maps are obtained after 5 minutes of sliding. During this sliding time temperature remains stable. It is possible that higher temperatures may occur at asperities before this steady state was reached. Such temperature spikes appear to be on a time and spatial scale smaller than the resolution of the IR camera.

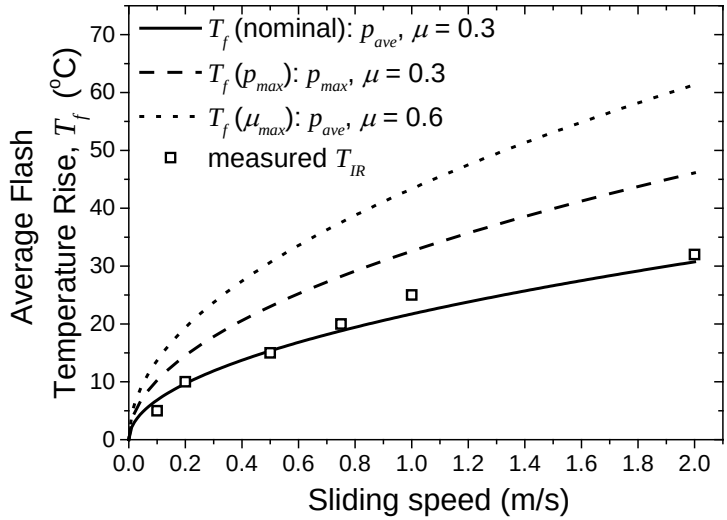

Figure 5.11. Flash temperatures calculated for stationary PEEK ball against rotating sapphire disc using the nominal and maximum contact conditions. A constant load of 10N was used. The labels and their corresponding conditions are: $\mathbf{T_f}$(**Nominal**)= nominal pressure, $\boldsymbol{\mu}$ = 0.3; $\mathbf{T_f}(\mathbf{p_{max}})$= maximum pressure, $\boldsymbol{\mu}$ = 0.3; $\mathbf{T_f}(\boldsymbol{\mu}_{\mathbf{max}})$= nominal pressure, $\boldsymbol{\mu}$ = 0.6; $\mathbf{T_{IR}}$ – contact temperature from IR thermography. Details of the predictions is in section 6.3 in the Appendix

The thermal conductivity of the counterface plays a significant role in determining the flash temperature T_f. Figure 5.12 shows predictions of T_f of a PEEK ball against sapphire, steel, glass and PEEK (see the appendix Section 5.6.3 for materials properties). Steel and sapphire are good thermal conductors. They have similar thermal conductivity K and diffusivity χ. Hence their predicted T_f are nearly identical (see solid line and dash line in Figure 5.12 for sapphire and steel respectively). Glass was not used as a counterface in any experiment, but it demonstrates how a thermal insulator may alter the surface temperature. Its predicted flash temperature rise reaches T_g ~150°C even for speeds lower than 1 m/s (dotted line, Figure 5.12). PEEK is a good thermal insulator and much softer than any of the other counterfaces. Its low thermal conductivity K and diffusivity χ as well as larger Hertzian contact area produces even

higher T_f than that of glass. Note, while the predicted T_f for glass and PEEK counterfaces is higher than T_g when U is larger than 1 m/s and 0.4 m/s respectively, in practice the contact temperature will be capped at the softening temperature of the PEEK balls.

The T_f prediction and the experimental contact temperature for PEEK-sapphire contact matches well, as shown in both Figures 5.11 and 5.12. Based on the T_f predictions, one would expect PEEK-steel contact to have similar temperature rise to that of PEEK-sapphire contact. Friction tests however, as presented in Figure 5.7, and also in Figure 5.12 (squares) shows that the contact temperature for PEEK-steel contact, as estimated by the local temperature of steel disc just next to the trailing edge of the contact, is higher than the predicted T_f. The T_f prediction with PEEK-PEEK contact might have provided the cause of such discrepancy. After friction tests PEEK debris and transfer films were found on steel counterfaces. This adhered debris likely facilitated frictional heating and resulted in much higher temperatures than that of PEEK-bare steel contact. Having said that, the measured temperature for PEEK-steel and the predicted T_f of PEEK-PEEK contact approaches T_g ~150°C at a sliding speed of 4 m/s and 0.4 m/s respectively. This may be due to two reasons. Firstly the measured temperature from PEEK-steel contact is obtained outside the contact (close to the trailing edge). Thus it is likely that the actual temperature inside the contact is higher. As a result transfer films found on steel counterfaces may have then been formed at temperatures at or above the glass transition T_g. Secondly, the PEEK transfer film is discontinuous. Hence during

rubbing the PEEK ball may be in contact of both transfer film and steel. The morphology and properties of transfer film will be discussed in section 5.4.2.

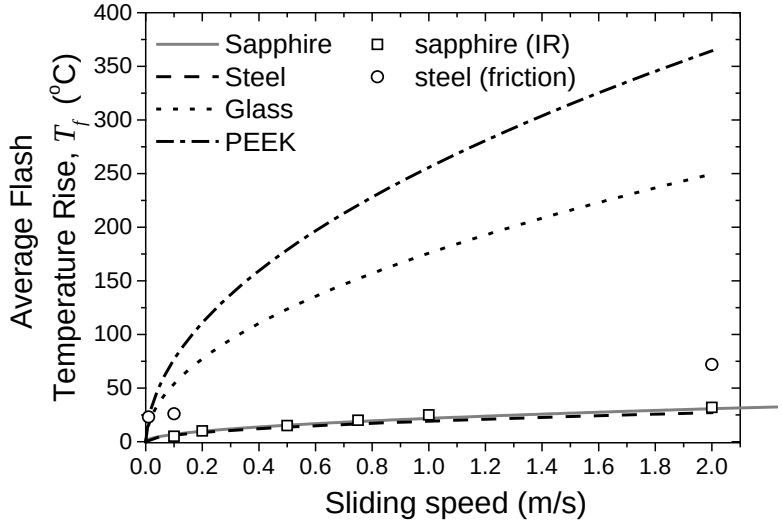

Figure 5.12. Predictions of lash temperatures for PEEK ball sliding against counterfaces of sapphire, steel, glass and PEEK. A constant load of 10 W, nominal pressure and μ = 0.3 were used for these predictions. All lines are predictions. The circles and squares are experimental results. Circles are temperature recorded for PEEK balls against sapphire disc with IR thermography. Squares are temperature recorded for PEEK balls against steel disc during friction tests with a thermocouple.

5.4.2 The Role Of Transfer Films On Friction Mechanisms.

The sliding friction behavior for PEEK was found to depend significantly upon the counterface material. Under identical test conditions, PEEK-sapphire and PEEK-steel contacts result in different frictional traces (see Figure 5.5). Both counterfaces had very low surface roughness (R_a 10 – 20 nm) and so ploughing components of friction are minimal. Observation of the ball and counterface following experiments suggests that adhesive friction plays an important role. The laser confocal micrographs (Keyence VK9700) in Figure 5.13 show the resulting wear scars on the PEEK balls after the

constant load friction tests (Figure 5.5). These wear scars are of similar size and indicate that the contact area was comparable between tests. However, the ball surface that slid against steel has a distinct red hue towards the edges of the wear scar, which is not observed on the PEEK balls that were rubbed against sapphire disc. The red hue is believed to be iron oxide Fe_2O_3 that was transferred from the steel counterface.

While the sapphire counterface remained clean, PEEK debris was observed on the steel surface following each experiment. The interaction between the steel and PEEK surfaces may explain the different friction responses observed. Compared to the steel counterface, sapphire is both harder and chemically inert. Both steel and sapphire counterfaces are very smooth (R_a 10 – 20 nm) and so it is quite difficult for debris to be physically entrapped by asperities. Examples of the debris found on steel counterfaces are shown in Figure 5.14. The adhesion of PEEK debris to the steel surface may be the result of chemical bonding. PEEK has been shown to be a suitable adhesive used in bonding steel surfaces together[180]. The adhesive strength however depends on the reaction products formed at the interface. Sugama suggested that adhesion of PEEK to steel results from metal-O complexes that form[180, 181]. Studies of the adhesive interface with X-ray photoelectron spectroscopy (XPS) revealed the formation of new peaks in the C_{1s} and O_{1s} spectra. It was believed that these peaks result from Fe-O-C and Cr-O-C compounds. These species may form due to a charge transfer reaction between C=O in the PEEK and elemental Fe or Cr in the stainless steel. Conditions in which Fe_2O_3 formed at the interface was found to correspond to decreased bond strength[180]. Similar reaction products may be responsible for the adhesive behavior of PEEK debris

to steel counterfaces. The formation of Fe_2O_3 during sliding could also result in weakly bound transfer films and the observed residue on the ball surface. In the studies by Sugama, the PEEK was bonded to steel at temperatures above 400°C[180, 181]. Such temperatures might be necessary to form the metal-O complexes they described. However, the activation energy for the formation of adhesive chemical bonds between PEEK and steel could be supplied by friction alone. For instance, Buckley used Auger spectroscopy to show evidence of chemical bonding when polyimide and PTFE were rubbed against metal surfaces [182]. For PTFE it has been observed that friction induced chain scission events facilitate the bonding of debris to steel surfaces[183, 184]. It is possible that chain scission events also underlie the bonding of PEEK debris to steel. However, these theories are difficult to prove and are beyond the scope of this work. Further chemical analysis of the interface between transfer film and steel counterfaces will be needed.

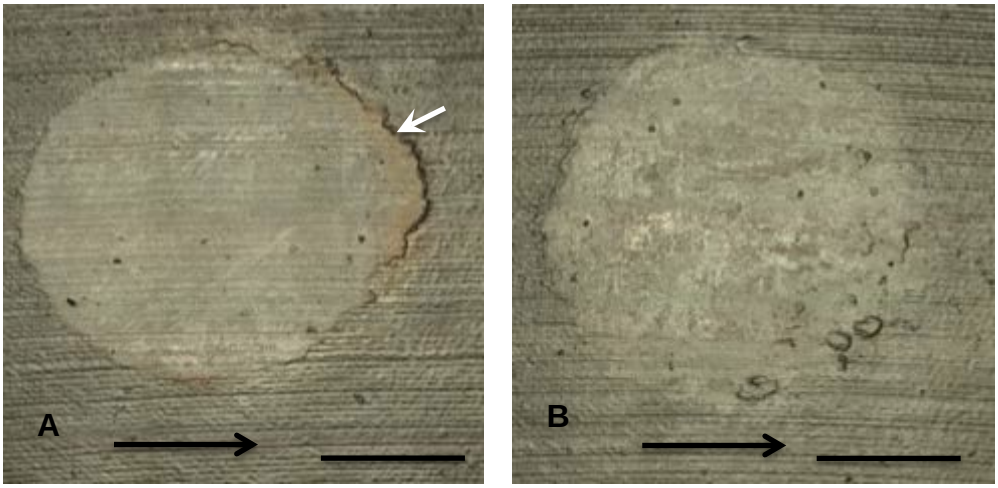

Figure 5.13. Ball surface after constant load experiment (as shown in Figure 5) A) Steel counterface B) Sapphire counterface with scale bar 500μm. The load was 10 N. *White arrow in A) highlights region of possible Fe_2O_3 transfer **Black arrow shows direction of disc sliding

The steel counterfaces from the friction experiments are shown in Figure 5.14. In Figure 5.14A and 5.14B debris from the constant speed increasing load experiment (Figure 5.4) is visible. Similarly, PEEK debris is also visible on the steel counterface from the constant load increasing speed experiment (Figure 5.5) in Figure 5.14C and 5.14D. The morphology of debris formed on the steel surface differs significantly between the experiments. The constant speed increasing load experiment results in the deposition of small discrete particles. However, long continuous sections of film are visible for the constant load increasing speed tests. Although these transfer films do not cover the steel surface uniformly some sections appear to be uniform in thickness and well adhered to the surface. These film sections are roughly 1 μm thick as measured by the confocal microscope (Keyence VK9700) and accompanying profilometry software. The formation and nature of this transfer films will affect the friction response observed

with PEEK-steel contact. As previously discussed, the surface debris can promote frictional heating in PEEK-steel contact and temperatures above T_g ~ 150°C can be reached with modest sliding speeds in PEEK-PEEK contact (see Figure 5.12). The PEEK-PEEK calculated flash temperatures suggest some sections of transfer film may have even been formed in a molten state. For PEEK this would require temperatures above 350°C. Ettles described this phenomenon and proposed a thermal control model for friction[137]. For this model, the melting point T_m is the maximum attainable surface temperature. Heat generated due to friction will go into melting more of the polymer rather than raising the surface temperature. Friction will also decrease with sliding speed due to increased melting of the bulk. However, the PEEK on steel friction coefficient remained stable for most velocities. Additionally, temperature measurements taken near the contact suggest temperatures well below T_m. High surface temperatures would also likely result in some visible changes to the steel surface. For instance “bluing” of stainless steel will occur during tempering. If melting does in fact occur during film formation, the friction and thermal effects remain localized. This localized melting could explain why films form as long continuous patches rather than a single sheet in Figure 14C.

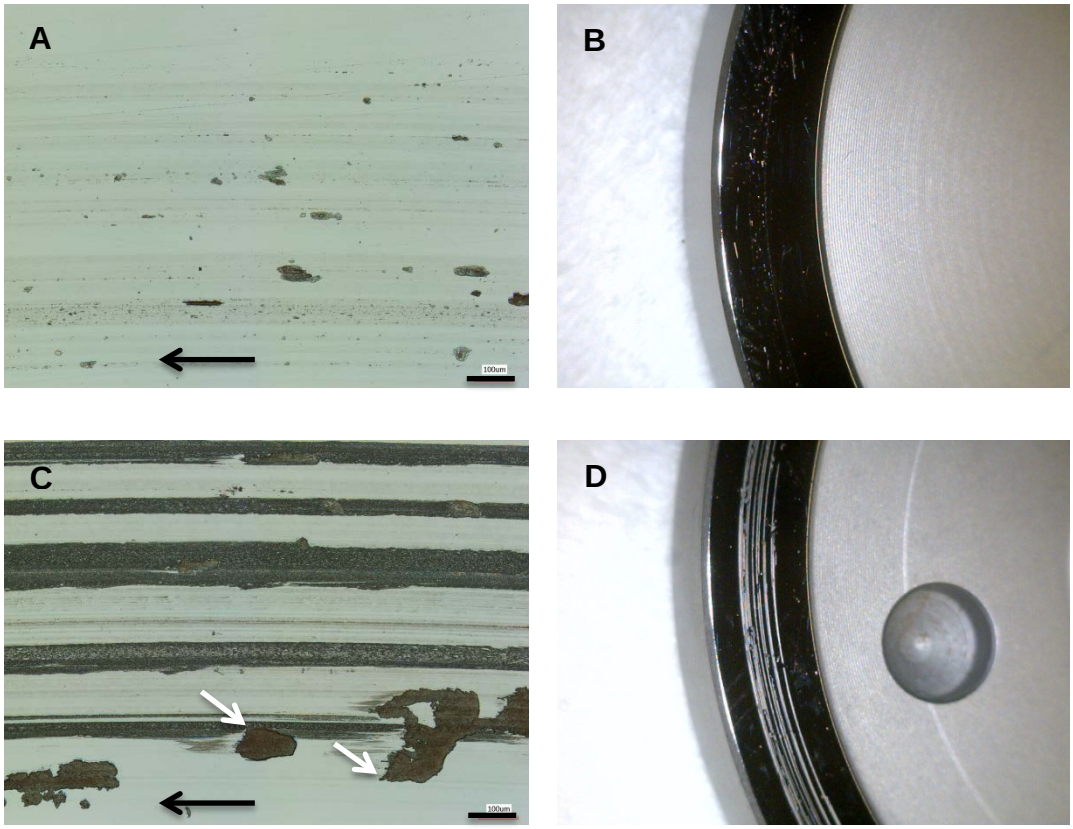

Figure 5.14. Debris transferred to steel counterfaces from A) constant velocity friction tests (see Figure 4) with scale bar 100μm B) counterface following constant velocity friction test C) constant load friction test (see Figure 5) with scale bar 100μm. D) counterface following constant load friction test. Black arrow represents the direction of sliding. White arrow highlights delaminated debris. The black and white regions of A and C correspond to PEEK film and steel surface respectively.

Differences in the friction response between PEEK-steel and PEEK-sapphire can also be attributed to the debris found in Figure 5.14. Recall in Figure 5.5 that for increasing sliding speed tests the PEEK-sapphire friction grew to a maximum before dropping off at speeds above 1m/s. However, PEEK sliding against steel exhibited a stable friction period across a wide range of speeds. The stability of this friction period may be as a result of localized surface phenomenon. The friction response does not

rapidly diminish with speed like in the thermal control model described by Ettles[137]. However, such a description is best extended to scenarios where melting of the entire bulk sliding body takes place. The formation of films observed in Figure 5.14C represent phenomenon extremely close to the sliding surface. The friction measurements and corresponding debris transfer show that PEEK sliding behavior is highly sensitive to environmental factors. Adhesion, deformation and delamination components of friction all may contribute to the observed response. The effect of adhesive friction is most apparent when comparing results from PEEK-steel and PEEK-sapphire contacts. Adhesive friction is typically described by the equation (1) [179].

$\mu_a = \frac{\tau_o}{\sigma_y} + \alpha$ Equation (1)

where the coefficient of friction due to adhesion μ_a is governed by the interfacial shear strength τ_o which corresponds to the frictional force f per unit area A, i.e. $\frac{f}{A}$. A pressure coefficient α is used to account for the fact that shear strength τ_0 will increase linearly with increasing pressure[179].The plastic flow stress or yield pressure σ_y will change the real contact area A_r depending on load W according to $A_r = \frac{W}{\sigma_y}$. Equation (5.1) can then be written as

$\mu_a = \frac{\tau_o A_r}{W} + \alpha$. Equation (5.2)

For the majority of sliding conditions as shown in Figure 5.4 and Figure 5.5, friction of PEEK-steel contact is greater than that of PEEK-sapphire contact. Differences in contact area will affect the measured friction coefficient and could account for the difference. A calculation of Hertzian contact (see appendix section 5.6.2) would produce

a contact diameter of 0.52mm for both sapphire and steel under a 10N static load. Figure 5.13 also indicates that wear scars are comparable with diameters ~1.5mm. Since it was not possible to observe changes in the contact area for PEEK-steel *in situ* a direct comparison cannot be made. Provided the contact areas and pressure coefficients are comparable between tests, it can be presumed that adhesive friction differs due to interfacial shear strength τ_0. The greater adhesive friction μ_a response results from greater surface forces between PEEK and steel compared to sapphire. Friction forces arise from the breaking of asperity contacts as well as shearing of bulk material in and around the contact. As shown in Figure 5.15, shearing will occur at some distance h below the surface. Debris will be removed from the bulk if the adhesive strength τ_i at the interface exceeds the bulk shear strength of the polymer τ_b. Subsurface cracks can also form and grow during sliding. The forces generated at this crack interface will contribute to friction and explains the high values observed during such debris formation. In Figure 14C there also appears to be thicker debris fragments that were sheared from the bulk and are highlighted by a white arrow. These fragments are much thicker than the 1μm transfer film sections and are roughly 3-5μm thick as measured by profilometry (Keyence VK9700). Figure 15C shows a larger section of thin continuous transfer film. The difference in such debris formation can contribute to different adhesive friction μ_a. As illustrated in Figure 5.15 the thicker debris would correspond to shearing of material further into the bulk. Such debris was also found for the constant load constant sliding speed tests (Figure 5.6) and was most prevalent for speeds above 2m/s. Recall there was greater fluctuation in the friction response for these higher sliding speeds as well. The

way in which debris is removed from the bulk could contribute to the observed friction responses for PEEK-steel sliding. In the absence of debris transfer, like for PEEK-sapphire, the friction response depends largely on changes in the contact area rather than shearing of the bulk.

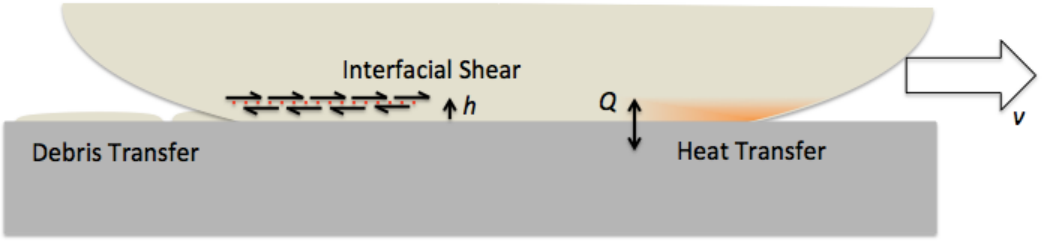

Figure 5.15. Illustration of interfacial processes that contribute to friction.

Blanchett described a similar delamination phenomenon for PTFE and discussed its relationship with sliding conditions[185]. Low wear and friction corresponded to drawing of fibrils across the sliding surface. However, severe wear was due to subsurface deformation and fracture. This transition from fibril drawing to delamination depends on how friction changes with temperature and sliding speed. Delamination occurs when the shear stress at the internal interface is less than the shear stress at the sliding surface[22]. Although fibril drawing is unlikely to occur in PEEK below T_g frictional heating at the surface can allow for smooth drawing of tribofilms. The presences subsurface cracks or penetration of heat into the bulk will disrupt this process as shown in Figure 5.15.

5.4.3 Transfer Film

The experimental results suggest that the sliding friction behavior of PEEK is highly dependent on the transfer of debris to the counterface. Briscoe explained that a polymer's ability to form thin continuous transfer layers is related to its drawability[179]. PEEK can undergo large deformations before break and when heated above T_g can be drawn into highly oriented films[74, 186, 187]. To further demonstrate the relationship between drawability and transfer film formation the infrared dichroic ratio of a PEEK film was measured. This technique has been shown to be able to assess orientation in PEEK[188, 189]. A transfer film formed on steel counterface during constant load friction experiment (Figure 5.5) was carefully removed from the disc and was examined with FTIR (Shimadzu IRAffinity-1) using an ATR accessory (PIKE MIRacle) and its spectra are shown in Figure 5.16. Measurements were taken using a ZnSe polarizer (Spectra-Tech) parallel and perpendicular to the sliding direction. Backgrounds were taken with the polarizer in place and only the polarizer was rotated between measurements. The dichroic ratio can be measured using the ratio of absorbance peaks from the parallel and perpendicular spectra $D = \frac{A_{\parallel}}{A_{\perp}}$. The results show similarly high dichroism at all wavenumbers and indicate that the film is stretched in the direction of sliding. The diphenyl ether peak at 1190 gives dichroic ratio of 3.4 and the 1648 band associated with stretching of carbonyl groups gives a dichroic ratio of 2.8. Typically, dichroic ratios D increase for increasing draw ratios λ but are not equivalent in value. Measurements were also taken of the wear scar and untested sections of the ball. Neither surface shows evidences of orientation from the polarized infrared spectra. The ball wear

surface may exhibit some orientation but the underlying bulk material masks the signal. Further work to understand film structure and any possible molecular orientation will be needed.

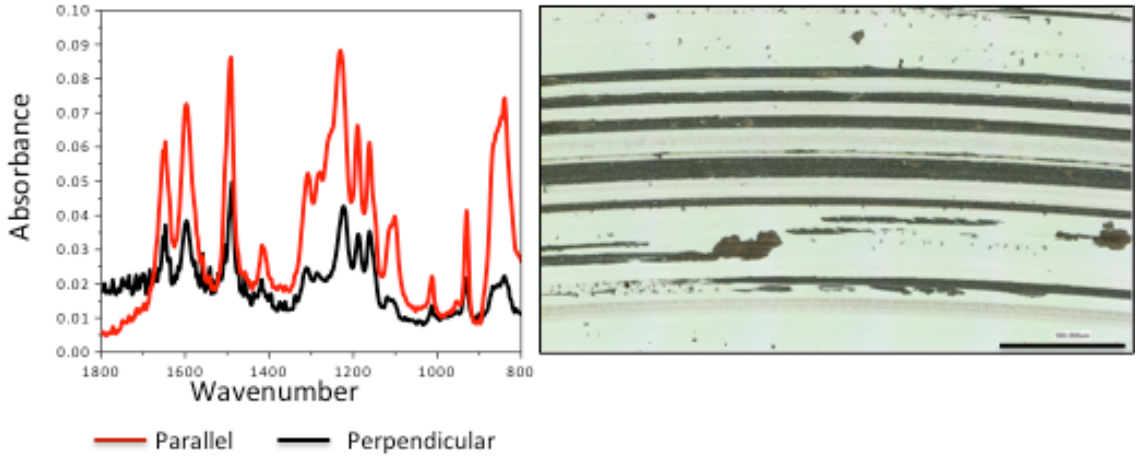

Figure 5.16. Polarized FTIR-ATR measurement of transfer film parallel and perpendicular to sliding and micrograph of the film with scale bar 500μm**.**

The dichroic ratio measurements support the notion that films form in a similar manner to drawing processes. For temperatures above the glass transition T_g PEEK films can be extruded to draw ratios $\lambda \sim 3$[74]. During sliding of PEEK, the deposition of debris on steel surfaces can promote frictional heating that increases the drawability of transfer layers. Subsurface delamination can disrupt this drawing process and result in increased friction. However, further understanding of PEEK transfer film formation and its adhesion to steel substrates will be needed.

5.5 Conclusion

In this study, the friction and surface temperature response of polyetheretherketone (PEEK) was monitored under dry sliding conditions with pressure and velocity as variables. Both stainless steel (AISI 52100) and sapphire counterfaces were used during friction studies. The counterfaces have similarly low roughness R_a 10-20nm but result in very different friction behavior. PEEK on steel appears to have a greater adhesive friction response than sapphire due to stronger electrostatic surface forces. Under all test conditions, PEEK debris was found transferred to the steel surface. Iron oxide residue also appears on the PEEK surfaces and indicates some chemical interaction took place during sliding. The transfer of debris to the surface explains how temperatures approaching melt or T_g can occur. Observation of frictional heating with full field infrared thermography supports this theory. Temperature maps of the contact for PEEK sliding against sapphire produces a temperature increase of 40°C with a 10N load and 2m/s sliding velocity. Although such a temperature rise is well below any thermal transition for PEEK, models for the average flash temperature match closely. Surface temperatures approaching the melt or T_g require sliding against an insulating material. Transfer films result from the localized heating of surface debris. The process is similar to drawing or extrusion of polymers at temperatures above the glass transition. Exposure to plasticizers or excessive sliding speed can disrupt this transfer film formation and lead to erratic and severe coefficients of friction. The friction and surface temperatures for PEEK depend on this transfer film formation process and cannot be explained by pressure and velocity alone.

5.6 Supplemental Materials

5.6.1 Calibration Curves

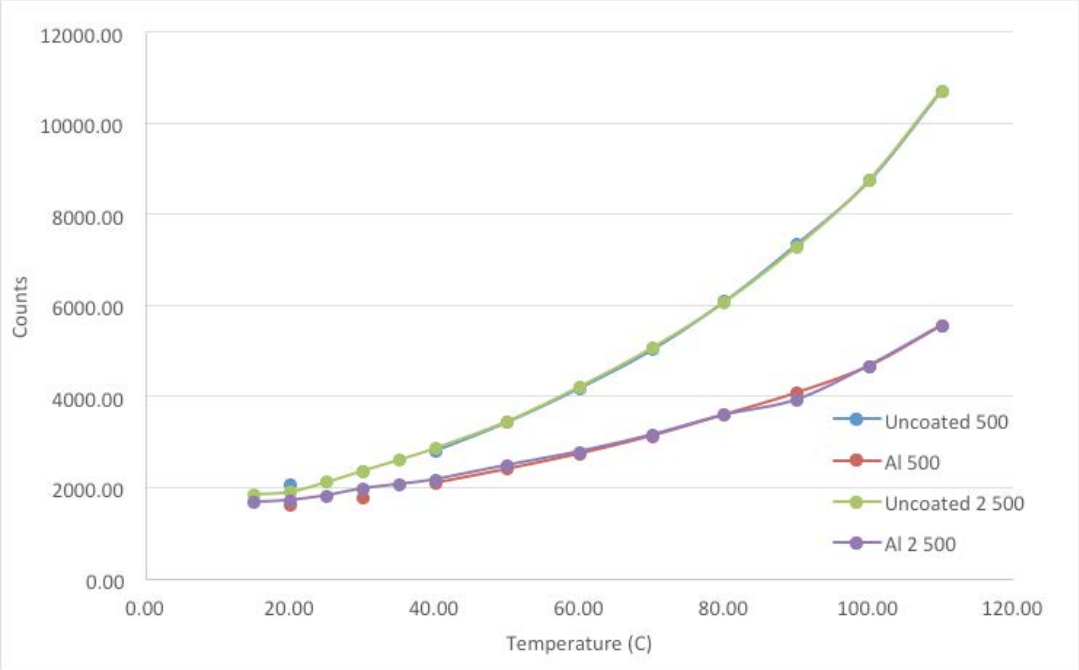

Figure 5.17. Single-pixel camera counts PEEK ball and uncoated and Al coated sapphire disc

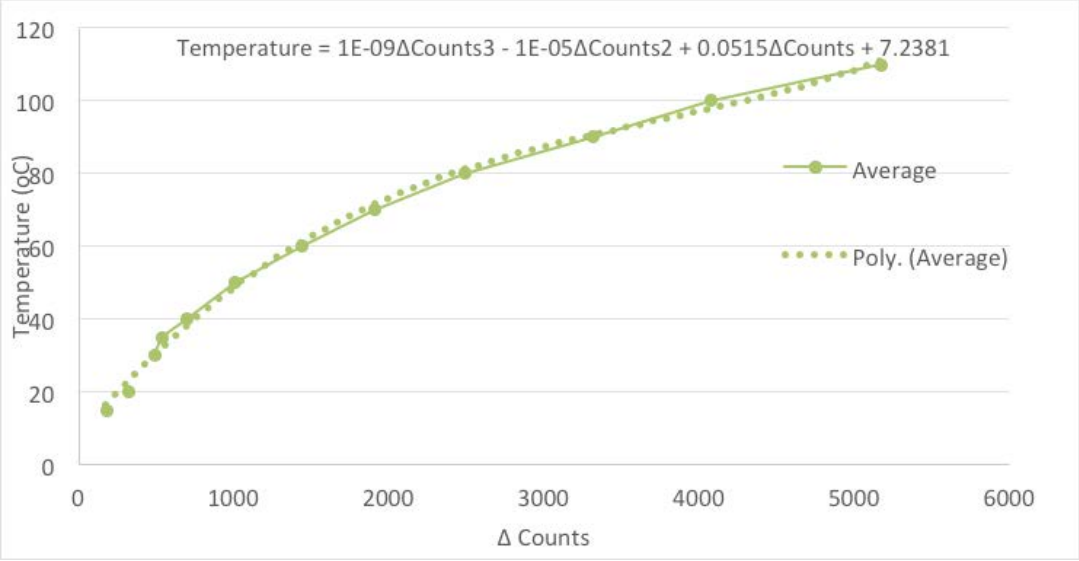

Figure 5.18. Calibration curve for IR experiment

5.6.2 Contact Mechanics

To calculate the nominal contact area and pressure the below equations and data are used. The material properties used in calculations is given in Table 5.2.

$$a = \sqrt[3]{\frac{3W}{8}\frac{(1-v_1^2)/E_1 + (1-v_2^2)/E_2}{1/d_1}}$$

$$p = \frac{W}{\pi a^2} \qquad p_{max} = \frac{3W}{2\pi a^2}$$

a Contact radius $[m]$

p Average contact pressure $[Pa]$

v_1 Poisson ratio Ball

v_2 Poisson ratio Disc

E_1 Elastic modulus Ball $[Pa]$

E_2 Elastic modulus Disc $[Pa]$

d_1 Ball diameter $[m]$

Table 5.2. Material properties for contact mechanics calculations.

Sample	PEEK	Steel	Glass	Sapphire
Poisson Ratio	0.38	0.3	0.22	0.25
Elastic Modulus (GPa)	3.6	200	90	345
Diameter (mm)	19	NA	NA	NA

5.6.3 Flash Temperature

Calculations for the average flash temperature are based on Jaegers model for a uniform circular source. The below equations and data are used for calculation. The material properties for calculation are given in Table 5.3.

$$T_f = \frac{0.903\dot{q}a}{0.849K_{disc}\sqrt{Pe}+1.064K_{ball}} \quad \alpha = \frac{0.849K_{disc}\sqrt{Pe}}{0.849K_{disc}\sqrt{Pe}+1.064K_{ball}}$$

T_f	Average flash temperature rise $[°C]$
α	Heat partition coefficient
μ	Coefficient of friction
W	Normal Load $[N]$
U	Relative sliding velocity $[m/s]$
a	Contact radius $[m]$
$A = \pi a^2$	Contact area
$p = W/A$	Average contact pressure $[Pa]$
$\dot{q} = \mu pU$	Heat flux per unit area $[W/m^2]$
K	Thermal conductivity $[W/mK]$
ρ	Density $[kg/m^3]$
σ	Specific heat $[J/kgK]$
$\chi = K/\rho\sigma$	Thermal diffusivity $[m^2/s]$
$Pe = Ua/\chi$	Peclet number

Table 5.3. Material properties for flash temperature calculations.

	$\chi[m^2/s]$	$K[W/mK]$	$\rho[kg/m^3]$	$\sigma[J/kgK]$
PEEK	1.41E-7	0.25	1320	1340
Steel	1.28E-5	46	7810	460
Glass	6.59E-7	1.1	2230	750
Sapphire	1.39E-5	42	3980	760

CHAPTER VI

RELATIONSHIP WITH HIGH TEMPERATURE DRAWING PROCESSES

The transfer films that are deposited on counterfaces are a frequently discussed topic in polymer tribology. Wear resistance is often ascribed to these films which protect the bulk polymer from abrasion by hard rough asperities. This behavior is common to the Polyetheretherketone (PEEK) family of polymers. However, little can be said regarding the underlying structure of PEEK transfer films. This chapter will focus on developing a deeper understanding of this behavior. Using a dual axis tribometer, PEEK pins were worn against a selection of counterfaces. Analysis of the transfer film and wear surface suggest that films form at temperatures above the glass transition T_g. Due to the inherently high friction and low thermal conductivity of PEEK such temperatures can easily occur when sliding against itself. Infrared thermal imaging of PEEK sliding on PEEK and glass surfaces was used to support this theory. The formation of transfer films resembles a unidirectional drawing process. Polarized FTIR-ATR measurements were used to assess chain orientation in the friction formed PEEK on steel transfer films.

6.1 Introduction

6.1.1 Wear of polymers

The need for advances in understanding of polymer wear behavior has been pointed out by a number of authors[190, 191]. Traditionally, wear studies have focused on how a particular polymer performs relative to some other polymer under a similar set of conditions. The resulting wear surfaces are then described in terms of the possible

mechanisms that might have occurred. Descriptions such as abrasive, adhesive, and fatigue have been used to link the observed damage to some material response. Briscoe further categorized these behaviors based on interfacial and cohesive zones[191]. However, challenges persist due to the inherent complexity of wear processes. It is possible for multiple wear mechanisms to occur simultaneously. The viscoelastic nature of polymers also means that bulk properties will change with temperature and strain rate. To date there are no a priori methods to determine a polymer wear behavior under a given set of conditions. Despite such shortcomings, significant advances have been made over the past half-century. In particular, the role molecular structure plays in the wear behavior of some polymers. This relationship is most well understood for linear semicrystalline polymers polyethylene and PTFE. In seminal work by Tabor et.al, it was found that the frictional response of these polymers could be related to their smooth molecular profiles[7, 27, 28]. This early work linking molecular structure to friction and wear has served as a wellspring for tribology research. The transfer film formation of PTFE is often exploited to create self-lubricating bearings. Processing conditions and fillers can even be tailored to promote this behavior. Similarly, knowledge of surface chain orientation in UHMWPE has been used to explain its sensitivity to cross shearing wear environments[8]. The current practice of crosslinking UHMWPE artificial joints can be credited to this understanding. Clearly, advances in the application of polymers to tribology depend on the ability to link structure-property relations to friction and wear[50].

The behavior of PEEK has been investigated in a number of wear configurations[14]. The vast majority have dealt with the wear of PEEK in pin-on-disc sliding[10]. Of particular interest has been the relationship between counterface surface roughness and wear[15-18]. Ovaert found that for unfilled PEEKs, an optimal surface roughness appears to exist[17, 19]. However, with increasing surface roughness there are only modest increases in wear. It is believed that this phenomenon can be attributed to the deposition of transfer films on the steel counterfaces. In theory, mechanically deposited films serve to protect the bulk from hard rough asperities. Laux and Schwartz later found that PEEK transfer film quality could be directly related to wear resistance[20, 21]. Most explanations contend that these films reduce wear by suppressing abrasion. Since the film modulus more closely matches the bulk, potential debris generating contact stress is reduced. However, this explanation neglects any changes in the polymer surface state that may beget wear resistance. Studies of the wear behavior of PAEK have indicated that oxidative crosslinking may take place during debris and transfer film formation[32, 34]. It is also likely that chain orientation takes place at the wear interface. It has been observed that PEEK is more sensitive to a cross shear wear environment than linear reciprocating possibly due to orientation strengthening[21]. Tanaka in fact observed a similar anisotropy in the friction response of PEEK and reported this amongst the unsolved problems in polymer tribology[11]. Despite evidence suggesting tribochemical changes in the surface of PEEK, there is no proof as to why or if such changes promote wear resistance.

6.1.2 PEEK Structure Properties

Polyetheretherketone (PEEK) is an aromatic backboned semicrystalline polymer belonging to the polyaryletherketone (PAEK) family of thermoplastics. As previously discussed, they are used extensively in tribological applications. Their high glass transition temperature T_g~150°C melting temperature T_m~350°C and solvent resistance make them an attractive engineering polymer for a wide range of environments. This has also meant PEEK is well studied and a wealth of knowledge exists regarding structure property relationships. PEEK typically achieves crystallinity between 30% and 45% depending on processing conditions and molecular weight[58]. Under identical conditions, lower molecular weight M_w PEEK will achieve a higher crystallinity compared to higher molecular weight M_w PEEK. The larger M_w will slow down chain folding and result in lower crystallinity. Chivers reported that increased crystallinity can increase the yield strength and elastic modulus but molecular weight alone does not have a significant effect[54]. Increasing molecular weight will however increase elongation at break. It has also been observed that molecular weight can influence fracture[39, 54] and fatigue[38] properties due to differences in microstructure. Typically, lower M_w PEEK forms larger spherulites with decreased tie chain density. Chu and Schultz found that lower M_w PEEK has reduced fracture toughness K_{IC} compared to higher M_w PEEK[39]. They also observed an increase in intraspherulitic fracture in lower M_w PEEK and attributed this to microstructure. Saib observed a strong relationship between M_w, crystallinity and tie chain density with fatigue behavior as well[38]. For higher M_w PEEK a Paris law stable crack growth behavior was found and this did not occur in the

lower M_w PEEK. Several authors have investigated a strain induced crystallization phenomenon in PEEK. Hamdan and Swallow reported that in compression crystallinity can increase for strain rates above 10^3/s[192, 193].

A number of researchers have attempted to improve mechanical properties of PEEK by tailoring microstructure through processing. Solid-state extrusion has been used to increase the modulus and strength of PEEK films along the drawing direction[73]. A die drawing process has also been employed to create samples with a modulus as high as 11GPa[76]. PEEK can achieve a preferred crystallographic orientation through extrusion and drawing processes[73, 76, 194, 195]. Films of PEEK grown through PTFE epitaxy are also found to achieve a similar structure[189]. Several spectroscopy studies of stretched PEEK films have been done to understand the influence of deformation on structure[196]. Daver and Cakmak employed a combined birefringence and wide-angle x-ray spectroscopy (WAXS) techniques to identify the structural ordering processes that occur during deformation of amorphous PEEK films in the rubbery state. Strain hardening was found to coincide with the appearance of nematic like ordering in the WAXS pattern[197]. PEEK and other semicrystalline polymers owe their naturally high draw ratio to such deformation induced structural changes[198]. When films of PEEK are stretched to draw ratios $\lambda>3$, chain orientation and strain induced crystallization impart substantial tensile strength[199]. In theory, a highly drawn and oriented PEEK surface would be more wear resistant. Briscoe attributed the transfer film formation observed in some polymers to drawability[179]. It might be expected that

PEEK transfer films undergo structural changes that contribute to improved wear performance.

6.2 Materials and Methods

In this work we will investigate the transfer film behavior of PEEK and how it relates to both wear resistance and drawability. The surface strains and frictional heating that occur during wear may contribute to some structural changes. However, the exact strain magnitude and temperature remain unknown and difficult to measure. To better understand the nature of transfer film and wear behavior in PEEK, a combined wear and spectroscopy study of will be performed.

6.2.1 Materials

In this work, samples from two different grades of PEEK material will be used. These grades are differentiated by weight average molecular weight M_W and are termed PEEK-L and PEEK-H. Gel permeation chromatography (GPC) was used to measure the molecular weight and the values for M_W are shown in Table 6.1. Wear pins were manufactured from the base PEEK material using an injection molding process described in previous work[20]. Rods of approximately 14mm diameter are extruded and machined into pins with a diameter of 6.35mm and length of 20mm. Samples were also molded into standard shapes for mechanical property measurements. Dynamic mechanical properties were measured using 40 x 11.5 x 3.3 mm bar shaped specimens molded in accordance with standard ASTM D790. A temperature sweep was performed using dynamic mechanical analysis (DMA) in torsion mode with a 1Hz frequency and 0.05% strain (TA Instruments, ARES-G2). The glass transition T_g as measured by the

peak value of tan δ is shown in Table 6.1. The crystallinity of the injection molded specimens were also measured using differential scanning calorimetry (DSC). The percent crystallinity (%X_c) was determined using the ratio of first heat melting enthalpy (ΔH_m) to the enthalpy of fusion for a perfect crystal (130 J/g)[104]. As shown in Table 6.1 the PEEK-L sample achieves a higher value of crystallinity compared to the higher M_W sample. The higher molecular weight inhibits chain folding and results in a lower %X_c. The injection molded bar specimens were cut into dog bones and tested in accordance with standard ASTM D638. Although there is a slight increase in modulus for PEEK-L it has significantly worse elongation at break compared to PEEK-H.

Table 6.1. Tabulated molecular weight M_w crystallinity %X_c and tensile properties for PEEK samples used.

Sample	M_w (kg/mol)	T_g[℃]	%X_c	Tensile Modulus E (GPa)	%Elongation ε	Tensile Strength σ (MPa)
PEEK-L	66.2	159	48	4.0	22	78
PEEK-H	114.4	158	42	3.8	51	82

6.2.2 Tribology Test Methods

In this work, wear testing is performed in a pin on plate configuration. A custom built multi axis tribometer is used which incorporates two programmable linear stages (Aerotech). Wear pins are mounted with a twist-lock style drill chuck and loaded against the counterface by pneumatically controlled actuators. The linear stages are stacked on top of eachother and can be programmed to move the counterface in a desired path. The counterface moves relative to the statically loaded pin. Wear results from the sliding of

the counterface against the pin surface. The counterface is made of D2 grade tool steel with both high carbon (1.5%C) and high chrome (11%Cr) content. The counterface is also unidirectionally ground to a R_a surface roughness of 0.5μm as shown in Figure 1. In this work, two different sliding paths will be used. A path termed multidirectional sliding results from the stages moving the counterface in a circle with a diameter of 20mm. This circular path and unidirectional counterface grinding means the angle between the pin sliding trajectory and counterface roughness are constantly changing. The sliding is done at a continuous speed of 100 and 200 mm/s for a total sliding distance of 2km. Loads of 32N and 160N are also used as test parameters and result in nominal contact pressures of 1 and 5MPa respectively. A sliding path termed linear reciprocating will also be used in which the counterface slides in a single direction. To compare the effects of linear reciprocation and multidirectional sliding tests will be done with the same 1 and 5MPa of nominal contact pressure. During reciprocation sliding is stopped and resumed at the end of travel and so a continuous velocity cannot be assigned. However, the average speed is fixed to be roughly 100 and 200 mm/s for comparative purposes. The sliding path has a distance of 75mm and tests are run for a sliding distance of 2km. It has been shown that the direction of asperities relative to sliding can be a contributing factor in polymer wear behavior[21, 200]. Tests were conducted with different sliding angles relative to the counterface roughness. The study were done with sliding perpendicular or 90° relative to the grinding direction with the previously described pressured and velocities. Additional studies were done with angles 0° or parallel to roughness as well as at 30° and 60°. Before testing, the wear surface of each pin was finished to a surface

roughness of approximately 0.2 μm Ra. Samples were ultrasonically cleaned, dried, and weighed before and after each test on a precision balance with a resolution of 0.01mg. The counterface was also wiped with acetone and then rinsed with deionized water to remove any contaminants prior to testing. After each test the change in mass was recorded and the reported density of the respective PEEK materials was used to calculate volumetric wear. Tests were all replicated four times and the standard error is reported with wear data.

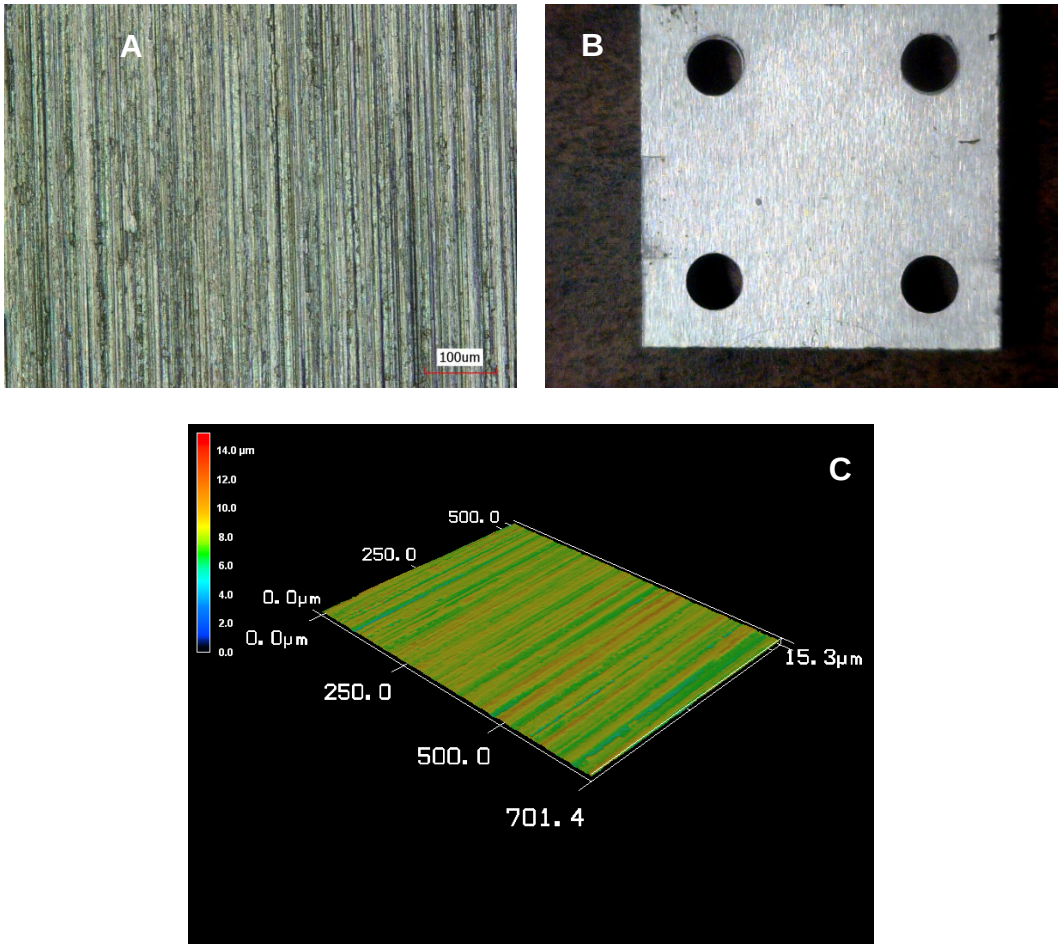

Figure 6.1. Images of the counterfaces used for wear and friction studies. A) Laser confocal micrograph of the steel counterface with scale bar 100 µm B) Counterface used for friction tests C) Topographical image of the counterface.

Friction data will also be collected for some sliding conditions. A three axis load cell (Interface) is used to monitor the forces that result from sliding. The counterface is mounted directly to the load cell and allows for real time monitoring of friction forces. A separate counterface is used for such studies since the counterfaces used in wear tests are too large to mount to the load cell. As shown in Figure 6.1B, a counterface with dimensions 50mm x 50mm with unidirectional surface roughness R_a of 0.5µm is used.

Sample counterfaces made of other materials such as glass and PEEK are also used in later studies but have a similar dimension. Friction data is collected at a rate of 250Hz.

6.2.3 Surface Imaging

Following wear tests surfaces were imaged using a number of methods. An ultraviolet laser confocal microscope (Keyence VK-9700) equipped with profilometry software was used. The microscope has a robotic stage and allows for images to be taken at magnification 10x-50x and stitched together into a complete image. An optical microscope (Olympus BX60) equipped with polarizers was also used in transmission mode to view possible birefringence or orientation in wear debris. A hand held digital microscope (Dino-lite) was used to take high resolution images of selected wear surfaces. Finally, scanning electron microscopy (SEM) was used to take high magnification images of wear surfaces and debris. Samples were coated with a 10nm thick layer of platinum with a Cressington108a auto sputter coater. A FEI-Quanta 600 electron microscope was then used to image the wear surface.

6.2.4 Temperature Measurement

Observations of the sliding temperature were done using an infrared camera (Fluke Ti45 IR Fusion) for PEEK pins sliding against glass and PEEK counterfaces. The camera has a temperature sensitivity of 0.08°C and uses a 160x120 Vanadium Oxide focal plane array. Calibration was performed for the temperature range -20°C to 350°C in accordance with manufacturer specifications[201]. The PEEK and glass counterfaces are assumed to have emissivity $\varepsilon \sim 0.95$ in the IR range of light. The IR temperature measurments of glass and PEEK counterfaces were also verified using a thermocouple.

The counterfaces were placed in an oven at 150°C and surface temperatures measured with the IR camera and thermocouple matched within 1°C.

6.2.5 Spectroscopy

Transfer films deposited on the steel counterfaces were studied to assess possible molecular orientation. Polarized Fourier transform infrared micoscopopy (FTIR) in attenuated total reflectance (ATR) mode was used to measure PEEK films. The dichroic ratio D was measured using infrared spectra taken with the IR source polarized parallel and perpendicular the direction of sliding. Similar techniques have been demonstrated to assess orientation in PEEK films[188, 189]. Transfer films were examined with FTIR (Shimadzu IRAffinity-1) using an ATR accessory (PIKE MIRacle). Measurements were taken using a ZnSe polarizer (Spectra-Tech) parallel and perpendicular to the sliding direction. Backgrounds were taken with the polarizer in place and only the polarizer was rotated between measurements. The dichroic ratio can be measured using the ratio of absorbance peaks from the parallel and perpendicular spectra $D = \frac{A_{\parallel}}{A_{\perp}}$.

6.3 Results and Discussion

6.3.1 Wear

The results from the wear studies are shown below in Figure 2 and Figure 3. In Figure 6.2 the effects of molecular weight M_W, contact pressure P, sliding velocity V, and wear path are all apparent. Wear is expressed in terms of wear volume (mm^3) in Figure 6.2A and Figure 6.2C. The same data is also expressed as a wear factor K (mm^3/Nm) as seen in Figure 6.2B and Figure 6.2D. Wear factor is calculated using the ratio of volumetric wear $Vol(mm^3)$to the product of sliding distance $d(m)$ and normal load

$F_N(N)$ and can be written $K = \frac{Vol}{F_N d}\left(\frac{mm^3}{Nm}\right)$. It should also be noted that Figure 6.2A and 6.2B correspond to the multidirectional sliding experiment and Figure 6.2B and 6.2C correspond to linear reciprocation.

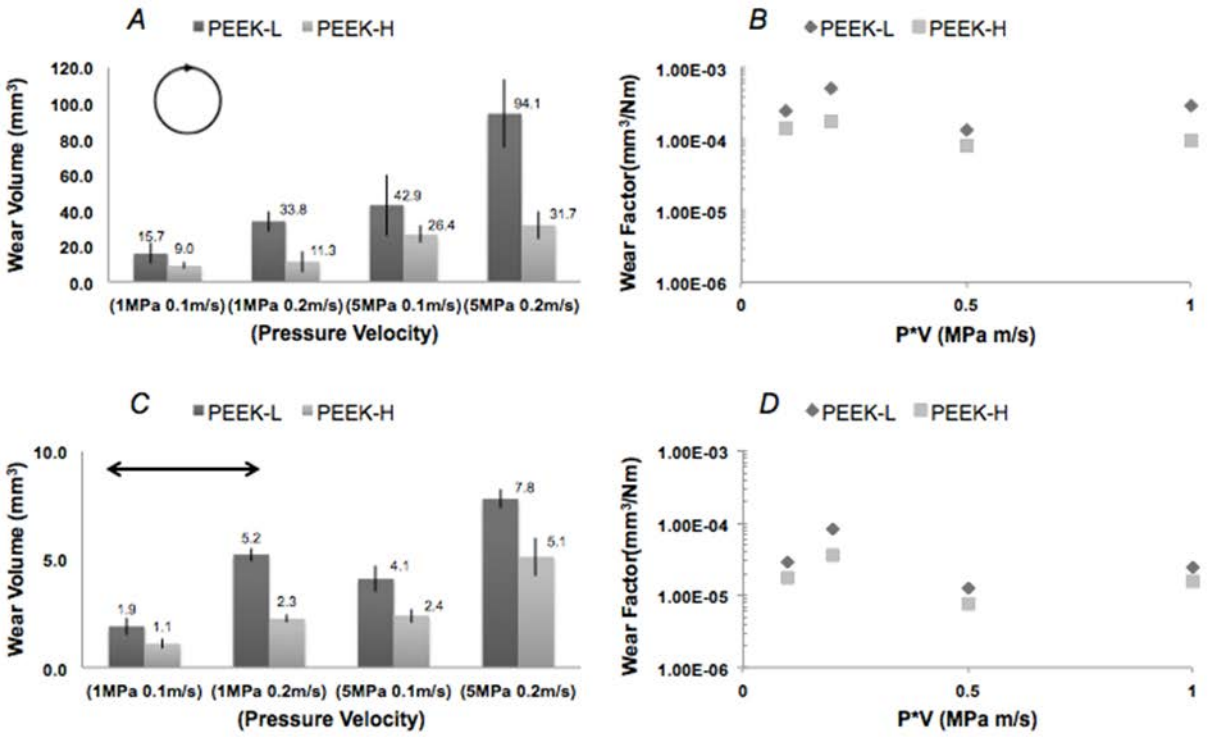

Figure 6.2. Wear volume and wear factor for PEEK-L and PEEK-H samples tested at different combinations of pressure and velocity. A) Multidirectional continuous sliding wear volume B) Multidirectional continuous sliding wear factor C) Linear reciprocating wear volume D) Linear reciprocating wear factor.

From the results it is apparent that molecular weight has a significant impact on wear performance in both multidirectional sliding and linear reciprocating. The difference is most extreme for multidirectional sliding under the highest combination of

pressure 5MPa and sliding velocity 0.2m/s. However, as the wear factors in Figure 6.2B and D indicate the higher M_W sample has consistently higher wear resistance. This relationship between wear rate and M_W in PEEK has been reported in a number of studies[10, 20, 21, 36]. From the mechanical properties in Table 1 it can be seen that PEEK-L has a much lower elongation at break than PEEK-H. The resulting lower ductility may play a part in explaining the lower wear resistance for PEEK-L. Additionally, the largest wear factor occurs at lower values of pressure velocity PV. With increased PV it is possible that frictional heat softens the surface. A softer more compliant surface would be less susceptible to cutting abrasive wear from the hard rough counterface asperities. The lower molecular weight samples will also have a lower shear viscosity η. This means that in the melt state the lower molecular weight material will flow under a smaller stress and may exhibit greater shear thinning[70]. If the frictional heating is great enough to melt some of the PEEK wear surface, the differences in wear behavior may be better explained by rheological properties than mechanical. However, the most striking observation in wear behavior is the difference between multidirectional sliding and linear reciprocating wear. This behavior was reported in a previous study[21] and the results are in line with those in Figure 6.2. It was reported that a reciprocating behavior produces transfer films that are both thinner and more continuous. A similar phenomenon is observed in this study such continuous films can be seen in Figure 6.4A. The transfer films are believed to cover hard rough asperities that will cut into the bulk. It is also suspected that the cross shearing from the circular multidirectional path can more easily remove debris from the bulk. In other polymers such as ultra high molecular

weight polyethylene (UHMWPE) and polytetrafluorethylene (PTFE) apparent orientation of polymer chains occur in the direction of sliding. For UHMWPE it has been observed that wear rates correspond to the degree of cross shearing[8]. Wang theorized that chains are oriented and sheared apart in a multidirectional environment and this explains the increased wear rate. In PTFE chains can be pulled from the bulk and form smooth running films that reduce wear[50]. Although PEEK does not share the same linear aliphatic structure, some orientation strengthening mechanism may underlie the observe difference in wear between the test conditions. To further investigate the influence of linear reciprocation on wear behavior tests were done with varying surface roughness direction. The results for reciprocation across different surface grinding angles are shown in Figure 6.3. Tests were done with a contact pressure of 5MPa and sliding speed 0.2m/s for a distance of 2km.

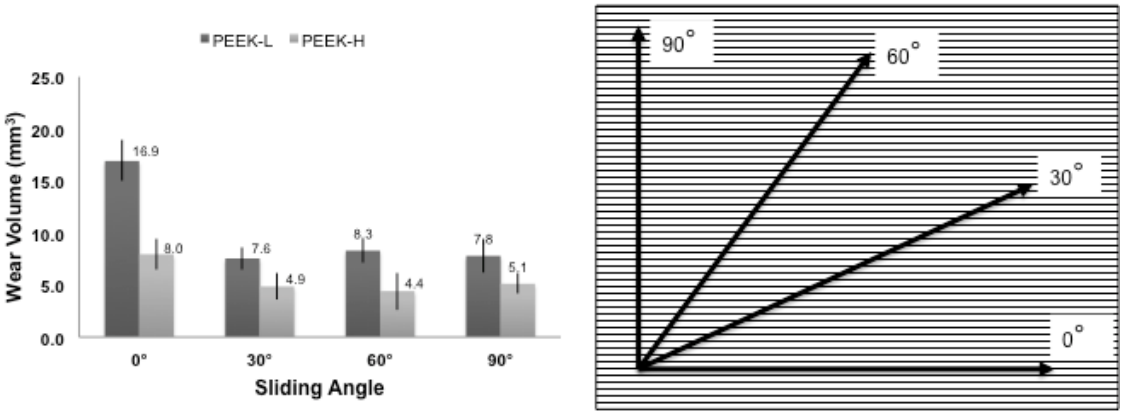

Figure 6.3. Wear volume resulting from linear reciprocation at varying angles relative to the surface roughness direction for PEEK-L and PEEK-H.

For both PEEK-L and PEEK-H the highest wear volume occurs for sliding parallel to the direction of grinding. In a study by Friedrich they also observed that the highest wear for unfilled PEEK corresponded to roughness aligned parallel to sliding[15]. A similar observation has also recently been made for a PTFE alumina Al_2O_3 composite[200]. As can be seen in Figure 4A, continuous transfer films are apparent on the counterface for sliding angles perpendicular to the grinding direction. At lower sliding angles films are still visible but appear sparser and less continuous. Sliding at angle 0° parallel to the grinding direction results in no visible film formation and debris is formed near the sliding periphery as seen in Figure 6.4B. Harris described a debris mobility phenomenon in the PTFE-Al_2O_3 system they studied[200]. They postulated that in order for a film to form debris must be retained in the wear track. Sliding perpendicular to the direction of roughness increases mechanical work and initiates a favorable tribochemical response in the PTFE-Al_2O_3 system. Bahadur suggested that for PEEK, the formation of a transfer film results from the mechanical entrapment of debris between conterface asperities[12]. Reciprocation perpendicular to the surface roughness direction causes debris to be deposited between asperity peaks. The enhanced mechanical anchoring means debris will be more readily retained and a transfer film can more easily be formed. However, the process by which wear debris forms into a transfer film is unclear. It is suspected that frictional heat may soften the retained debris and causes it to agglomerate into a continuous sheet[21]. The mechanism by which debris forms into a transfer film and how it relates to wear resistance will be further discussed.

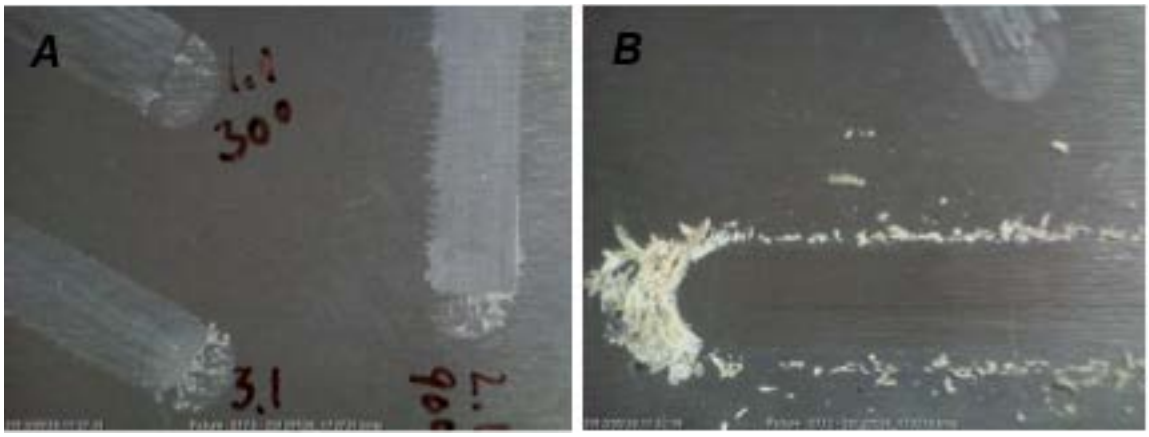

Figure 6.4. Counterfaces transfer films and debris formed sliding A) Perpendicular to the surface grinding direction B) Parallel to the surface grinding direction.

6.3.2 Transfer Film Formation

A selection of transfer films was formed under linear reciprocation with varying pressure and velocity. This was done in order to study the mechanisms responsible for film formation and how it relates to wear. Films were formed with reciprocation perpendicular to the surface roughness direction and the PEEK-H material was used for all tests. In Figure 6.5 an illustration of the process is shown along with the pin surface and accompanying transfer film. In order to accommodate the load cell used in friction measurements the reciprocation distance was limited to 20mm.

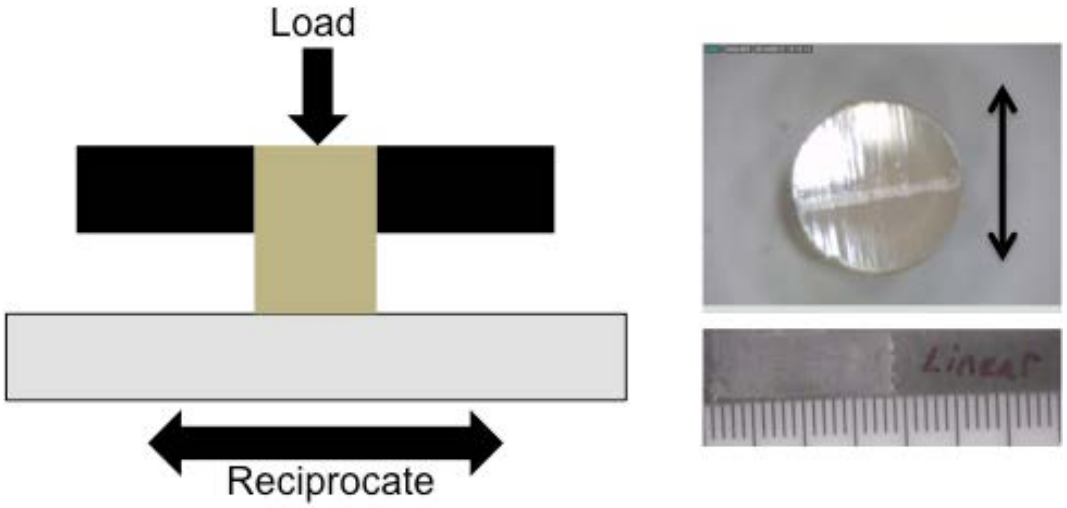

Figure 6.5. Illustration of the loading configuration and motion profile used in fretting tests. The transfer film and pin surface following the test are also shown.

Sliding was done for a total of 2,000 cycles, which corresponds to a sliding distance of 8m. This sliding distance is significantly lower than the 2km of sliding used in wear studies. However, it appears that under the selected pressure and velocity conditions a film will readily form within the first few thousand cycles. In Figure 6 the friction trace for sliding with a load of 200N and sliding frequency 2Hz (80mm/s) is shown. The dynamic friction trace within the first few hundred cycles is shown in Figure 6.6A and Figure 6B corresponds to roughly one thousand sliding cycles. Spikes in friction at the beginning and end of sliding show up in the friction trace for the first few hundred sliding cycles. With increasing cycles the static spikes in the friction trace are not longer visible but the friction response appears more erratic. It can be seen in Figure 6.6B that small fluctuations occur in the friction trace during sliding. It was observed that during this period transfer films become visible on the counterface. Although

transfer films appear linked to lower wear in PEEK it appears that they do little to reduce the magnitude of the friction forces.

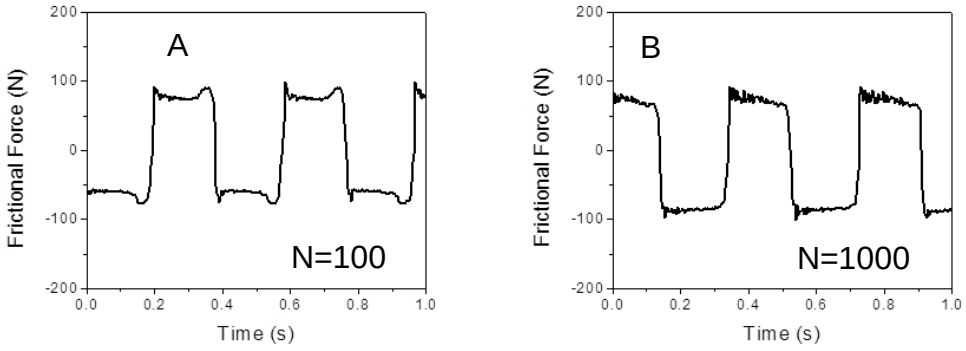

Figure 6.6. Friction profiles for PEEK pin sliding against steel counterface with pressure 5 MPa and sliding at 2Hz or 80 mm/s for A) 100 sliding cycles B) 1000 sliding cycles.

Examples of films formed with different loads and sliding velocity are show in Figure 6.7. Additionally, the resulting pin surfaces are shown in Figure 6.8. It can be seen that there is an apparent pressure and velocity limit on the tenacity of the transfer films. Increasing pressure and velocity causes films to flake off and become detached from the counterface. It might be presumed that under these sliding conditions the adhesion between the film and the counterface is overcome by the sliding frictional forces. At high sliding velocity the debris also appears to be discolored indicating possible oxidation. It may also be reasoned that the observed behavior results from the buildup of frictional heat at the wear surface. The formation of large sheet like debris particles at high combinations of pressure and velocity has been well reported in PEEK. Zhang described such PEEK debris in terms of the fractal dimension[23, 202]. They had

observed that larger plate like debris occurred at larger loadings. Additionally, they observed “filmy laces” emanating from the trailing edge of the wear pins[23]. Zhang suggested that frictional heat resulted in debris becoming plastically deformed and extruded between the pin and counterface. Ovaert observed a similar phenomenon and indicated that the retention of debris was critical for transfer film formation[17-19]. The wear particle and transfer film thickness also corresponded to the location of subsurface stress maxima[19]. They indicated that the formation of transfer films and plate like debris resembled a delamination process. It is difficult to determine whether the transfer film seen in Figure 6.7A and detached debris seen in Figure 6.7D were formed as the result of the same process. The detached debris may be due to previously formed film becoming debonded from the counterface. However, it is possible that increasing load disrupts transfer film formation and promotes the delamination debris For PTFE Blanchett described a similar phenomenon[185]. Low wear corresponded to the formation of highly oriented debris that consisted of individual PTFE fibrils. This fibril formation process however could be disrupted by the propagation of subsurface cracks and the formation of large debris flakes. Although PEEK will not fibrillate in the way observed for PTFE, there could be a similar mechanism that competes with delamination.

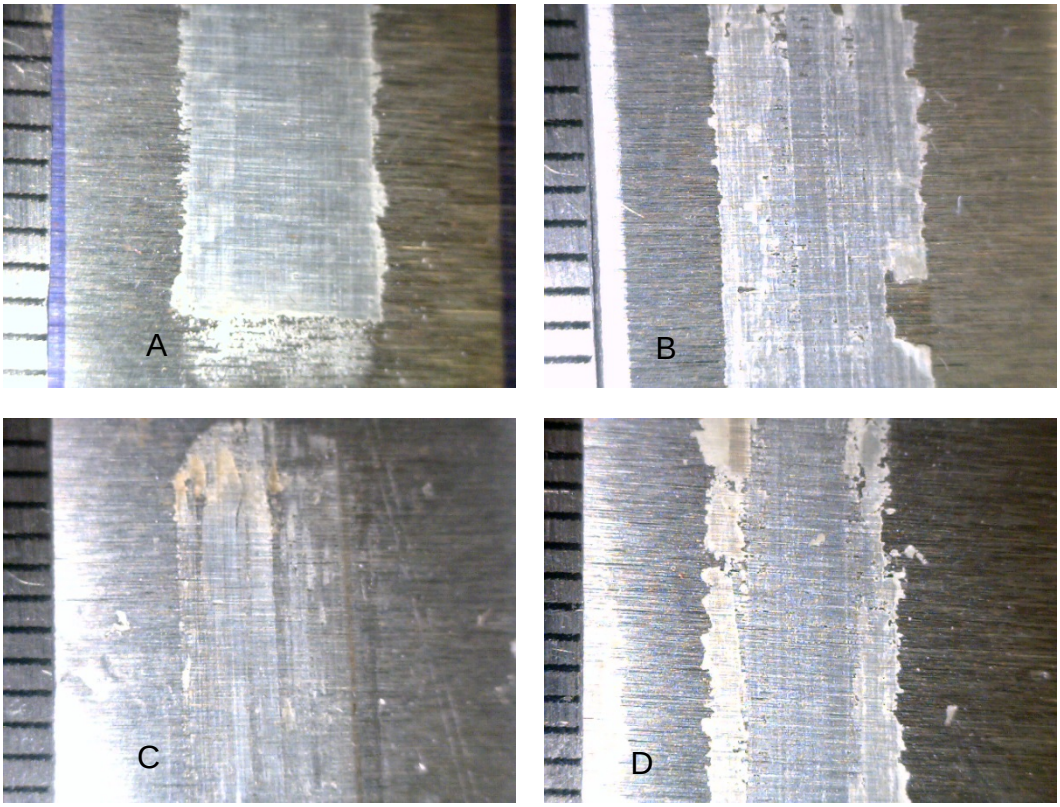

Figure 6.7. Transfer film and debris deposited on counterfaces after sliding for 1000 cycles. A) 5MPa contact pressure 2Hz (80 mm/s) sliding speed B) 10MPa contact pressure 5Hz (200 mm/s) sliding speed C) 5MPa contact pressure 10Hz (400 mm/s) sliding speed D) 20MPa contact pressure 2Hz (80 mm/s) sliding speed.

The notion that plastic flow takes place at the wear interface is supported by observation of the wear pin surface. Figure 8 shows the pin surface for transfer films formed with a 160N (5MPa) load and sliding at 2Hz (80mm/s). There are several surface features that show up prominently on the wear surface. In Figure 6.8A grooves can be seen on the surface parallel to the direction of sliding as indicated by the black arrow in the figure. There also appears to be a region of interest perpendicular to the direction of sliding. A magnified view of the wear surface can be seen in Figure 6.8B. As can be

seen, ripples appear within the surface grooves and are also aligned with the direction of sliding. Similar surface features have been observed in wear studies of PEEK[21, 36] and UHMWPE[148]. It is believed that such ripples occur due to plastic flow of the wear surface. As the polymer slides over the counterface frictional heating occurs. If the temperature exceeds the glass transition T_g~150°C the polymer will be in a rubbery state. The more rubbery polymer surface can then be stretched or plastically deformed during sliding. A similar phenomenon occurs in rubber and are referred to as Schallamach waves[203]. It is believed the periodicity of these ripples in rubber corresponds to the sticking and slipping of asperity contacts[204]. Recall in Figure 6.6 friction response became increasingly erratic with increased sliding cycles. This friction response likely corresponds to the formation of the observed ripple features. However, it is unclear whether temperatures approaching T_g~150°C had occurred and will be further discussed.

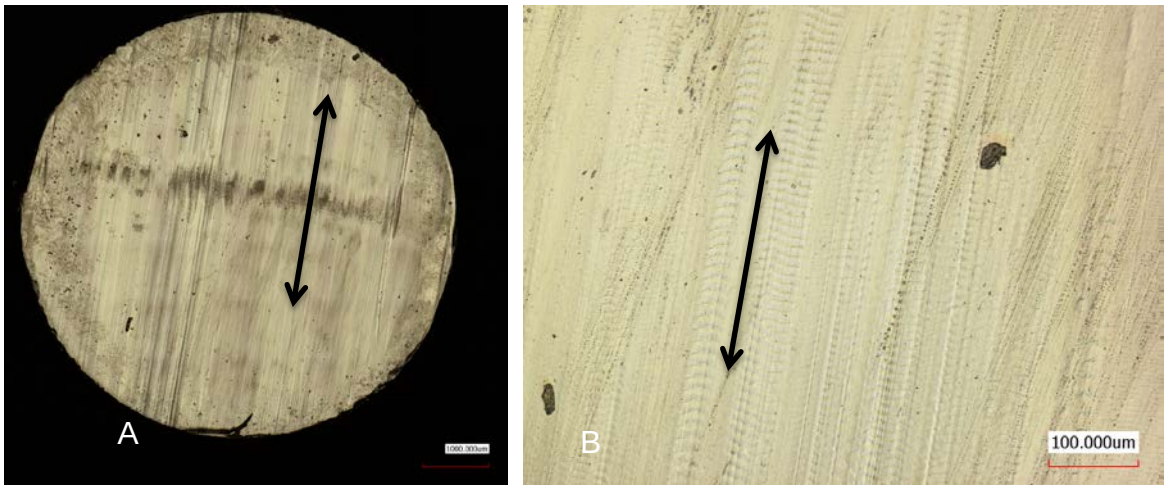

Figure 6.8. Laser confocal micrographs of wear pin surface after sliding with pressure 5 MPa and speed 80 mm/s A) Arrow indicates sliding direction B) Scale bar is 100 μm

With increasing pressure and velocity the pin surface appears increasingly damaged as shown in Figure 6.9. Deep ruts are also visible on the surface parallel to the direction of sliding. Interestingly, many of the same features found in Figure 6.8 are also visible. Although ripples are less prominent, these features are still apparent in Figure 6.9B. The increased pressure and velocity results in both a loss of transfer film integrity and also greater damage to the pin surface. There appears to be a limit on pressure and velocity beyond which transfer films offer no benefit to wear reistance. Rather, the films become third bodies that abrade the bulk pin surface and contribute to greater frictional heating.

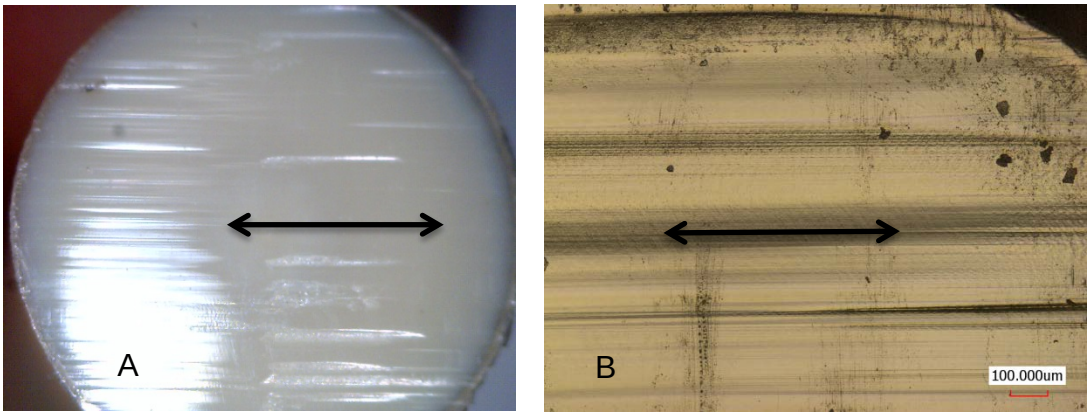

Figure 6.9. Wear pin surface after sliding with contact pressure 20 MPa sliding speed 80 mm/s A) Arrow indicates sliding direction B) Scale bar 100 μm

The transfer film in Figure 6.7A was further examined using scanning electron microscopy (SEM) in Figure 6.10. It was assumed that the tenacity of the transfer film

depended largely on its adhesion to the counterface. Inspection of the SEM image shows some intriguing features that may be used to describe the film formation and behavior. Although the film appears as a large continuous sheet, there are a number of holes and voids. The film in Figure 6.10A appears to be made up of compacted and coalesced debris fragments. Zooming in on some regions also shows that these fragments are connected by fibrils. These fibrils may serve as weak points within the film structure. During sliding, the shear stress imparted on the film from the reciprocating pin can cause sections of the film to break and become detached from the bulk. The fibrils are also oriented in the direction of sliding. This may also in part explain the difference in wear behavior between multidirectional sliding and linear reciprocation. The cross shearing experienced during multidirectional sliding would inhibit such fibril formation. It has been suggested that transfer film formation in polymers depends on drawability[179]. Obsevations of the transfer film and pin surface during linear reciprocation suggest that they had been strained in the direction of sliding. Further discussion of the relationship between film formation and drawability will be further discussed.

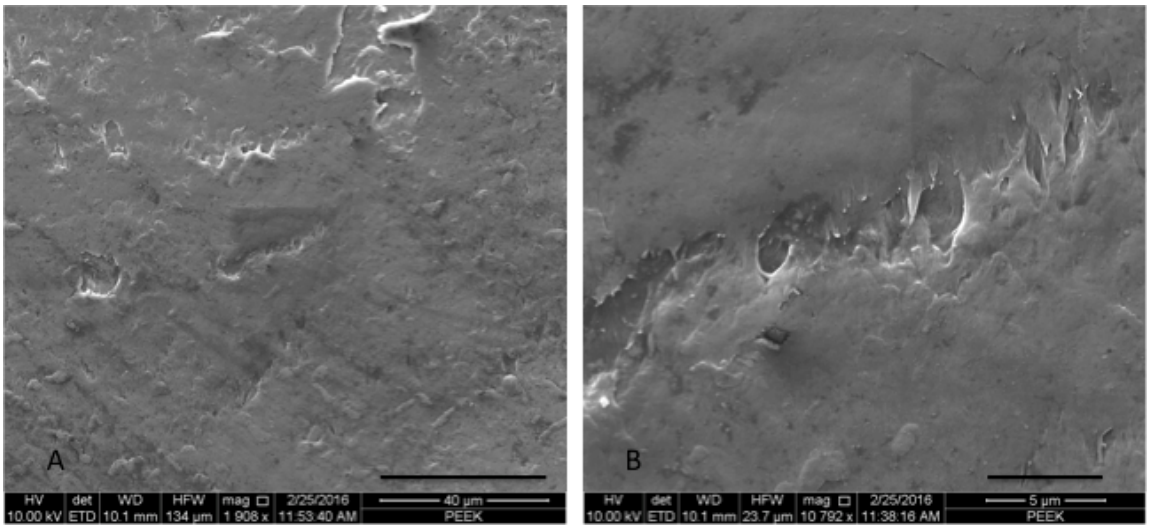

Figure 6.10. Scanning electron micrograph of transfer film with scale bars A) 40 μm and B) 5 μm

6.3.3 Transfer Film Structure and Drawability

To further explore the structure of the transfer films sections of film were analyzed to assess possible orientation. The high quality film in Figure 6.7A and the detached film from 6.7D were examined. Figure 11 shows the polarized optical micrograph of the film from 6.7D. Under the cross polarizers the film shows a high degree of birefringence. The film section also is transparent and does not show any evidence crystalline structures. Previous analysis of wear debris suggested that the films had been heated to temperatures above melt and quenched into an amorphous state.

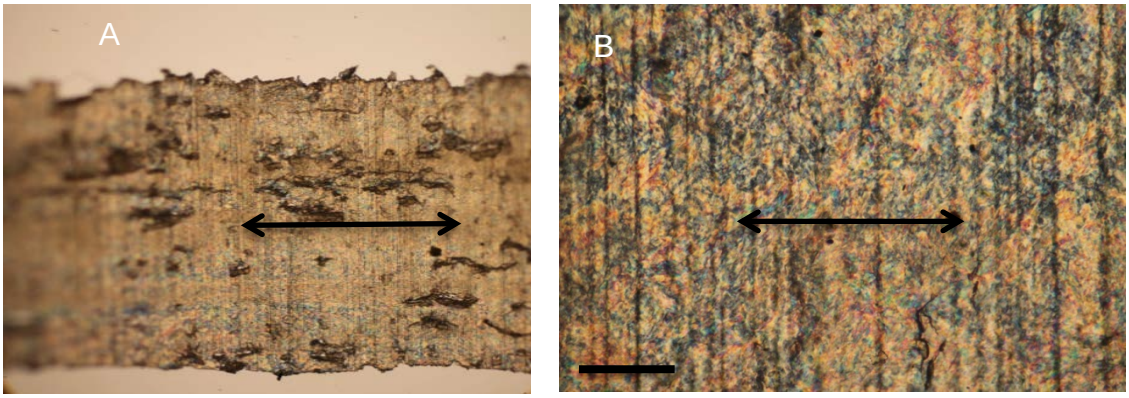

Figure 6.11. Micrograph taken of detached debris fragment with an optical microscope. Image is taken in transmission mode with the light source linearly polarized. Scale bar is 20μm and arrows indicate the direction of sliding.

Transfer films from Figure 6.7A and detached debris from Figure 6.7D were measured using polarized FTIR-ATR spectroscopy. The absorbance spectra are shown in Figure 6.12 with the infrared source polarized parallel and perpendicular to the sliding direction. The pin surface was also measured but does not exhibit any difference in the spectra. The spectra from both the transfer film and debris appear to be oriented in the direction of sliding. Interestingly, some portions of the spectra are more drawn than others. The dichroic ratio can be measured using the ratio of parallel and perpendicular spectra $D = \frac{A_{\parallel}}{A_{\perp}}$ and dichroic ratios are shown in Figure 13.

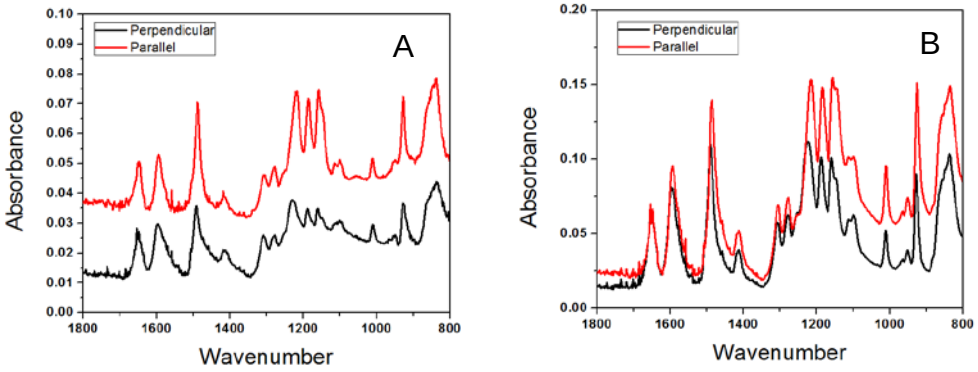

Figure 6.12. Polarized FTIR-ATR spectra from A) Transfer film deposited on steel counterface B) Detached debris fragment.

The previous results demonstrated that the sliding friction and wear behavior of PEEK depended strongly on the deposition and integrity of transfer films. It is believed that a polymer's ability to form thin continuous transfer layers is related to its drawability[179]. Studies have shown that PEEK may undergo large deformations before break and when heated above T_g can be drawn into highly oriented films[74, 186, 187]. It is common for PEEK films to be drawn to ratios $\lambda \sim 3$ when temperatures above T_g are used[74]. Interestingly, the measured transfer film and debris dichroic ratios are similar for some wavenumbers as shown below. In particular the wavenumbers from the diphenyl ether segments show much stronger dichroism than that of other segments. For instance the peak at 1645, which corresponds to the carbonyl group, does not exhibit any dichroism. Although the dichroic ratio does not directly correspond to draw ratio it is an indication of orientation. Typically, the more oriented a polymer film the higher the dichroic ratio. Comparison of the debris and film also suggest that the transfer film may be slightly more oriented. Comparing wavenumbers between 1100 and 1300 show

consistently higher dichroic ratios *D*. It might be reasoned that films achieve greater integrity and tenacity when they can be drawn to achieve the highest possible orientation.

Wavenumber	Pin	Plate	Debris
930	0.95	2.42	2.48
1012	0.94	2.48	2.66
1162	0.97	2.67	1.69
1188	1.00	1.86	1.56
1227	1.00	1.99	1.48
1284	0.96	2.73	2.35
1309	1.02	2.51	1.25
1490	1.00	2.08	1.34
1598	1.00	1.16	1.15
1645	0.99	0.99	1.08

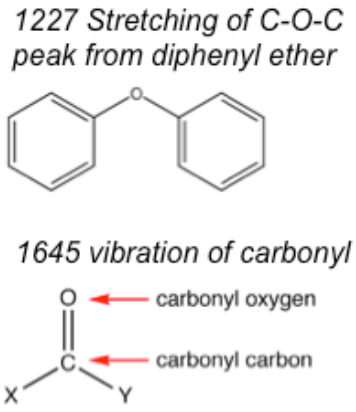

Figure 6.13. Measured dichroic ratios for wear pin, transfer film and detached debris. The diphenyl ether and carbonyl groups are also depicted.

6.3.4 Frictional Heating

It is believed that frictional heating contributes to the wear behavior of PEEK. This frictional heating may be especially pronounced when the PEEK pin surface slides over previously deposited debris fragments. Typically polymer on polymer sliding does not produce favorable friction or wear behaviors[205-207]. When polymers slide against themselves greater adhesive friction forces often arise. Polymers are also thermal insulators and so frictional heat cannot easily dissipate away from the sliding surface. In PEEK surface temperatures exceeding the glass transition are observed in gear assemblies and are attributed to the high friction and low thermal conductivity[13].

Apparent excessive frictional heating has also been observed when PEEK slides against itself but no surface temperature measurements are provided[127]. Tanaka made a similar observation for PEEK sliding against glass counterfaces[139].

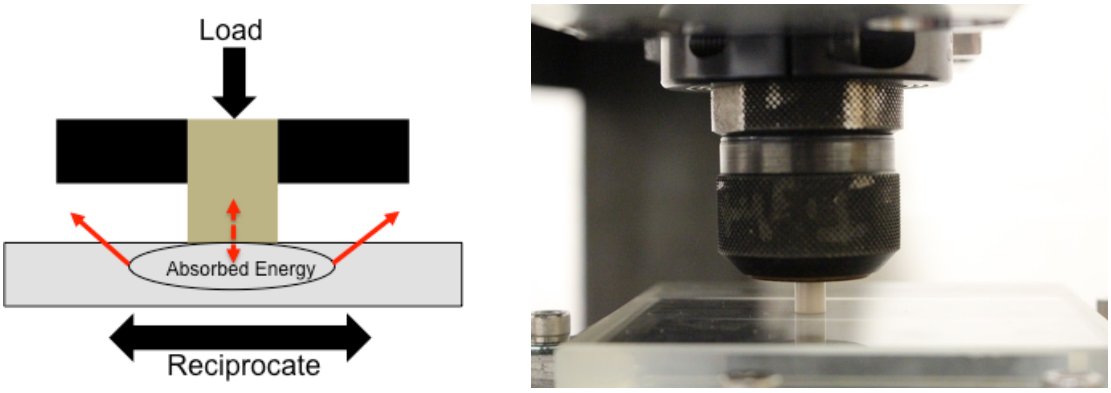

Figure 6.14. Illustration and experimental setup for measurement of surface temperature.

It is believed that frictional heating contributes to the wear behavior of PEEK. This frictional heating may be especially pronounced during transfer film formation. The deposition of debris to the steel counterface creates periods of PEEK on PEEK sliding. In order to demonstrate the potential for surface temperatures to reach thermal transitions experiments are performed with PEEK and glass counterfaces. The results are also compared with that predicted by flash temperature theory. Surface temperature was discussed in a previous section and a similar calculation methodology is used. During sliding heat is generated at the surface and the heat flux can be calculated as $\dot{q} = \mu p U$. In the equation the average heat flux $\dot{q}$ is calculated using the coefficient of friction μ along

with the nominal contact pressure p and sliding speed U. The average temperature rise T_f is then calculated using Jaeger's solution for a uniform circular souce[152, 154, 155].

$$T_f = \frac{0.903\dot{q}a}{0.849K_{Plate}\sqrt{Pe}+1.064K_{Pin}} \quad \text{(Equation 6.1)}$$

In the equation the thermal conductivity $K[W/mK]$ of the pin and plate are used and the values used are listed in Table 6.2. Additionally the Peclet number is calculated according to $Pe = Ua/\chi$. In the equation the thermal diffusivity $\chi = K/\rho\sigma$ is used along with the sliding speed U and radius of contact a.

Table 6.2. Thermal properties diffusivity *X*, conductivity *K*, density ρ, and specific heat σ for counterfaces used in experiments.

	X [m2/s]	*K [W/mK]*	*ρ[kg/m3]*	*σ[J/kgK]*
PEEK	1.41E-07	0.25	1320	1340
Steel	5.63E-06	20	7700	461
Glass	6.59E-07	1.1	2225	750

Figure 6.15 shows the predicted flash temperature rise T_f for different counterfaces with increasing sliding speed U. In the calculation it is assumed that the coefficient of friction μ is a constant 0.3 and the pin surface is in full contact with the counterface giving a contact radius a of 3.2 mm. The average contact pressure is assumed to be 5 MPa in order to provide comparison with the previous wear studies. As might be expected the largest flash temperature rise corresponds to the counterface with the lowest thermal conductivity. This is in stark contrast to PEEK sliding against steel where a temperature rise of only 4°C is predicted at a 300 mm/s sliding speed.

Furthermore the temperature rise for PEEK on PEEK sliding is well below any thermal transition such as the glass transition T_g~150°C.

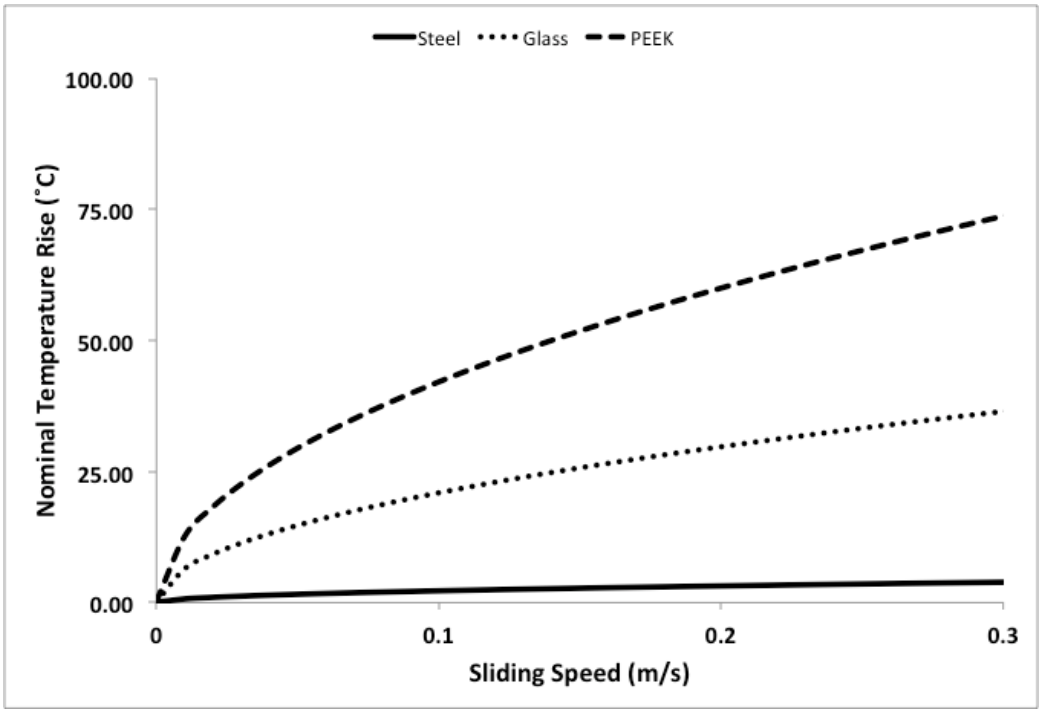

Figure 6.15. Predicted flash temperature rise with increasing sliding speed for a PEEK pin with a contact pressure of 5 MPa sliding against stainless steel, glass, and PEEK counterfaces.

The predicted temperature rise for sliding conditions used in wear studies indicates that frictional heating would not become significant. However, during sliding some portion of heat is retained within the sliding track. Using a glass counterface and a 25 mm diameter pin loaded to 5 MPa of contact pressure the sliding surface temperature is monitored with an infrared camera (Fluke Ti45 IR Fusion). Initially, the camera detects a modest temperature rise. However, after roughly 1,000 sliding cycles a significant temperature rise is detected as shown in Figure 6.16. In the figure the pin

slides a distance of 75 mm before reversing direction. Heat that is generated within the pin contact will continuously rise with repeated traversals.

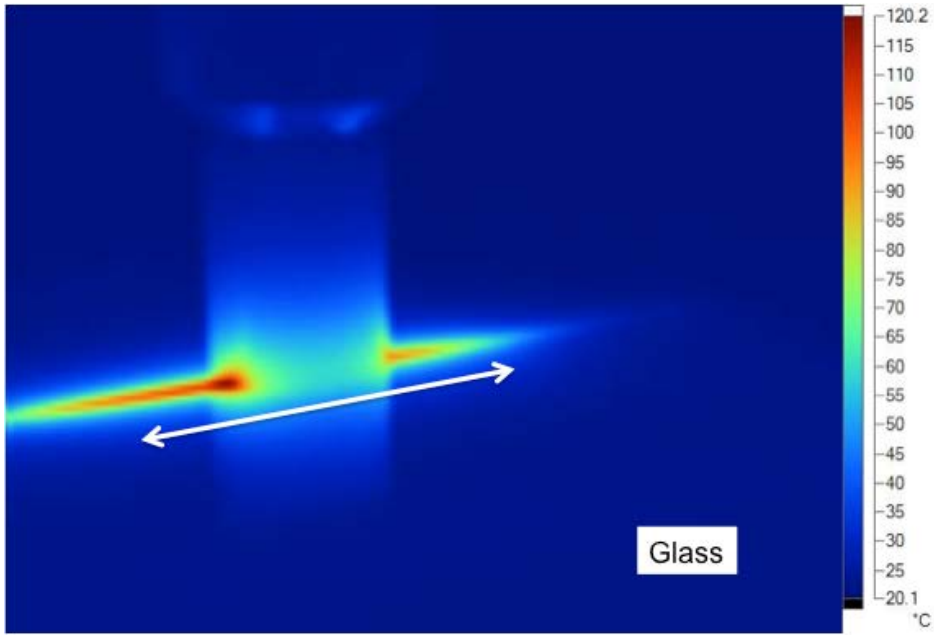

Figure 6.16. Infrared image of a PEEK pin sliding on a glass counterface with a contact pressure of 5 MPa and sliding speed of 200 mm/s.

The infrared camera temperature measurements were repeated with the 6.35 mm diameter pins with both glass and PEEK counterfaces. With contact pressure 5 MPa and sliding speed were set to 200 mm/s and the counterface temperature was monitored with the infrared camera. As shown in Figure 6.17 the heat is retained within the sliding track. The surface temperatures increase with increasing sliding cycles until eventually the sliding track approaches the glass transition T_g. Figure 6.17A shows the surface after the first 100 sliding cycles. During this period a flash temperature rise T_f of only 30°C is observed. The flash temperature model predicted a similar temperature rise as seen in

Figure 6.15. It can be presumed that during the first few sliding cycles the contact transitioned from partial to full contact. In Figure 6.17B the surface temperature after 500 sliding is shown and in Figure 6.17C the surface temperature after 1000 cycles is shown. Interestingly the measured surface temperature reaches a point above the glass transition T_g. When the glass surface temperature reaches 170°C after 1000 sliding cycles there is a noticeable change in the polymer surface. Figure 6.18 shows wear pin surfaces after sliding on glass for 1000 cycles. The polymer appears to have been softened and deformed in the direction of sliding. This observation corresponds with the measured surface temperature of 170°C. The 5 MPa of contact pressure and 200 mm/s sliding velocity were sufficient to heat the surface above the glass transition when a glass counterface is used.

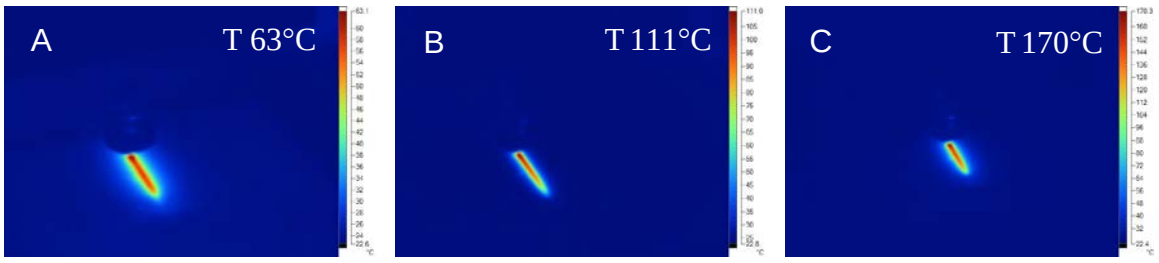

Figure 6.17. Infrared images for PEEK pin sliding on glass counterface with a contact pressure of 5 MPa and sliding speed of 200 mm/s. A) Surface after 100 cycles B) Surface after 500 cycles C) Surface after 1000 cycles

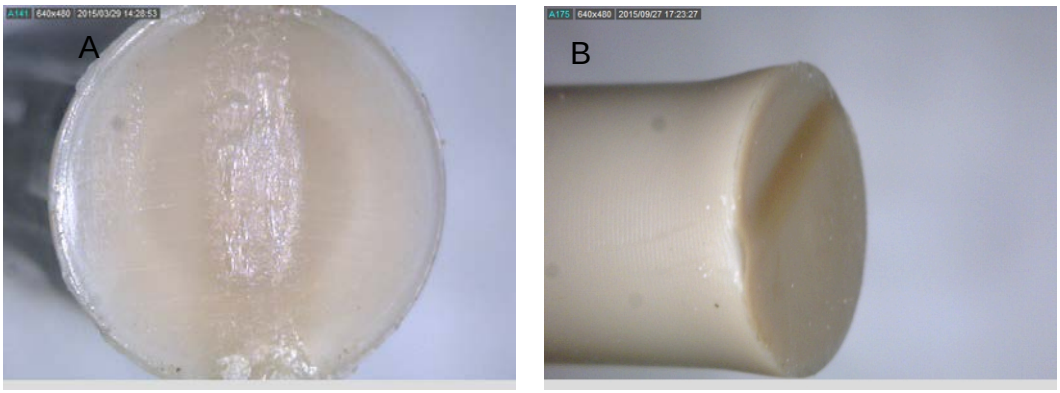

Figure 6.18. Illustration of transfer film formation process. Debris is heated due to friction and joined to debris deposited in adjacent asperities.

The same sliding test conditions were used with the PEEK pin sliding on a PEEK counterface. After the first 200 sliding cycles significant frictional heating takes place. Similar to glass the surface reaches a temperature of 170°C, which is above the glass transition temperature. As shown in Figure 6.19 the sliding track reaches such temperatures and also results in significant changes in both the pin and PEEK counterface. The edges of the PEEK pin have completely been worn off and the counterface shows evidence of plastic flow. This response is counterintuitive to what is observed during PEEK transfer film formation. It is believed that transfer film formation results from the heat generated due to PEEK on PEEK sliding. However, PEEK on PEEK sliding appears to result in a catastrophic loss of sample integrity. It appears that during transfer film formation the heating at the surface remains localized and close to the wear interface. During film formation temperatures approaching the glass transition do not penetrate into the bulk as observed with glass or PEEK counterfaces.

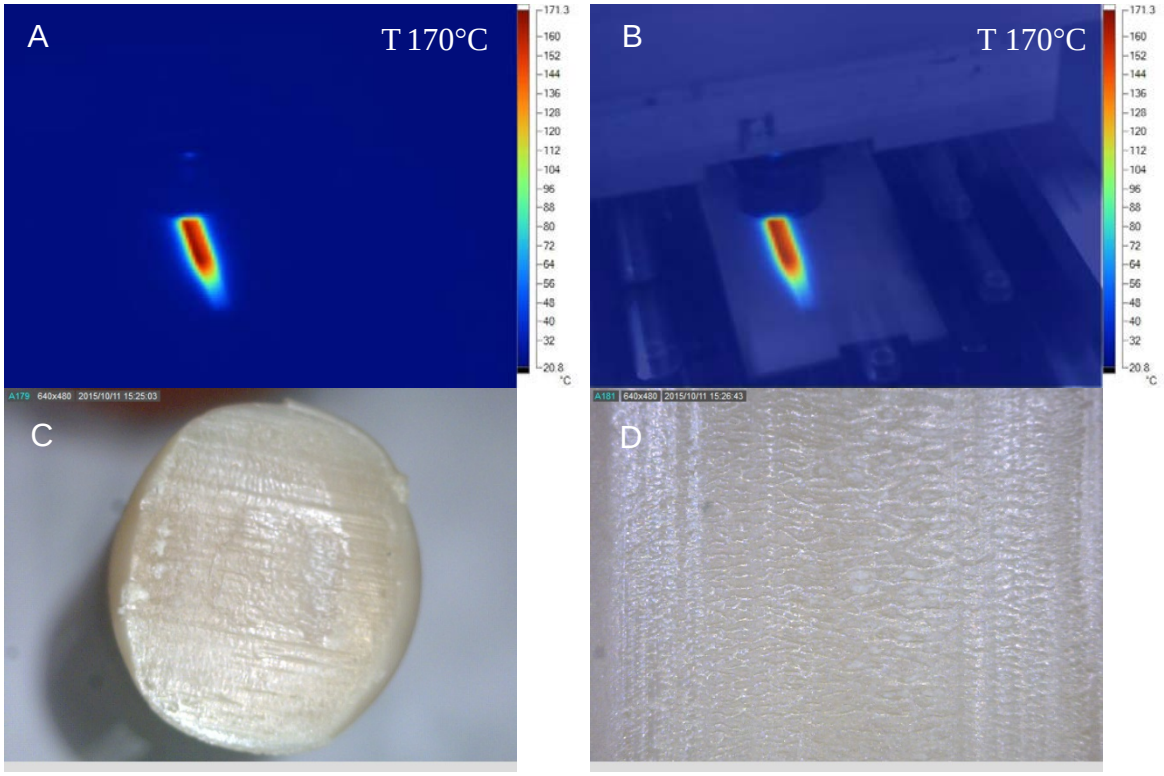

Figure 6.19. Selected images from PEEK on PEEK sliding with a contact pressure of 5 MPa and sliding speed 200 mm/s. A) Infrared image with max temperature 170°C. B) Infrared image overlaid on top of real image. C) Pin surface after 200 sliding cycles. D) PEEK counterface after 200 sliding cycles.

6.4 Conclusion

The results of this study demonstrate PEEK polymer's sensitivity to multidirectional sliding compared to a linear reciprocating environment. The sensitivity is especially pronounced for lower molecular weight M_W material. It is also observed that wear resistance can be partially attributed to the formation of transfer films. When sliding perpendicular to the surface grinding direction well adhered films form on the surface but are entirely absent when sliding along the grinding direction. The absence of

a transfer film corresponds to an increase in wear. However the presence of a transfer film alone does not explain the order of magnitude increase in wear rate during multidirectional sliding. Observations of the wear surface and transfer film indicate that formation occurs in a rubbery state. Measurements of the film with polarized FTIR-ATR spectroscopy suggest that the film is oriented in the direction of sliding. Such observations indicate that the wear surface and film formation resemble a drawing process. PEEK can be drawn at temperature near the glass transition T_g to ratios $\lambda \sim 3$. Such draw ratios produce films with improved mechanical strength in the direction of drawing. It can be reasoned that the transfer film and wear surface experience similar orientation strengthening, which can be attributed to wear resistance. The formation of such transfer films is also aided by frictional heating as illustrated in the below Figure 6.20. During the first few sliding cycles debris becomes detached and imbedded between counteface asperities. The sliding of the PEEK pin against such third body debris can quickly elevate the surface temperature above T_g. The insulating nature of PEEK also means that the surface temperature will grow with increasing sliding cycles. Such phenomenon was demonstrated with PEEK and glass counterfaces. The heat retained in the sliding track can be observed to grow until it reaches the glass transition of 150°C. Interestingly the pin surface begins to melt and lose its integrity with glass and PEEK counterfaces but is largely undamaged when sliding against a transfer film on metal counterface. Although the exact nature of transfer films is not fully known it appears strongly linked to the drawability of the PEEK wear surface.

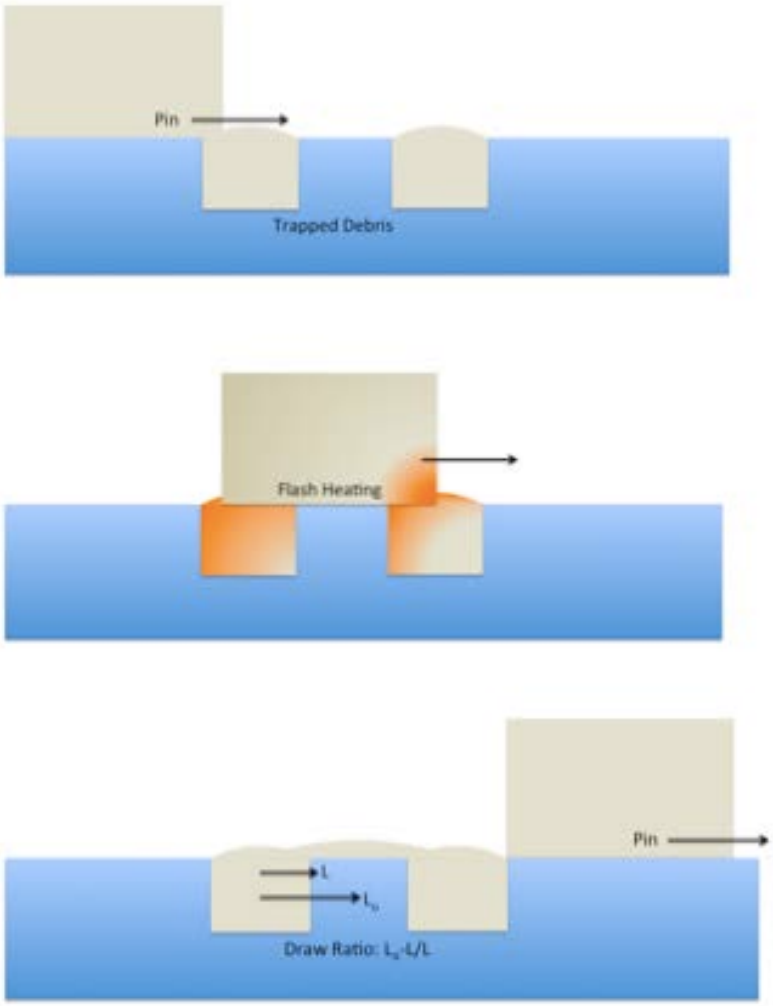

Figure 6.20. Illustration of transfer film formation process. Debris is heated due to friction and joined to debris deposited in adjacent asperities.

CHAPTER VII

CONCLUSIONS AND CONSIDERATIONS FOR FUTURE RESEARCH

7.1 Summary and Conclusions

Experimental work and analysis of results were performed in order to gain a deeper understanding of adhesive wear processes in polyaryletherketone (PAEK) polymers. The focuses of this study were as follows:

1. Develop an experimental methodology to simulate adhesive fatigue damage in PAEK material. Utilizing this methodology, investigate the role of PAEK structure properties and environmental conditions on the fretting response.
2. Measure the static friction response of PAEK systems. Relate the static friction response to how the material will behave in a fretting environment.
3. Investigate how surface properties affect the sliding friction and flash temperature of PEEK polymers. Perform in-situ temperature measurements to validate the predicted flash temperature behavior.
4. Describe how changes in PEEK structure arise during the wear and transfer film formation. In particular, understand the relationship between transfer film formation and drawability of the PEEK wear surface.

The experimental study using a selection of polyaryletherkeone (PAEK) polymers show the effect of material properties on the adhesive wear behavior. The repeated sticking and slipping of adhesively joined asperities results in fretting damage. The severity of this fretting response is strongly linked to the PAEK fracture properties.

It was observed that during fretting, fracture occurred for lower M_w PEEK material and the PEK member of the PAEK family. Although fillers could greatly improve the fretting response in dry conditions, the lower M_w PEEK material also exhibited catrastrophic fractures in wet conditions. Studies of the static friction response demonstrate how changes in the wear surface contribute to fretting wear. In wet conditions, the penetration of fluid into the bulk reduces the interfacial shear strength and promotes slipping of asperities. For dry sliding conditions, frictional heating softens the surface and increases the magnitude of static friction. The damage observed in dry fretting remains localized to regions affected by this frictional heating.

Analyzing the debris and wear surface shows the importance of frictional heating on determining the material response. In both fretting and dry sliding conditions debris was found to be largely amorphous. Figure 7.1A shows the wide angle X-ray diffraction pattern for both wear debris and the as received “amorphous” powder. Neither material shows evidence of crystal structure and implies that the material has been quenched from a temperature above the melt. As shown in Figure 7.1B the crystal structure does not disappear until reaching temperatures above 340°C.

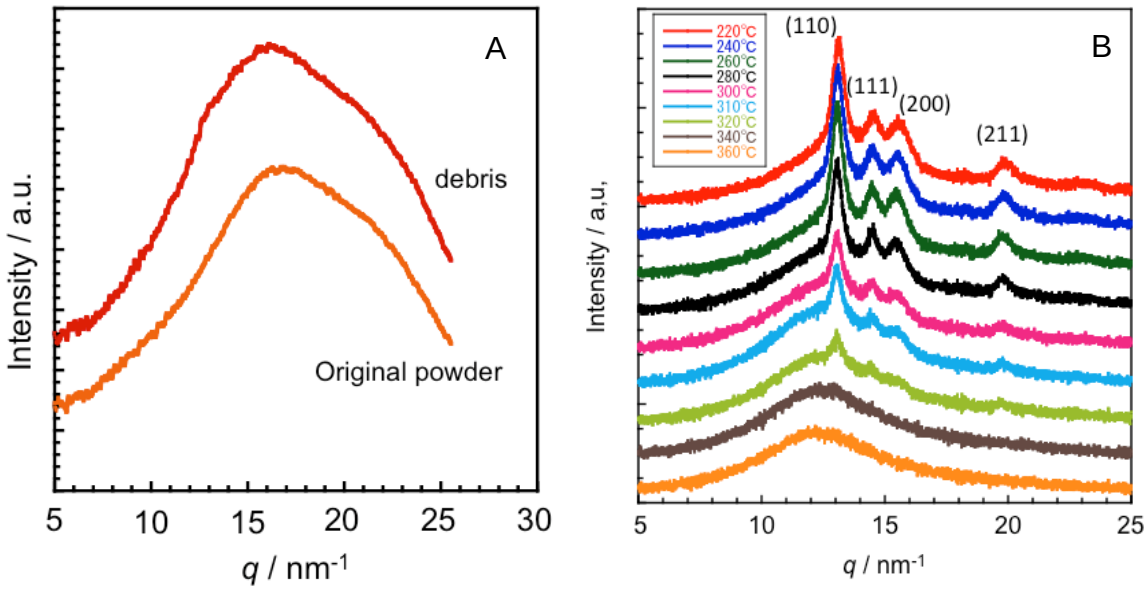

Figure 7.1. Wide angle X-Ray diffraction pattern for PEEK wear debris and original amorphous powder. B) Spectra of powder between 220°C and 350°C.

However, in situ measurement reveals only a modest rise in the surface temperature. Figure 7.2 illustrates the findings taken using infrared thermography. The measured surface temperature rise closely matches the results predicted by flash temperature theory. When debris can become entrapped within the sliding contact, localized heating takes place. The inherently low thermal conductivity of PEEK and the high PEEK on PEEK friction increase the resulting sliding surface temperature. The localized heating and shearing of material in the sliding contact can also result in the formation of a transfer film. This process resembles high temperature drawing and the films appear oriented in the direction of sliding.

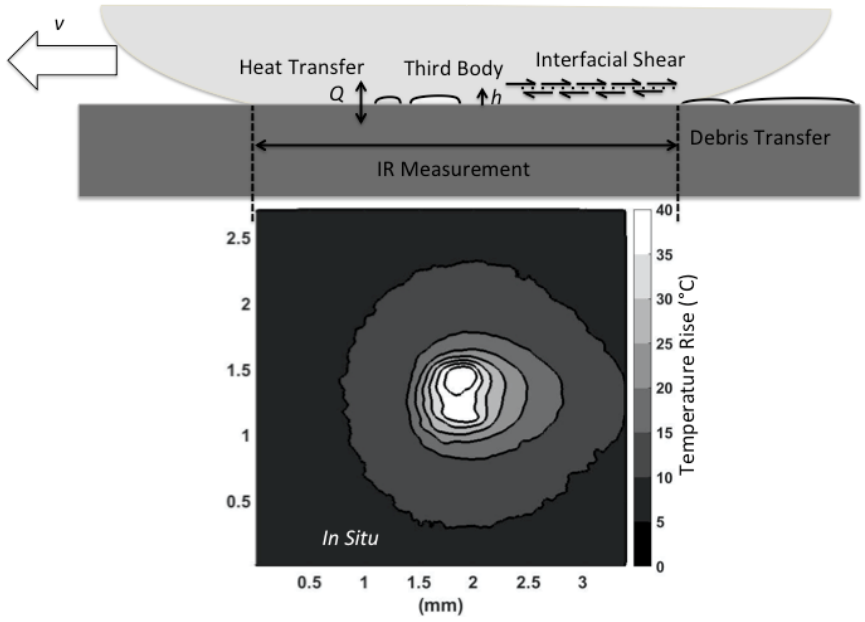

Figure 7.2. Illustration of frictional heating and transfer film formation process.

The localized heating also explains the sensitivity of PEEK wear behavior to molecular weight Mw and sliding direction. Figure 7.3 shows the dynamic mechanical behavior for a low and high M_w PEEK sample. With increasing temperature the shear modulus G' drops and molecular mobility becomes more favorable. The increased molecular mobility at temperatures above the glass transition T_g will promote debris formation. The cross shearing of the PEEK surface from multidirectional sliding will increase the wear rate as a result. The localized heating also explains the drastic difference in behaviors between the various grades and type of PAEK material tested. Figure 7.4 shows the stress strain hysteresis behavior for a low and high M_w PEEK sample tested at 175C. It can be seen that the energy dissipated due to hysteresis is much

greater in the lower M_w PEEK sample. The greater hysteric heating will cause greater softening of the bulk polymer and will contribute to wear behavior.

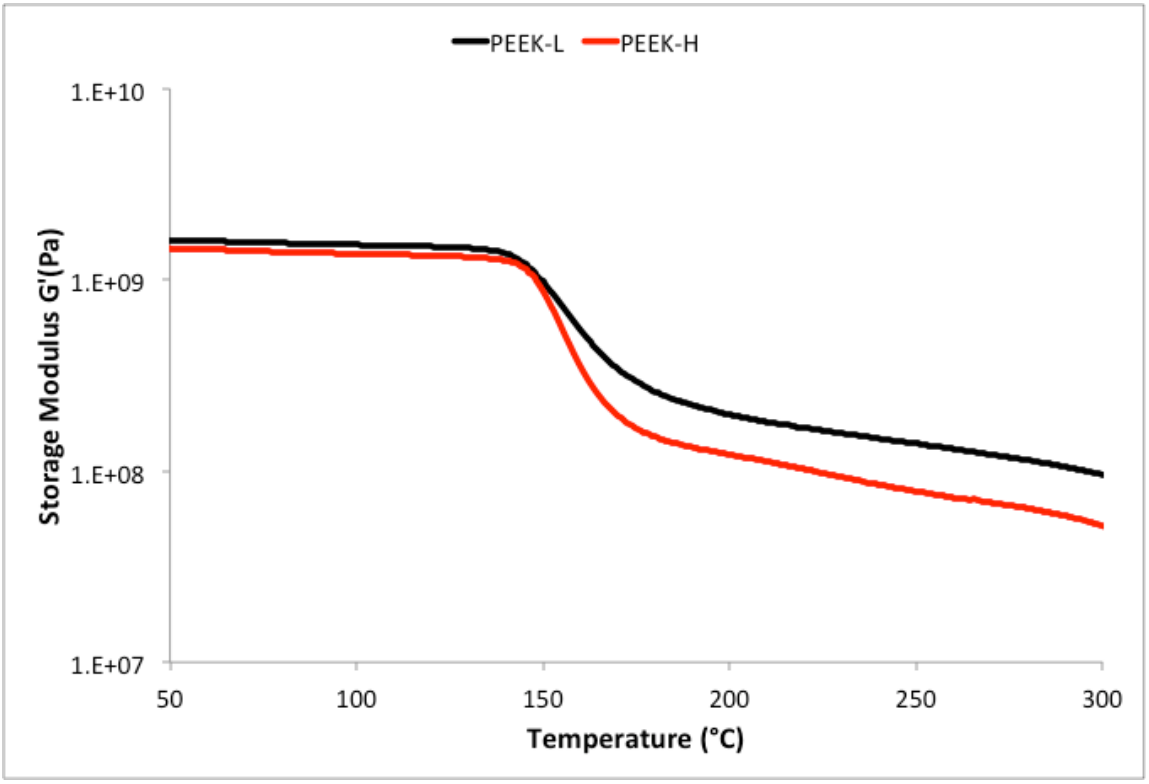

Figure 7.3. Dynamic mechanical temperature sweep for PEEK-L and PEEK-H samples.

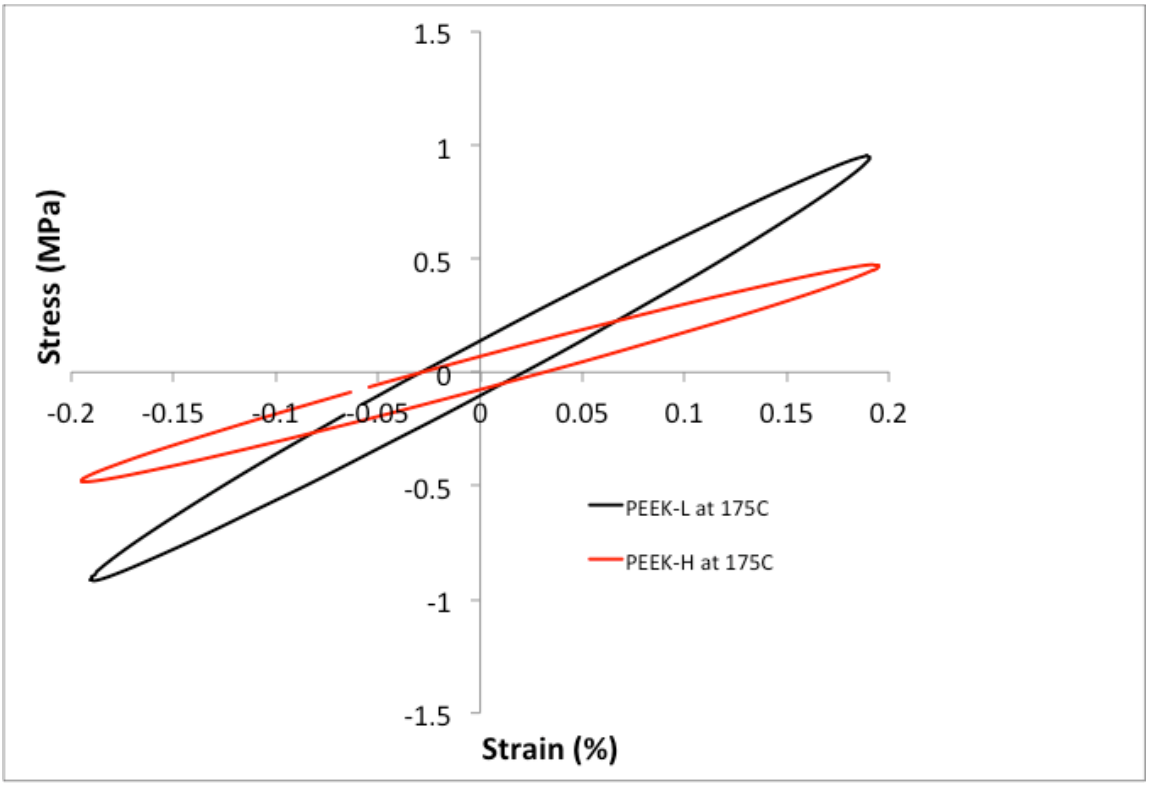

Figure 7.4. Hysteresis loops for PEEK-L and PEEK-H samples taken at 175°C.

The experimental results demonstrate how the varied material parameters and test conditions contribute to adhesive wear. Although wear cannot be predicted a priori these studies allow for some behavioral predictions to be made for PEEK based material. Further work in understanding the relationship between material properties and wear of PEEK is needed.

7.2 Considerations for Future Research

The findings presented in this dissertation offer greater insight into the fundamentals of friction and wear in PAEK based materials. Although many questions were answered, there are many areas that require additional work. The research findings

can also be used to design improved PAEK based material for application in tribological environments.

7.2.1 Model for Subsurface Damage Mechanisms

In this work it became apparent that the severity of wear and damage to the pin surface corresponded to how material is sheared away from the bulk. Low wear corresponded to instances in which transfer films formed as thin continuous sheets. More severe wear coincided with thicker delaminated sheets of debris. Blanchett described a similar process for the behavior of PTFE[185] and an illustration is shown in Figure 7.5. The sliding conditions such as pressure, velocity, and surface roughness will all contribute to the subsurface stress distribution. Additionally, changes in surface properties that occur during wear can also contribute to how material is sheared from the bulk. Future work to model this contact stress distribution would be highly beneficial.

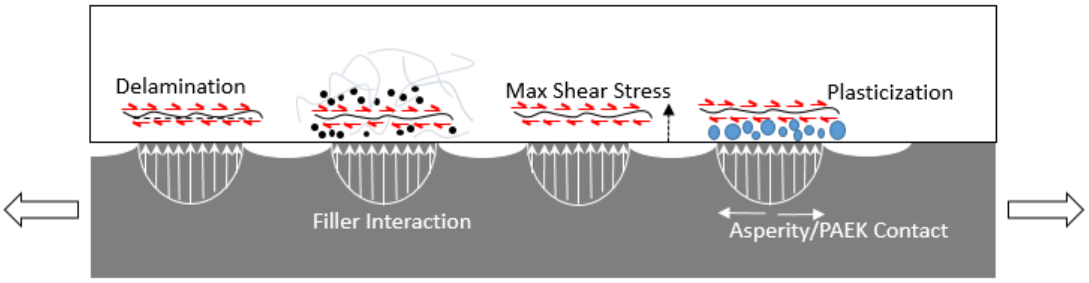

Figure 7.5. Illusstration of subsurface shear stress and contributing factors.

A model of how the presence of a transfer film changes the contact stress distribution would also be necessary. It is believed that transfer films reduce wear since they protect the bulk from abrasion of hard rough asperities. The film modulus closely matches that of the bulk as seen in the nanoindentation load vs. depth graph in Figure 7.6. However, it is uncertain what factors dictate the tenacity of these films and their effectiveness in reducing wear. Attempts have been made to incorporate such transfer film effects on contact stress by some researchers[208]. An effective model would also describe how heat is distributed within the film[209].

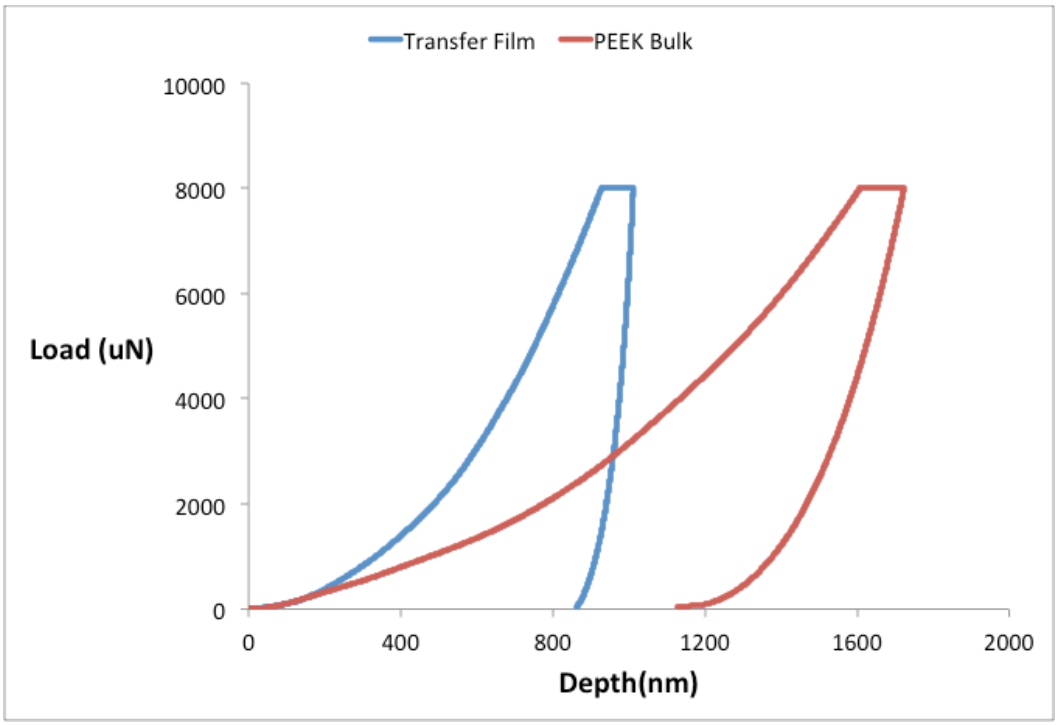

Figure 7.6. Nanoindentation of transfer film and bulk PEEK material.

7.2.2 Nanoparticles to Improve Transfer Film Deposition

Fillers are often added to PEEK and may result in lower friction and improved wear resistance. The most common fillers are PTFE, graphite, and carbon fiber and are used both individually and in combination with each other. However, the use of filler to improve tribological behavior can reduce mechanical properties. Nanoparticles are an increasingly attractive choice for filler[48]. When such nanoparticles are well dispersed in the polymer matrix they can interact with cracks or other damage features. Due to the particle size they will not act as a stress concentrator that promotes crack propagation. Many nanoparticles are also multifunctional in the sense that they can improve strength, lower friction and promote transfer film formation all at the same time. Work to incorporate well dispersed nanomaterial into a PEEK matrix would be extremely valuable.

7.2.3 Chemical Adhesion Between Debris and Surface

Another area that lacks comprehensive knowledge is the adhesion between transfer films and counterfaces. The tenacity of the transfer film depends on how strongly it is bonded to the counterface. When the shear strength of this bond is overcome the transfer film will be removed and no longer offer any protection from abrasion. To better understand the nature of this bonding between PEEK film and the counterface chemical spectroscopy can be performed. In previous work with PTFE focused ion beam milling was used to remove sections of transfer film bonded to counterfaces[210]. The cross section of the transfer film and counterface could then be examined with transmission electron microscopy (TEM). Chemical analysis of the cross

section can also be done to assign chemistry to the adhesion mechanism. Such a procedure would also be beneficial for understanding how different counterface materials and fillers influence the wear behavior.

REFERENCES

1. Pitenis, A., D. Dowson, and W. Gregory Sawyer, *Leonardo da Vinci's Friction Experiments: An Old Story Acknowledged and Repeated.* Tribology Letters, 2014. **56**(3): p. 509-515.

2. Archard, J.F. and W. Hirst. *The wear of metals under unlubricated conditions*. in *Proceedings of the Royal Society of London A: Mathematical, Physical and Engineering Sciences*. 1956. The Royal Society.

3. Ludema, K.C. and D. Tabor, *The friction and visco-elastic properties of polymeric solids.* Wear, 1966. **9**(5): p. 329-348.

4. Tabor, D., *Surface forces and surface interactions.* Journal of colloid and interface science, 1977. **58**(1): p. 2-13.

5. Lancaster, J.K., *Abrasive wear of polymers.* Wear, 1969. **14**(4): p. 223-239.

6. Kato, K. and K. Adachi, *Wear mechanisms.* Modern tribology handbook, 2001. **1**: p. 273-300.

7. Pooley, C.M. and D. Tabor, *Friction and molecular structure: the behaviour of some thermoplastics.* Proceedings of the Royal Society of London. Series A, Mathematical and Physical Sciences, 1972: p. 251-274.

8. Wang, A., *A unified theory of wear for ultra-high molecular weight polyethylene in multi-directional sliding.* Wear, 2001. **248**(1–2): p. 38-47.

9. Briscoe, B.J. and S.K. Sinha, *Wear of polymers.* Proceedings of the Institution of Mechanical Engineers, Part J: Journal of Engineering Tribology, 2002. **216**(6): p. 401-413.

10. Lu, Z.P. and K. Friedrich, *On sliding friction and wear of PEEK and its composites.* Wear, 1995. **181**: p. 624-631.

11. Tanaka, K., *Some interesting problems that remain unsolved in my work on polymer tribology.* Tribology International, 1995. **28**(1): p. 19-22.

12. Bahadur, S., *The development of transfer layers and their role in polymer tribology.* Wear, 2000. **245**(1–2): p. 92-99.

13. Hoskins, T.J., et al., *The wear of PEEK in rolling–sliding contact–Simulation of polymer gear applications.* Wear, 2014. **309**(1): p. 35-42.

14. Stuart, B.H., *Tribological studies of poly (ether ether ketone) blends.* Tribology International, 1998. **31**(11): p. 647-651.

15. Friedrich, K., J. Karger-Kocsis, and Z. Lu, *Effects of steel counterface roughness and temperature on the friction and wear of PE (E) K composites under dry sliding conditions.* Wear, 1991. **148**(2): p. 235-247.

16. Elliott, D.M., J. Fisher, and D.T. Clark, *Effect of counterface surface roughness and its evolution on the wear and friction of PEEK and PEEK-bonded carbon fibre composites on stainless steel.* Wear, 1998. **217**(2): p. 288-296.

17. Ovaert, T.C. and H.S. Cheng, *Counterface topographical effects on the wear of polyetheretherketone and a polyetheretherketone-carbon fiber composite.* Wear, 1991. **150**(1): p. 275-287.

18. Ramachandra, S. and T.C. Ovaert, *The effect of controlled surface topographical features on the unlubricated transfer and wear of PEEK.* Wear, 1997. **206**(1): p. 94-99.

19. Ovaert, T.C. and H.S. Cheng, *The unlubricated sliding wear behavior of polyetheretherketone against smooth mild-steel counterfaces.* Journal of Tribology, 1991. **113**(1): p. 150-157.

20. Laux, K.A. and C.J. Schwartz, *Effects of contact pressure, molecular weight, and supplier on the wear behavior and transfer film of polyetheretherketone (PEEK).* Wear, 2013. **297**(1–2): p. 919-925.

21. Laux, K.A. and C.J. Schwartz, *Influence of linear reciprocating and multi-directional sliding on PEEK wear performance and transfer film formation.* Wear, 2013. **301**(1–2): p. 727-734.

22. Suh, N.P., *An overview of the delamination theory of wear.* Wear, 1977. **44**(1): p. 1-16.

23. Zhang, M.Q., Z.P. Lu, and K. Friedrich, *On the wear debris of polyetheretherketone: fractal dimensions in relation to wear mechanisms.* Tribology international, 1997. **30**(2): p. 87-102.

24. Dickens, P.M., J.L. Sullivan, and J.K. Lancaster, *Speed effects on the dry and lubricated wear of polymers.* Wear, 1986. **112**(3): p. 273-289.

25. Zhang, G., et al., *Effects of sliding velocity and applied load on the tribological mechanism of amorphous poly-ether–ether–ketone (PEEK).* Tribology International, 2008. **41**(2): p. 79-86.

26. Schelling, A., H.H. Kausch, and A.C. Roulin, *Friction behaviour of polyetheretherketone under dry reciprocating movement.* Wear, 1991. **151**(1): p. 129-142.

27. Briscoe, B.J., M.C.M. Pooley, and D. Tabor, *Friction and transfer of some polymers in unlubricated sliding*, in *Advances in Polymer Friction and Wear*. 1975, Springer. p. 191-204.

28. Makinson, K.R. and D. Tabor, *Friction and Transfer of Polytetrafluoroethylene.* Nature, 1964. **201**(4918): p. 464-466.

29. Marcellan, A., et al., *Third body effects in the wear of polyamide: micro-mechanisms and wear particles analysis.* Wear, 2009. **266**(9): p. 1013-1020.

30. Stuart, B.H., *The application of Fourier transform Raman spectroscopy to polymer tribology.* Spectrochimica Acta Part A: Molecular and Biomolecular Spectroscopy, 1997. **53**(1): p. 111-118.

31. Feng, X., Z. Lu, and R. Zhang, *Analysis of electron spectroscopy for chemical analysis of the transferred film formed during sliding wear for carbon fibre reinforced polyetheretherketone and its composites.* Journal of materials science, 1999. **34**(14): p. 3513-3524.

32. Li, T.Q., et al., *Friction induced mechanochemical and mechanophysical changes in high performance semicrystalline polymer.* Polymer, 1999. **40**(16): p. 4451-4458.

33. Elliott, D.M., et al., *A tri-pin-on-disk apparatus for in situ X-ray photoelectron spectroscopy of worn surfaces.* Wear, 1999. **236**(1): p. 308-314.

34. Zhang, M.Q., Z.P. Lu, and K. Friedrich, *Thermal analysis of the wear debris of polyetheretherketone.* Tribology International, 1997. **30**(2): p. 103-111.

35. Zhang, M.Q., et al., *Frictional surface temperature determination of high-temperature-resistant semicrystalline polymers by using their double melting features.* Journal of Applied Polymer Science, 1997. **63**(5): p. 589-593.

36. Zhang, G. and A.K. Schlarb, *Correlation of the tribological behaviors with the mechanical properties of poly-ether-ether-ketones (PEEKs) with different molecular weights and their fiber filled composites.* Wear, 2009. **266**(1): p. 337-344.

37. Omar, M.K., A.G. Atkins, and J.K. Lancaster, *The role of crack resistance parameters in polymer wear.* Journal of Physics D: Applied Physics, 1986. **19**(2): p. 177.

38. Saib, K.S., W.J. Evans, and D.H. Isaac, *The role of microstructure during fatigue crack growth in poly(aryl ether ether ketone) (PEEK).* Polymer, 1993. **34**(15): p. 3198-3203.

39. Chu, J.-N. and J. Schultz, *The influence of microstructure on the failure behaviour of PEEK.* Journal of Materials Science, 1990. **25**(8): p. 3746-3752.

40. Berer, M., Z. Major, and G. Pinter, *Elevated pitting wear of injection molded polyetheretherketone (PEEK) rolls.* Wear, 2013. **297**(1): p. 1052-1063.

41. Mizobe, K., et al. *Fourier Transform Infrared Spectroscopy for Wear Debris Adhesion on PEEK Bearing Surface*. in *Applied Mechanics and Materials*. 2013. Trans Tech Publ.

42. Stolarski, T.A. and R. Gawarkiewicz, *Peculiarities associated with testing polyetheretherketone (PEEK) in a model rolling contact.* Tribology International, 2015. **81**: p. 9-18.

43. Berer, M., et al., *Investigation of the dynamic mechanical behavior of polyetheretherketone (PEEK) in the high stress tensile regime.* Mechanics of Time-Dependent Materials, 2014. **18**(4): p. 663-684.

44. Berer, M., D. Tscharnuter, and G. Pinter, *Dynamic mechanical response of polyetheretherketone (PEEK) exposed to cyclic loads in the high stress tensile regime.* International Journal of Fatigue, 2015. **80**: p. 397-405.

45. Iqbal, T., B.J. Briscoe, and P.F. Luckham, *Surface Plasticization of Poly (ether ether ketone).* European Polymer Journal, 2011. **47**(12): p. 2244-2258.

46. Briscoe, B.J., et al., *The failure of poly (ether ether ketone) in high speed contacts.* Wear, 1993. **162**: p. 407-417.

47. Pan, G., et al., *Fretting wear behaviors of nanometer Al2O3 and SiO2 reinforced PEEK composites.* Wear, 2009. **266**(11–12): p. 1208-1215.

48. Friedrich, K., Z. Zhang, and A.K. Schlarb, *Effects of various fillers on the sliding wear of polymer composites.* Composites Science and Technology, 2005. **65**(15): p. 2329-2343.

49. Harsha, A.P. and U.S. Tewari, *The effect of fibre reinforcement and solid lubricants on abrasive wear behavior of polyetheretherketone composites.* Journal of reinforced plastics and composites, 2003. **22**(8): p. 751-767.

50. Sawyer, W.G., et al., *Mechanistic Studies in Friction and Wear of Bulk Materials.* Annu. Rev. Mater. Res, 2014. **44**: p. 16.1-16.33.

51. Stober, E.J., J.C. Seferis, and J.D. Keenan, *Characterization and exposure of polyetheretherketone (PEEK) to fluid environments.* Polymer, 1984. **25**(12): p. 1845-1852.

52. Hay, J.N. and D.J. Kemmish, *Environmental stress crack resistance of and absorption of low-molecular-weight penetrants by poly (aryl ether ether ketone).* Polymer, 1988. **29**(4): p. 613-618.

53. Ogale, A.A. and R.L. McCullough, *Physical aging characteristics of polyether ether ketone.* Composites science and technology, 1987. **30**(2): p. 137-148.

54. Chivers, R.A. and D.R. Moore, *The effect of molecular weight and crystallinity on the mechanical properties of injection moulded poly (aryl-ether-ether-ketone) resin.* Polymer, 1994. **35**(1): p. 110-116.

55. Talbott, M.F., G.S. Springer, and L.A. Berglund, *The effects of crystallinity on the mechanical properties of PEEK polymer and graphite fiber reinforced PEEK.* Journal of Composite Materials, 1987. **21**(11): p. 1056-1081.

56. Medellin-Rodriguez, F.J. and P.J. Phillips, *Crystallization and structure-mechanical property relations in poly (aryl ether ether ketone)[PEEK]*. Polymer Engineering & Science, 1990. **30**(14): p. 860-869.

57. Atkinson, J.R., J.N. Hay, and M.J. Jenkins, *Enthalpic relaxation in semi-crystalline PEEK.* Polymer, 2002. **43**(3): p. 731-735.

58. Kemmish, D., *Update on the Technology and Applications of Polyaryletherketones*. 2010: ISmithers.

59. Reitman, M., et al., *Morphology and Crystalline Architecture of Polyaryletherketones.* PEEK Biomaterials Handbook, 2011: p. 49.

60. Blundell, D.J. and B.N. Osborn, *The morphology of poly (aryl-ether-ether-ketone).* Polymer, 1983. **24**(8): p. 953-958.

61. Rueda, D.R., et al., *Polymer communications: X-ray diffraction study of die drawn poly (aryletherketone)(PEEK).* Polymer communications, 1983. **24**(9): p. 258-260.

62. Jin, L., et al., *Crystallization behavior and morphological characterization of poly (ether ether ketone).* Polymer, 2014. **55**(20): p. 5255-5265.

63. Cebe, P. and S.-D. Hong, *Crystallization behaviour of poly (ether-ether-ketone).* Polymer, 1986. **27**(8): p. 1183-1192.

64. Bassett, D.C., R.H. Olley, and I.A.M. Al Raheil, *On crystallization phenomena in PEEK*. Polymer, 1988. **29**(10): p. 1745-1754.

65. Hsiao, B.S., et al., *Time-resolved X-ray study of poly (aryl ether ether ketone) crystallization and melting behaviour: 1. Crystallization.* Polymer, 1993. **34**(19): p. 3986-3995.

66. Krüger, K.N. and H.G. Zachmann, *Investigation of the melting behavior of poly (aryl ether ketones) by simultaneous measurements of SAXS and WAXS employing synchrotron radiation.* Macromolecules, 1993. **26**(19): p. 5202-5208.

67. Verma, R.K., et al., *SAXS studies of lamellar level morphological changes during crystallization and melting in PEEK.* Polymer, 1996. **37**(24): p. 5357-5365.

68. Lattimer, M.P., et al., *On the origin of the multiple endotherms in PEEK.* Polymer, 1992. **33**(18): p. 3971-3973.

69. Sobieraj, M.C. and C.M. Rimnac, *Fracture, Fatigue, and Notch Behavior of PEEK.* PEEK Biomaterials Handbook, 2011: p. 61.

70. White, K.L., et al., *Rheological and thermal behaviors of commercial poly (aryletherketone) s.* Polymer Engineering & Science, 2013. **53**(3): p. 651-661.

71. Jonas, A. and R. Legras, *Thermal stability and crystallization of poly (aryl ether ether ketone).* Polymer, 1991. **32**(15): p. 2691-2706.

72. Day, M., J.D. Cooney, and D.M. Wiles, *The thermal stability of poly (aryl-ether–ether-ketone) as assessed by thermogravimetry.* Journal of applied polymer science, 1989. **38**(2): p. 323-337.

73. Lee, Y., J.-M. Lefebvre, and R.S. Porter, *Uniaxial Draw Of Poly(aryl-ether-ether-ketone) by solid-state extrusion.* Journal of Polymer Science Part B: Polymer Physics, 1988. **26**(4): p. 795-805.

74. Lee, Y., J.M. Lefebvre, and R.S. Porter, *Uniaxial Draw Of Poly (aryl-ether-ether-ketone) by solid-state extrusion.* Journal of Polymer Science Part B: Polymer Physics, 1988. **26**(4): p. 795-805.

75. Voice, A.M., D.I. Bower, and I.M. Ward, *Molecular orientation in uniaxially drawn poly(aryl ether ether ketone): 1. Refractive index and X-ray measurements.* Polymer, 1993. **34**(6): p. 1154-1163.

76. Richardson, A., et al., *The production and properties of poly(aryletherketone) (PEEK) rods oriented by drawing through a conical die.* Polymer Engineering & Science, 1985. **25**(6): p. 355-361.

77. Cebe, P., *Annealing study of poly (etheretherketone).* Journal of materials science, 1988. **23**(10): p. 3721-3731.

78. Lee, Y. and R.S. Porter, *Crystallization of poly (etheretherketone)(PEEK) in carbon fiber composites.* Polymer Engineering & Science, 1986. **26**(9): p. 633-639.

79. Waterhouse, R.B., *Fretting fatigue*. 1981: Elsevier Science & Technology.

80. Mutoh, Y., S.E. Kinyon, and D.W. Hoeppner, *Fretting fatigue: advances in basic understanding and applications*. Vol. 1425. 2003: ASTM International.

81. Hills, D.A., *Mechanics of fretting fatigue.* Wear, 1994. **175**(1): p. 107-113.

82. Play, D., *Mutual overlap coefficient and wear debris motion in dry oscillating friction and wear tests.* ASLE transactions, 1985. **28**(4): p. 527-535.

83. Feeny, B., et al., *A historical review on dry friction and stick-slip phenomena.* Applied Mechanics Reviews, 1998. **51**(5): p. 321-341.

84. Etsion, I., *Revisiting the Cattaneo–Mindlin concept of interfacial slip in tangentially loaded compliant bodies.* Journal of Tribology, 2010. **132**(2): p. 020801.

85. Hoeppner, D., S. Adibnazari, and M.W. Moesser, *Literature Review and Preliminary Studies of Fretting and Fretting Fatigue Including Special Applications to Aircraft Joints*. 1994, DTIC Document.

86. Gordelier, S.C. and T.C. Chivers, *A literature review of palliatives for fretting fatigue.* Wear, 1979. **56**(1): p. 177-190.

87. Kang, C. and N.S. Eiss Jr, *Fretting wear of polysiloxane-polyimide copolymer coatings as a function of varying humidity.* Wear, 1992. **158**(1-2): p. 29-40.

88. Higham, P.A., F.H. Stott, and B. Bethune, *Mechanisms of wear of the metal surface during fretting corrosion of steel on polymers.* Corrosion Science, 1978. **18**(1): p. 3-13.

89. Gaydos, P., *Fretting wear of polymeric coatings.* Wear of Materials 1989., 1989. **2**: p. 529-535.

90. Zhou, Z.R. and L. Vincent, *Lubrication by thin polystyrene coating in fretting.* Wear, 1999. **231**(2): p. 179-184.

91. Kang, C. and N.S. Eiss, *Fretting of polyimide coatings Part I: Structure and moisture effects.* Wear, 1995. **181–183, Part 1**(0): p. 94-100.

92. Dahmani, N., et al., *Velocity accommodation in polymer fretting.* Wear, 1992. **158**(1–2): p. 15-28.

93. Rabbe, L.M., et al., *Fretting deterioration of orthopaedic implant materials: Search for solutions.* Clinical Materials, 1994. **15**(4): p. 221-226.

94. Briscoe, B.J., et al., *Contact damage of poly(methylmethacrylate) during complex microdisplacements.* Wear, 2000. **240**(1–2): p. 27-39.

95. Chateauminois, A., M. Kharrat, and A. Krichen, *Analysis of fretting damage in polymers by means of fretting maps.* Astm special technical publication, 2000. **1367**: p. 352-368.

96. Briscoe, B.J., et al., *Fretting wear behaviour of polymethylmethacrylate under linear motions and torsional contact conditions.* Tribology International, 1998. **31**(11): p. 701-711.

97. Briscoe, B.J. and A. Chateauminois, *Measurements of friction-induced surface strains in a steel/polymer contact.* Tribology International, 2002. **35**(4): p. 245-254.

98. Briscoe, B.J., et al., *Acoustic noise emission in a model PMMA/steel fretting contact.* Tribology Series, 2001. **39**: p. 673-681.

99. Chateauminois, A. and B.J. Briscoe, *Nano-rheological properties of polymeric third bodies generated within fretting contacts.* Surface and Coatings Technology, 2003. **163–164**(0): p. 435-443.

100. Higham, P.A., B. Bethune, and F.H. Stott, *Changes in the surface morphology of polycarbonate induced by fretting.* Journal of Materials Science, 1977. **12**(12): p. 2503-2510.

101. Terekhina, S., M. Salvia, and S. Fouvry, *Contact fatigue and wear behaviour of bismaleimide polymer subjected to fretting loading under various temperature conditions.* Tribology International, 2011. **44**(4): p. 396-408.

102. Krichen, A., et al., *Surface damage of poly (methylmethacrylate) under fretting loading.* Wear, 1999. **230**(2): p. 146-155.

103. Guo, Q. and W. Luo, *Mechanisms of fretting wear resistance in terms of material structures for unfilled engineering polymers.* Wear, 2001. **249**(10–11): p. 924-931.

104. Blundell, D.J. and B.N. Osborn, *The morphology of poly(aryl-ether-ether-ketone).* Polymer, 1983. **24**(8): p. 953-958.

105. *Annual Book of ASTM Standards*, in *15.03*. 2002, ASTM International: West Conshohocken, Pa. USA.

106. Briscoe, B.J. and T.A. Stolarski, *Combined rotating and linear motion effects on the wear of polymers.* 1979.

107. Briscoe, B.J. and T.A. Stolarski, *Transfer wear of polymers during combined linear motion and load axis spin.* Wear, 1985. **104**(2): p. 121-137.

108. Stachowiak, G. and A.W. Batchelor, *Engineering tribology*. 2013: Butterworth-Heinemann.

109. Baumberger, T. and C. Caroli, *Solid friction from stick–slip down to pinning and aging.* Advances in Physics, 2006. **55**(3-4): p. 279-348.

110. Xia, Z.Y., H.J. Sue, and T.P. Rieker, *Morphological evolution of poly (ethylene terephthalate) during equal channel angular extrusion process.* Macromolecules, 2000. **33**(23): p. 8746-8755.

111. Hay, J.N., J.I. Langford, and J.R. Lloyd, *Variation in unit cell parameters of aromatic polymers with crystallization temperature.* Polymer, 1989. **30**(3): p. 489-493.

112. Zhang, G., et al., *Temperature dependence of the tribological mechanisms of amorphous PEEK (polyetheretherketone) under dry sliding conditions.* Acta Materialia, 2008. **56**(10): p. 2182-2190.

113. Kemmish, D., *Update on the Technology and Applications of Polyaryletherketones; iSmithers: Shropshire.* United Kingdom, 2010.

114. Díez-Pascual, A.M., et al., *High-performance nanocomposites based on polyetherketones.* Progress in Materials Science, 2012. **57**(7): p. 1106-1190.

115. Scharf, T.W. and S.V. Prasad, *Solid lubricants: a review.* Journal of Materials Science, 2013. **48**(2): p. 511-531.

116. Bahadur, S. and D. Gong, *The action of fillers in the modification of the tribological behavior of polymers.* Wear, 1992. **158**(1): p. 41-59.

117. Bahadur, S., D. Gong, and J.W. Anderegg, *The investigation of the action of fillers by XPS studies of the transfer films of PEEK and its composites containing CuS and CuF 2.* Wear, 1993. **160**(1): p. 131-138.

118. Bahadur, S. and C.J. Schwartz, . *The influence of nanoparticle fillers in polymer matrices on the formation and stability of transfer film during wear.* Tribology and Interface Engineering Series, 2008. **55**: p. 17-34.

119. Burris, D.L. and W.G. Sawyer, *A low friction and ultra low wear rate PEEK/PTFE composite.* Wear, 2006. **261**(3): p. 410-418.

120. Zhang, G., Z. Rasheva, and A.K. Schlarb, *Friction and wear variations of short carbon fiber (SCF)/PTFE/graphite (10vol.%) filled PEEK: Effects of fiber orientation and nominal contact pressure.* Wear, 2010. **268**(7): p. 893-899.

121. Lancaster, J.K., *A review of the influence of environmental humidity and water on friction, lubrication and wear.* Tribology International, 1990. **23**(6): p. 371-389.

122. Evans, D.C. *Polymer-fluid interaction in relation to wear*. in *Proceedings of the third Leeds–Lyon symposium on tribology, the wear of non-metallic materials*. 1978.

123. Briscoe, B.J. and B.H. Stuart, *The surface plasticisation and lubrication of poly (ether ether ketone) by third body formation.* Tribology Series, 1996. **31**: p. 69-78.

124. Briscoe, B.J., T.A. Stolarski, and G.J. Davies, *Boundary lubrication of thermoplastic polymers in model fluids.* Tribology international, 1984. **17**(3): p. 129-137.

125. Mohammed, M.H., et al., *Physical properties of poly (ether ether ketone) exposed to simulated severe oilfield service conditions.* Polymer Degradation and Stability, 2013. **98**(6): p. 1264-1270.

126. Unal, H. and A. Mimaroglu, *Friction and wear characteristics of PEEK and its composite under water lubrication.* Journal of reinforced plastics and composites, 2006. **25**(16): p. 1659-1667.

127. Yamamoto, Y. and T. Takashima, *Friction and wear of water lubricated PEEK and PPS sliding contacts.* Wear, 2002. **253**(7–8): p. 820-826.

128. Yamamoto, Y. and M. Hashimoto, *Friction and wear of water lubricated PEEK and PPS sliding contacts: Part 2. Composites with carbon or glass fibre.* Wear, 2004. **257**(1): p. 181-189.

129. Jacobs, O., et al., *On the effect of counterface material and aqueous environment on the sliding wear of various PEEK compounds.* Tribology letters, 2005. **18**(3): p. 359-372.

130. Laux, K.A., et al., *Wear Behavior of Polyaryletherketones Under Multi-directional Sliding and Fretting Conditions.* Tribology Letters, 2015. **58**(3): p. 1-13.

131. ABAQUS. *ABAQUS® Analysis User's Manual, Version 6.9*. Available from: www.simulia.com

132. Cho, D.-H., B. Bhushan, and J. Dyess, *Mechanisms of static and kinetic friction of polypropylene, polyethylene terephthalate, and high-density polyethylene pairs during sliding.* Tribology International, 2016. **94**: p. 165-175.

133. Maeda, N., et al., *Adhesion and friction mechanisms of polymer-on-polymer surfaces.* Science, 2002. **297**(5580): p. 379-382.

134. Berman, A.D., W.A. Ducker, and J.N. Israelachvili, *Origin and characterization of different stick-slip friction mechanisms.* Langmuir, 1996. **12**(19): p. 4559-4563.

135. Bowden, F.P. and D. Tabor, *The Friction and Lubrication of Solids*. Vol. 1. 2001: Oxford University Press.

136. Menezes, P.L. and S.V. Kailas, *Effect of roughness parameter and grinding angle on coefficient of friction when sliding of Al–Mg alloy over EN8 steel.* Journal of tribology, 2006. **128**(4): p. 697-704.

137. McC. Ettles, C.M., *Polymer and elastomer friction in the thermal control regime.* ASLE transactions, 1987. **30**(2): p. 149-159.

138. Lancaster, J.K., *Estimation of the limiting PV relationships for thermoplastic bearing materials.* Tribology, 1971. **4**(2): p. 82-86.

139. Tanaka, K. and Y. Uchiyama. *Friction, wear and surface melting of crystalline polymers*. in *Abstracts of papers of the american chemical society*. 1974. AMER CHEMICAL SOC 1155 16TH ST, NW, WASHINGTON, DC 20036.

140. Kurtz, S.M. and J.N. Devine, *PEEK biomaterials in trauma, orthopedic, and spinal implants.* Biomaterials, 2007. **28**(32): p. 4845-4869.

141. Rowntree, R.A. and M.J. Todd. *A review of European trends in space tribology and its application to spacecraft mechanism design*. in *MRS Proceedings*. 1988. Cambridge Univ Press.

142. Burris, D.L. and W.G. Sawyer, *Hierarchically constructed metal foam/polymer composite for high thermal conductivity.* Wear, 2008. **264**(3): p. 374-380.

143. Bijwe, J., S. Sen, and A. Ghosh, *Influence of PTFE content in PEEK–PTFE blends on mechanical properties and tribo-performance in various wear modes.* Wear, 2005. **258**(10): p. 1536-1542.

144. Dyson, J. and W. Hirst, *The true contact area between solids.* Proceedings of the Physical Society. Section B, 1954. **67**(4): p. 309.

145. McCutchen, C.W., *Optical systems for observing surface topography by frustrated total internal reflection and by interference.* Review of Scientific Instruments, 1964. **35**(10): p. 1340-1345.

146. O'Callaghan, P.W. and S.D. Probert, *Prediction and measurement of true areas of contact between solids.* Wear, 1987. **120**(1): p. 29-49.

147. Blok, H., *The flash temperature concept.* Wear, 1963. **6**(6): p. 483-494.

148. Plumlee, K.G. and C.J. Schwartz, *Surface layer plastic deformation as a mechanism for UHMWPE wear, and its role in debris size.* Wear, 2013. **301**(1–2): p. 257-263.

149. Rhee, S.H. and K.C. Ludema, *Mechanisms of formation of polymeric transfer films.* Wear, 1978. **46**(1): p. 231-240.

150. Archard, J.F., *The temperature of rubbing surfaces.* wear, 1959. **2**(6): p. 438-455.

151. Archard, J.F. and R.A. Rowntree, *The temperature of rubbing bodies; part 2, the distribution of temperatures.* Wear, 1988. **128**(1): p. 1-17.

152. Jaeger, J.C. *Moving sources of heat and the temperature of sliding contacts*. in *J. and Proc. Roy. Soc. New South Wales*. 1942.

153. Tian, X. and F.E. Kennedy, *Maximum and average flash temperatures in sliding contacts.* Journal of Tribology, 1994. **116**(1): p. 167-174.

154. Kennedy, F.E., *Frictional heating and contact temperatures.* Modern tribology handbook, 2001. **1**: p. 235-259.

155. Rowe, K.G., et al., *In situ thermal measurements of sliding contacts.* Tribology International, 2013. **62**: p. 208-214.

156. Laraqi, N., et al., *Temperature and division of heat in a pin-on-disc frictional device—exact analytical solution.* Wear, 2009. **266**(7): p. 765-770.

157. Le Rouzic, J. and T. Reddyhoff, *Development of infrared microscopy for measuring asperity contact temperatures.* Journal of Tribology, 2013. **135**(2): p. 021504.

158. Bennett, A.I., K.G. Rowe, and W.G. Sawyer, *Dynamic In Situ Measurements of Frictional Heating on an Isolated Surface Protrusion.* Tribology Letters, 2014. **55**(1): p. 205-210.

159. Putignano, C., et al., *A theoretical and experimental study of viscoelastic rolling contacts incorporating thermal effects.* Proceedings of the Institution of Mechanical Engineers, Part J: Journal of Engineering Tribology, 2014: p. 1350650114530681.

160. Fortunato, G., et al., *General theory of frictional heating with application to rubber friction.* Journal of Physics: Condensed Matter, 2015. **27**(17): p. 175008.

161. Underwood, G.S., *Wear Performance of Ultra-Performance Engineering Polymers at High PVs*. 2002, SAE Technical Paper.

162. Stolarski, T.A., *Tribology of polyetheretherketone.* Wear, 1992. **158**(1): p. 71-78.

163. Burris, D.L., et al., *Polymeric nanocomposites for tribological applications.* Macromolecular materials and engineering, 2007. **292**(4): p. 387-402.

164. Zhao, Q. and S. Bahadur, *The mechanism of filler action and the criterion of filler selection for reducing wear.* Wear, 1999. **225**: p. 660-668.

165. Jacobs, O., et al., *On the effect of counterface material and aqueous environment on the sliding wear of carbon fibre reinforced polyetheretherketone (PEEK).* Tribology Letters, 2005. **19**(4): p. 319-329.

166. Rebelo de Figueiredo, M., et al., *Adhesion tendency of polymers to hard coatings.* International Polymer Processing, 2013. **28**(4): p. 415-420.

167. Instruments, P.C.S., *MTM (Mini Traction Machine).* 2016.

168. Bahadur, S., *Dependence of polymer sliding friction on normal load and contact pressure.* Wear, 1974. **29**(3): p. 323-336.

169. Archard, J.F. *Elastic deformation and the laws of friction*. in *Proceedings of the Royal Society of London A: Mathematical, Physical and Engineering Sciences*. 1957. The Royal Society.

170. Bowers, R.C., *Coefficient of friction of high polymers as a function of pressure.* Journal of Applied Physics, 1971. **42**(12): p. 4961-4970.

171. Quaglini, V. and P. Dubini, *Friction of polymers sliding on smooth surfaces.* Advances in Tribology, 2011. **2011**.

172. McC. Ettles, M.C., *Heat generation and friction in rotating bands.* ASLE transactions, 1986. **29**(3): p. 312-320.

173. Clerico, M., *Tribological behaviour of polyacetals.* Wear, 1980. **64**(2): p. 259-272.

174. Watanabe, M. and H. Yamaguchi, *The friction and wear properties of nylon.* Wear, 1986. **110**(3): p. 379-388.

175. Vinogradov, G.V., V.A. Mustafaev, and Y.Y. Podolsky, *A study of heavy metal-to-plastic friction duties and of the wear of hardened steel in the presence of polymers.* Wear, 1965. **8**(5): p. 358-373.

176. Jones, D.P., D.C. Leach, and D.R. Moore, *Mechanical properties of poly (ether-ether-ketone) for engineering applications.* Polymer, 1985. **26**(9): p. 1385-1393.

177. *Victrex PEEK™ 450G datasheet. Victrex Ltd. Available from: http://www.victrex.com/en/peek-450g-polymer.php.*

178. Myshkin, N.K., M.I. Petrokovets, and A.V. Kovalev, *Tribology of polymers: adhesion, friction, wear, and mass-transfer.* Tribology International, 2006. **38**(11): p. 910-921.

179. Briscoe, B.J. and D. Tabor, *Friction and wear of polymers: the role of mechanical properties.* British Polymer Journal, 1978. **10**(1): p. 74-78.

180. Sugama, T., N.R. Carciello, and M. Miura, *Adhesion of crystalline polyphenyletheretherketone (PEEK) in metal-to-metal joints.* International journal of adhesion and adhesives, 1992. **12**(1): p. 27-37.

181. Sugama, T. and N.R. Carciello, *Polyphenyletherketone and polyphenylethersulfone adhesives for metal-to-metal joints.* International Journal of Adhesion and Adhesives, 1993. **13**(4): p. 257-266.

182. Buckley, D.H. and W.A. Brainard, *The atomic nature of polymer-metal interactions in adhesion, friction, and wear*, in *Advances in polymer friction and wear*. 1974, Springer. p. 315-331.

183. Harris, K.L., et al., *PTFE tribology and the role of mechanochemistry in the development of protective surface films.* Macromolecules, 2015. **48**(11): p. 3739-3745.

184. Sawyer, W.G., et al., *Mechanistic studies in friction and wear of bulk materials.* Annual Review of Materials Research, 2014. **44**: p. 395-427.

185. Blanchet, T.A. and F.E. Kennedy, *Sliding wear mechanism of polytetrafluoroethylene (PTFE) and PTFE composites.* Wear, 1992. **153**(1): p. 229-243.

186. Bassigny, V., et al., *Tensile drawing of poly (aryl ether ether ketone): 1. birefringence, infra-red dichroism and shrinkage-stress measurements.* Polymer, 1993. **34**(19): p. 4052-4059.

187. Lee, L.H., J.J. Vanselow, and N.S. Schneider, *Effects of mechanical drawing on the structure and properties of PEEK.* Polymer Engineering & Science, 1988. **28**(3): p. 181-187.

188. Daly, H.B., et al., *An experimental technique for the characterization of molecular orientation through the thickness of plastic products.* Polymer Engineering & Science, 1999. **39**(10): p. 1982-1992.

189. Damman, P., et al., *Liquid-liquid phase separation and oriented growth of poly (aryl ether ether ketone) on friction-transferred poly (tetrafluoroethylene) substrates.* Macromolecules, 1995. **28**(24): p. 8272-8276.

190. Zhang, S.W., *State-of-the-art of polymer tribology.* Tribology International, 1998. **31**(1–3): p. 49-60.

191. Briscoe, B., *Wear of polymers: an essay on fundamental aspects.* Tribology International, 1981. **14**(4): p. 231-243.

192. Hamdan, S. and G.M. Swallowe, *The strain-rate and temperature dependence of the mechanical properties of polyetherketone and polyetheretherketone.* Journal of materials science, 1996. **31**(6): p. 1415-1423.

193. Hamdan, S. and G.M. Swallowe, *Crystallinity in PEEK and PEK after mechanical testing and its dependence on strain rate and temperature.* Journal of Polymer Science Part B: Polymer Physics, 1996. **34**(4): p. 699-705.

194. Voice, A.M., D.I. Bower, and I.M. Ward, *Molecular orientation in uniaxially drawn poly(aryl ether ether ketone): 2. Infra-red spectroscopic study.* Polymer, 1993. **34**(6): p. 1164-1173.

195. Lee, Y. and R.S. Porter, *Crystallization of poly(ether ether ketone) oriented by solid-state extrusion.* Macromolecules, 1991. **24**(12): p. 3537-3542.

196. Blundell, D.J., et al., *Orientation changes during the cold drawing and subsequent annealing of PEEK.* Polymer, 1994. **35**(18): p. 3875-3882.

197. Daver, F., A. Blake, and M. Cakmak, *Stages of Structural Ordering Leading to Stress Induced Crystallization of PEEK Films: A Mechano-Optical Study on Deformation, Relaxation and Retraction.* Macromolecules, 2009. **42**(7): p. 2626-2633.

198. Séguéla, R., *On the Natural Draw Ratio of Semi-Crystalline Polymers: Review of the Mechanical, Physical and Molecular Aspects.* Macromolecular Materials and Engineering, 2007. **292**(3): p. 235-244.

199. Li, W., et al., *Preparation and Characterization of high-strength poly (ether ether ketone) films.* Journal of Applied Polymer Science, 2014. **131**(9).

200. Harris, K.L., et al., *Wear Debris Mobility, Aligned Surface Roughness, and the Low Wear Behavior of Filled Polytetrafluoroethylene.* Tribology Letters, 2015. **60**(1): p. 1-8.

201. *http://media.fluke.com/documents/flexcam.*

202. Zhang, M.Q., et al., *Predictability of wear status provided by fractal dimensions of wear particles.* Journal of materials science letters, 1996. **15**(15): p. 1288-1290.

203. Schallamach, A., *How does rubber slide?* Wear, 1971. **17**(4): p. 301-312.

204. Maegawa, S. and K. Nakano, *Mechanism of stick-slip associated with Schallamach waves.* Wear, 2010. **268**(7): p. 924-930.

205. Jia, B.-B., et al., *Tribological behaviors of several polymer–polymer sliding combinations under dry friction and oil-lubricated conditions.* Wear, 2007. **262**(11): p. 1353-1359.

206. Erhard, G., *Sliding friction behaviour of polymer-polymer material combinations.* Wear, 1983. **84**(2): p. 167-181.

207. Lavielle, L., *Polymer-polymer friction: relation to adhesion.* Wear, 1991. **151**(1): p. 63-75.

208. Youn, J.R. and C.L. Su, *Elastic contact stress analysis of semi-crystalline polymers under normal and tangential loading.* Polymer Engineering & Science, 1987. **27**(13): p. 999-1005.

209. Kadiric, A., R.S. Sayles, and E. Ioannides, *Thermo-mechanical model for moving layered rough surface contacts.* Journal of Tribology, 2008. **130**(1): p. 011016.

210. Radcliffe, C., *Sealing material developments for reciprocating gas compressors.* Sealing Technology, 2005. **2005**(11): p. 7-11.